The PHILOSOPHICAL MAGAZINE

FIRST PUBLISHED IN 1798

VOL. 45 SEVENTH SERIES No. 364 May 1954

A Journal of Theoretical Experimental and Applied Physics

PRICE 15s. 0d.

Annual Subscription £8 0s. 0d. payable in advance

TED AND PUBLISHED BY TAYLOR & FRANCIS LTD., RED LION COURT, FLEET ST., LONDON, E.C.4.

ATOMIC ENERGY

A SURVEY

by

PROFESSOR J. ROTBLAT

Published April 1954

Given as a course of lectures at the University of London under the auspices of the Atomic Scientists' Association *and the Department of Extra-Mural Studies*

CONTENTS

Atomic Research at Harwell

Speaker: Sir JOHN D. COCKCROFT, K.C.B., SC.D., LL.D., F.R.S.

Chairman: Sir RODERIC HILL, K.C.B., M.C., A.F.C., M.A.

Atomic Weapons

Speaker: Professor O. R. FRISCH, O.B.E., D.SC., F.R.S.

Chairman: Professor P. M. S. BLACKETT, M.A., D.SC., F.R.S.

Power from Atomic Energy

Speaker: Professor F. E. SIMON, C.B.E., PH.D., F.R.S.

Chairman: Sir CHRISTOPHER HINTON, M.I.C.E., M.I.MECH.E.

Radiation Hazards of Atomic Energy

Speaker: Dr. J. F. LOUTIT, M.D., M.R.C.P.

Chairman: Sir ERNEST ROCK CARLING, F.R.C.S., F.R.C.P.

Medical Uses of Atomic Energy

Speaker: Dr. E. E. POCHIN, M.D., F.R.C.P.

Chairman: Sir HENRY DALE, O.M., G.B.E., F.R.C.P., F.R.S.

Atomic Energy and Moral Issues

Speakers: Professor KATHLEEN LONSDALE, D.SC., F.R.S.
Sir GEORGE P. THOMSON, D.SC., LL.D., F.R.S.

Chairman: Professor A. V. HILL, C.H., O.B.E., SC.D., F.R.S.

Paper bound: 4/9 (70 cents) Cloth bound: 6/9 ($1) (including postage)

Printed and Published by
TAYLOR & FRANCIS, LTD.,
RED LION COURT, FLEET STREET, LONDON, E.C.4

LIV. *The Surface of a Nucleus*

By J. M. C. Scott
Cavendish Laboratory, Cambridge*

[Received January 31, 1954]

Summary

In interpreting experiments on nuclear reactions, a common procedure includes the use of a ' radius ' of the form $r_0A^{1/3}$ or $r_0(A_1^{1/3}+A_2^{1/3})$, with $r_0=14{\cdot}5\times10^{-14}$ cm. Certain recent experiments indicate a rather high density of nuclear matter, and imply that r_0 is 20% smaller than this ; but whereas some nuclear reaction data also suggest a smaller radius, others seem to require a larger one.

With the object of improving this situation, a theoretical analysis of neutron scattering data is given which yields information on the form of the outermost part of the nuclear field. Using the hypothesis of charge-independence, the field affecting protons is deduced from that affecting neutrons. The potential barrier calculated in this way for protons is much less severe when the energy is near the top of the barrier than it would be on the customary assumption of a sharp nuclear boundary. Approximate formulae for the penetrability are given for limiting cases.

The neutron data are found to be difficult to reconcile with two-body nuclear forces with the conventional Yukawa shape, but are consistent with any of the short-tailed potentials.

§1. Introduction

The formula $R=r_0A^{1/3}$ for the radius of a nucleus is widely used, especially in calculating the penetrability of potential barriers, but there is some uncertainty about the best value of r_0 to use. The penetrability may vary by a substantial factor with different choices of radius : it is nevertheless difficult to check the correctness of whatever radius is assumed, because differences in penetrability can be largely offset by adjusting the unknown ' reduced level-width '. Since the absolute value of the reduced level-width is something one would like to know, this is not a satisfactory situation.

The surface of the nucleus is certainly not a sharp boundary. Different phenomena, therefore, may very well yield different values of the radius

* Communicated by the Author.

when interpreted in terms of a sharp-boundary model, as the following rough figures illustrate :

Method	Value of r_0 (unit $=10^{-14}$ cm)	Reference
(1) Mirror nuclei (2) Fast neutron cross sections (3) Alpha-decay lifetimes	14 to 15	Text-books, e.g. Blatt and Weisskopf (1952)
(4) Fast electron scattering	11	Bitter and Feshbach (1953)
(5) x-rays from captured mesons	12	Fitch and Rainwater (1953)

Of these, (5) and perhaps (4) correspond to a radius chosen so as to give the right central density, whereas (2) and (3) are reaction radii depending on the distance at which nuclear forces begin to act strongly on an approaching particle : it is not altogether surprising that the latter are larger, both because of the non-zero range of the nuclear forces and because of the gradual tailing-off of the probability-density of the nucleons. The high value given by method (1) is due mainly to the neglect of exchange energy (Wigner and Feenberg 1941), and partly also to the last-mentioned ' tail ' effect (Wilson 1952).

It will be shown here (§4) how quantitative information about the outer fringe of the nuclear field can be obtained from data on neutron cross sections. In §5 the application of the results to proton reactions is briefly considered.

§2. Models of the Nucleus

This section contains a preliminary discussion of the basic ideas used in the later sections, since both the validity of the argument and the interpretation of the data depend on them. Though space does not permit a complete discussion, it is desirable to be as explicit as possible about the assumptions involved.

2.1. *The Independent-Particle Model (Weak Interaction)*

2.1.1. *Bound States*

By a ' model ' we shall mean some simplified description of the nucleus which permits us to deduce or calculate some of its properties. Such descriptions differ in their implications for the phenomena considered in §§4 and 5. They vary from very specific models of doubtful validity to general but less informative ones.

At one extreme there is the independent-particle model (Condon and Shortley 1935, pp. 158–160), which is the basis of most theoretical work on the properties of atoms, and has been much used for nuclei (Inglis 1953). The original objections raised against it, which are still often heard, seem to be somewhat ill founded. It is said (i) that it is successful with atoms

because the electrons are mainly controlled by the Coulomb field of the nucleus, whereas in nuclei there is no fixed centre of force, and (ii) the nuclear forces produce a very strong force when two nucleons are within a short range of each other (which tends to make one-particle wave functions useless). It is often overlooked that these objections should apply equally to the theory of atomic spectra : for (i) the atomic field is just as much due to the electrons as to the nucleons (the two contributions are about equally strong for the outer electrons to which spectroscopic theory is usually applied) ; (ii) the Coulomb force is also very strong for two electrons close together, as they may well be if their spin co-ordinates are unlike. The second objection would also apply to the theory of the conduction electrons in metals. In view of the usefulness of the independent particle treatment of atoms, then, there is no need to be pessimistic about nuclei.

Mathematically, the model which we wish to consider here implies the use of a wave function consisting of a sum of products of a set of one-nucleon wave functions, which can be described by a configuration symbol. All the particles are regarded as moving in the same field $V(r)$ (not as in the Hartree self-consistent field). This forms the starting point of a perturbation or a variation treatment, in which the difference between the true forces $U(\mathbf{r}_1, \mathbf{r}_2)$ and the smoothed-out field V,

$$\sum_{i>k}\sum U(\mathbf{r}_i, \mathbf{r}_k) - \sum_k V(r_k), \quad . \quad . \quad . \quad . \quad . \quad . \quad . \quad . \quad (1)$$

is the perturbation ; the first-order perturbation is relied on to give the splitting of the configuration into terms. However V may be defined, its usefulness depends really on the smallness of the perturbation. Naturally this method of approach does not tell us everything—but on the whole it is very successful in predicting the *relative* positions of atomic energy levels, and it *may* well therefore be a good approximation for nuclei.

2.1.2. *Nuclear Reactions*

Although these ideas are usually only applied to bound states of nuclei, it is worth while to carry them over to the phenomena of reactions at low energies, and to consider what they would imply.

When a nucleon with low kinetic energy interacts with a target nucleus, and a resonance level is observed, this virtual level may, according to the weak-interaction model, be of either of two types.

(*a*) It may be that the virtual level of the compound nucleus belongs to the same configuration as the separated system target-plus-nucleon (ignoring the question of the principal quantum number of the incident nucleon), and is a level with the same symmetry properties, as expressed by appropriate symmetry quantum numbers. The behaviour of the system can then be described approximately in terms of an equivalent single-particle problem : the wave function is replaced by a product

$$\psi(\mathbf{r}_1) \, . \, \phi(\mathbf{r}_2, \ldots, \mathbf{r}_N), \quad . \quad . \quad . \quad . \quad . \quad . \quad . \quad . \quad . \quad (2)$$

and the residual target nucleus is described throughout by the same

function ϕ and plays only a passive part. Then the break-up of the compound nucleus is only prevented by the potential barrier, or in the case of slow neutrons by the effect of long wavelength which is responsible for the well-known relations $\sigma_{\text{abs}} \propto 1/v$ and $\Gamma_n \propto v$. As the situation is similar to that in the ordinary theory of alpha decay, virtual levels of this kind may perhaps be conveniently described for brevity as Gamow levels. The situation when the particle is uncharged was discussed by Kapur and Peierls (1938) and more recently on similar lines by Feshbach, Peaslee and Weisskopf (1947) and others. (Strictly speaking, (2) ought to be antisymmetrized, and the analysis becomes much more complicated in appearance. In a detailed treatment (Lane 1953, Lane and Thomas 1954), case (*a*) is the case in which the fractional parentage coefficient is large.)

(*b*) It may be however that either the virtual level belongs to a configuration which does not include a nucleon of the same kind and with the same angular momentum as the emitted nucleon, so that break-up is only rendered possible by configuration-mixing, or else that break-up is hindered by a selection rule and proceeds only in virtue of mixing of like terms in the same configuration. Such levels may for brevity be called Auger levels, because of the analogy with the radiationless transitions of atoms known as auto-ionization or Auger effect.

The ' Auger ' levels should be much more numerous and closely spaced than the ' Gamow ' levels, but in so far as the weak-interaction model is valid they should have smaller widths.

2.2. *Strong Interaction*

If the perturbation (1), and the consequent configuration-mixing, are so strong as to make any sort of perturbation theory useless, it is necessary to fall back on the general formal theory of nuclear reactions developed by Wigner and others, from which few detailed predictions can be made. The decomposition (2) is only supposed to be applicable when $\mathbf{r}_1$ is outside a sphere drawn so large that the incident neutron is entirely free ; then by integrations carried out over the rest of phase-space one can deduce the general behaviour of $(1/\psi)\, d\psi/dr_1$ at the surface of the sphere as the energy varies. For example, if processes other than elastic scattering with $l=0$ are neglected, one finds a relation of the form

$$\frac{r\psi}{\partial(r\psi)/\partial r} = \sum_n \frac{\gamma_n{}^2}{E_n - E}, \qquad \ldots\ldots\ldots \quad (3)$$

in which the sum is extended over all resonance levels E_n of the compound nucleus. By proceeding in this way, Wigner and others (1947) have constructed a general theory of resonance reactions which includes the commonly used Breit–Wigner formulae for cross sections as a special case.

In particular, the phase-shift which determines the scattering of slow neutrons by a nucleus is directly related to (3). In the case of strong interaction, little can be said about the constants γ_n beyond the fact that they are real. If they are all of comparable magnitude, the scattering

would be much influenced by the levels E_n that happen to lie nearest, and large positive or negative scattering amplitudes would occur if the available energy E lies just above or just below a resonance level. On the other hand, in the limit of very weak interaction, γ_n would be small for what we have called the Auger levels, and large for the much less numerous Gamow levels. In that case the scattering would usually depend on the nearest Gamow level, and be little affected by the much closer (but narrower) Auger levels, unless of course one of them should happen to be very close indeed.

2.3. *Medium-Interaction Models*

Weisskopf and others (Feshbach, Porter and Weisskopf 1953, Blatt and Weisskopf 1952, pp. 345–358) have made use of a potential-well model of the nucleus, in which an incident neutron is described by a single-particle wave function, not only outside the nucleus but for some distance below the surface. Instead of requiring that the neutron wave can reach the centre suffering only refraction, as in the zero-order approximation of the weak-interaction model, they describe the interaction between the neutron and the nuclear matter by an extinction coefficient. This model, sometimes called the ' cloudy crystal ball ' or the ' continuum theory ', has had some success in interpreting experiments on the scattering of fast neutrons.

It is possible to make this type of theory somewhat less phenomenological, at the cost of extra mathematical complication, by starting from the general formal theory (§ 2.2), and supposing that the function $\psi(r_1)$ can be extended some distance into the nucleus, i.e. well within the minimum sphere of § 2.2, before the junction is made with the interior solutions. This extension of $\psi(r_1)$ is regarded merely as a zero-order approximation, but if the effective potential which determines it is suitably chosen the error may be taken into account as a first-order perturbation at the expense of some complication in the mathematics of the formal dispersion theory.

§ 3. The Effective Potential

3.1. *Depth of Well*

The weak- and the medium-coupling models lead to the notion of an effective potential similar in principle to that which is used in discussing complex atoms. It is often assumed to be a square well (depth W, say), though of course it must actually be rounded off somewhat at the edge ; a parabolic bowl shape (oscillator potential) is often mathematically more convenient, and is doubtless a better approximation for the lightest nuclei.

We shall need later a rough estimate of the depth W of the well. This is readily obtained from considerations of statistical mechanics. If we have N neutrons filling a well of radius $R=r_0A^{1/3}$ to a maximum kinetic energy $p^2/2M$ then allowing two neutrons to each h^3 of phase space we obtain

$$\frac{p}{\hbar}=\left(\frac{9\pi}{4}\frac{N}{A}\right)^{1/3}\frac{1}{r_0}=\frac{1{\cdot}58}{r_0} \quad . \quad . \quad . \quad . \quad . \quad . \quad (4)$$

approximately, for the propagation constant of a neutron at the top of the Fermi distribution. The numerical relation connecting propagation constant (2π divided by wavelength) with energy will frequently be required : it is

$$\frac{\sqrt{E}}{p/\hbar} = \frac{\hbar}{\sqrt{(2M)}} = 45{\cdot}51 \times 10^{-14} \text{ cm MeV}^{1/2} = \frac{1}{2{\cdot}197 \times 10^{12}} \text{ cm MeV}^{1/2}. \quad (5)$$

Using $r_0 = 12 \times 10^{-14}$ cm, the energy of the top neutron will be 35 MeV above the bottom of the well ; and assuming that the addition of 7 MeV binding energy would make it free, the total depth W will be 42 MeV. With a larger value of r_0, say $14{\cdot}2 \times 10^{-14}$ cm, W would be reduced to 32 MeV.

3.2. *The Surface of the Nucleus*

The effective potential $V(r)$ cannot be a simple square well, but the transition from the value $-W$ inside to zero outside must be somewhat gradual. It will appear later that it is the outermost part of this transition region that is the most interesting, both theoretically and experimentally. The ' tail ' of the potential $V(r)$ will ultimately decrease to zero like $\exp\{-(r-R)/b\}$, where b is a constant fairly small compared with the size of the nucleus (except for the lightest nuclei which are not considered here). This is because the ultimate behaviour of V for larger nuclei may depend either on the diminution of the nuclear forces with increasing distance, or on the decrease of the probability-density of nuclear matter, whichever is ultimately the slower ; and whichever is slower will be asymptotic to an exponential and will determine the value of b.

If b is determined by the tailing-off of the density $|\Psi|^2$ of the individual nucleons in the target nucleus, the following argument leads to the estimate that

$$1/b \simeq (2/\hbar)\sqrt{(2MB)}, \quad . \quad . \quad . \quad . \quad . \quad . \quad . \quad (6)$$

in terms of the binding energy B of the most easily-removed neutron in the target nucleus. If we consider the part of co-ordinate space in which one nucleon, say a neutron, is a little distance outside the conventional ' interior ', so that $|\Psi|^2$ is rather small, then the probability of finding a second nucleon also outside the interior region is very much smaller still, for energetic reasons, and can be neglected. This implies that the wave function can be expressed in product form (2) in terms of a single-particle wave function and a factor describing the inert residue. The wave equation then indicates that $\psi(r_1)$ must fall off exponentially with the coefficient $\hbar/\sqrt{(2MB)}$ for large enough r_1. This rather rough argument leads to a value of b of about 8×10^{-14} cm.

Turning now to the various types of nuclear forces that are commonly considered, the assumption that pairs of nucleons are acted on by an attraction described by a Yukawa potential implies that b will be determined by the range of that potential if the range is long enough. According to figures given by Salpeter (1951), we have in this case $b = (14{\cdot}1 \pm 0{\cdot}6) \times 10^{-14}$ cm based on neutron–proton scattering at low

energies (triplet interaction). In the case of the exponential shape, the corresponding constant is $b=6{\cdot}8\times10^{-14}$ cm. The Gaussian shape falls off faster than any exponential function, and therefore cannot ultimately compete with the superimposed effect of the nucleon wave functions (6); and the same applies to the square-well shape.

It thus appears that if a determination of b from experimental data is feasible, it may give some information on nuclear forces, if they are of a 'long-tailed' type.

Before proceeding further we return to the consideration of the distribution of nucleons just 'outside' the nucleus in a little more detail. The formula (6) rests on the tacit assumption that the nucleon which could be removed by supplying energy B could be removed with orbital angular momentum zero, which implies that the residual nucleus (corresponding to ϕ in (2)) has the same parity as the original nucleus and spin differing by $\frac{1}{2}$. Among the 69 cases considered below, this is true for Sn and Te and possibly one or two others, but is in general false. If we do consider the binding energy B in the ordinary sense, the first factor $\psi(r_1)$ in (2) may involve a high angular momentum l; e.g. for ^{88}Sr ($I=0+$) the residual nucleus is ^{87}Sr with $I=\frac{9}{2}(+)$ in the ground state. The value of B to be used in the formula (5) would thus apparently have to be increased by the amount of the centrifugal barrier

$$\frac{l(l+1)}{R^2}\,\frac{\hbar^2}{2M},$$

which is here of the order of 13 MEV. Alternatively we can contemplate removing a neutron with $l=0$, but we must then include in the energy-deficit the extra energy to excite the residual nucleus ^{87}Sr to the lowest level that has $I=\frac{1}{2}(+)$. Again the value of B has to be increased, probably by several MEV at least.

Both in this case, and in general, far too little is known of the excited states of the residual nuclei to settle whether one of these extremes or some compromise between them represents the 'most easily removed nucleon', in the sense of determining the effective (i.e. greatest) value of b. It appears from these considerations that B should be taken somewhere between 8 and 20 MEV; an argument using an idealized statistical model is given in Appendix I, which leads to a value 10 MEV more than the conventional neutron binding energy, say $7+10=17$ MEV. This implies

$$b=5{\cdot}5\times10^{-14}\text{ cm}. \qquad \ldots\ldots \quad (7)$$

We conclude that b, averaged over a number of nuclei, probably lies within the limits $(6\pm1)\times10^{-14}$ cm, unless of course the value determined by the range of nuclear forces is greater, but that in a few exceptional cases it may be as high as 8×10^{-14} cm.

Another possible cause for the lack of sharpness of the surface of the nucleus is the zero-point motion associated with the deformation oscillations that are invoked to explain fission. The relevant functions fall

off faster than an exponential, and this effect need not be considered further.

§4. Deductions from Experimental Data

When we look for experimental data bearing on the nuclear radius, and the unsharpness of the nuclear surface which we have described in terms of the rounding off of the edge of the potential well, the most obvious course might seem to be to study the penetrabilities which affect the absorption or emission of a charged particle. We at once encounter two difficulties ; the analytical difficulty of solving the wave equation for a ' rounded-off ' barrier when there are three variable parameters ; and the lack of satisfactory data : for the very precise data on natural radioactivity cannot be used without considering the structure of the alpha particle, and the data on level widths for proton emission are not sufficiently extensive and accurate.

The data on the scattering of slow neutrons appears best suited to our purpose. It is the scattering length, a, for coherent scattering (Fermi and Marshall 1947, Cassels 1950) which will be used, rather than the cross section, partly because the sign of the scattered wave is significant for our purpose, and partly because of a property which will appear in §4.2.

The scattering depends on the phase δ in the wave function

$$\psi \propto (1/r) \sin (kr+\delta)$$

which describes an s neutron when it is beyond the range of attraction of the nucleus. According to the weak-interaction and the medium-interaction models, the wave function can be extended through the boundary layer of the nucleus and into the potential-well region, in a zero-order approximation at any rate, and the phase δ of the long wavelength waves outside depends on the phase of the short waves below the surface of the nucleus in some way to be considered later. At this stage the models differ : in the medium-interaction model the internal phase is effectively random, depending on where the energy of the system happens to fall among the resonance levels of the compound nucleus, which form a closely-spaced spectrum. In the weak-interaction model, however, the phase depends on the distance in wavelengths to the centre of the nucleus and back, just as in the classical phenomenon of refraction by a transparent sphere. This distance increases steadily through several wavelengths as we traverse the periodic table.

On examining a list of the coherent scattering lengths (Hughes 1953) of all available nuclei, excluding the lightest, it is difficult to see any systematic variation of the kind that might be expected with the extreme weak-coupling assumption. Ford and Bohm (1950) have plotted the scattering lengths against mass number, and claim that there is some indication of such a regularity, which they call a size-resonance. The evidence has been accidentally exaggerated by their method of plotting : while it is indeed remarkable that three out of the very few known

negative values occur close together (Ti, ^{51}V, ^{55}Mn), these appear in their diagram as six points—which would be a much more striking coincidence. On the other hand, the adjacent nuclei Cr and ^{54}Fe have positive scattering lengths of about the normal magnitude. Still, although Ford and Bohm consider that the evidence is by no means conclusive, it has been strengthened by the recent discovery of a negative scattering length in ^{152}Sm (Koehler and Wollan 1953), and the effect is very probably real.

Incidentally, if Ford and Bohm's interpretation is right, the value of about 45 Mev which they find for the well-depth confirms the estimate of §3.1.

If the indication of a size-resonance effect is accepted as real, then the conditions in nuclei are on the borderline between the weak-interaction theory and the domain in which only the medium-interaction is applicable. Any systematic variation of the internal phase with mass-number is almost completely masked in some way, e.g. by perturbations causing configuration-mixing or by fluctuations in the well-depth or both. Bearing in mind, as well, that the available nuclei are distributed throughout most of the periodic table, one may safely regard the internal phases as being a random sample, even if there is a slight correlation between the phases in adjacent elements.

In the medium interaction model, the internal phases ought also to be random.

We accordingly shall analyse the known coherent scattering lengths as a statistical sample on the basis of this postulate of randomness.

4.1. *The Sharp-Boundary Assumption*

First of all, the data will be analysed on the basis of the sharp-boundary hypothesis. Although this is not in fact correct, most of the analysis can be taken over unchanged and used in the more correct theory of §4.4 below. For the present, then, the neutron is regarded as moving in an effective potential $V(r)$, which is a square well of radius R and depth $-W$. The de Broglie wave numbers outside and inside are specified by

$$k=(1/\hbar)\sqrt{(2ME)}, \quad . \quad . \quad . \quad . \quad . \quad . \quad . \quad (8\,a)$$

which is small for slow neutrons, and

$$K=(1/\hbar)\sqrt{\{2M(E+W)\}}\simeq(1/\hbar)\sqrt{(2MW)} \quad . \quad . \quad . \quad (8\,b)$$

which is large. The wave function just inside the nucleus is specified by

$$\chi\equiv r\psi=C_1\sin(Kr+\beta), \quad . \quad . \quad . \quad . \quad . \quad . \quad (9)$$

where $\beta=0$ in the weak interaction theory and β is random in the medium interaction theory. Both K and β are practically independent of E in the small range of energies covered by thermal neutrons.

The wave function outside the nucleus is specified by

$$\chi=C_2\sin(kr+\delta), \quad . \quad . \quad . \quad . \quad . \quad . \quad . \quad (10)$$

where δ is the phase-shift of s-wave scattering, as usually defined.

The boundary conditions require that $(1/\chi)\, d\chi/dr$ be continuous where r takes the value $R=r_0A^{1/3}$, and this gives

$$\delta+kR=\tan^{-1}\{(k/K)\tan(KR+\beta)\}. \quad . \quad . \quad . \quad (11)$$

The Fermi scattering length is therefore

$$a\equiv\lim_{k\to 0}(-\delta/k)=R-(1/K)\tan(KR+\beta),$$

or we may write

$$a=R+S\tan\theta, \quad . \quad . \quad . \quad . \quad . \quad . \quad . \quad . \quad (12)$$

where θ can be taken to be between $-\frac{1}{2}\pi$ and $+\frac{1}{2}\pi$, and is uniformly distributed in that interval among the sample of nuclei to be considered, and

$$S=1/K. \quad . \quad . \quad . \quad . \quad . \quad . \quad . \quad . \quad (13)$$

Hence $a-R(=x)$ is distributed according to the law :

$$\left\{\begin{matrix}\text{Probability of}\\ x \text{ lying in } dx\end{matrix}\right\}=\frac{1}{\pi}\frac{S\,dx}{x^2+S^2}. \quad . \quad . \quad . \quad . \quad . \quad (14)$$

If we choose those values of $a-R$ which are derived from coherent scattering by pure isotopes with spin zero (this restriction will presently be removed), we have a sample from a probability distribution (14), which is a distribution law very different from the Gaussian error curve, and is sometimes called the Cauchy distribution.

In order to make full use of the data, we need to examine some questions of probability theory relating to the Cauchy distribution.

4.2. *The Cauchy Distribution*

The problem of estimation in statistics is the problem of deducing, from a finite sample, information about the parameters of the distribution (' population ') from which it was drawn. In the case of the Cauchy distribution

$$P(x)\,dx=\frac{1}{\pi}\frac{S\,dx}{(x-X)^2+S^2}, \quad . \quad . \quad . \quad . \quad . \quad . \quad (15)$$

the parameters are the central value X, and the width, or what we may call the ' spread ' of the distribution, S. Whereas with the Gaussian error law the arithmetic mean of a sample is the best statistic that can be calculated from the sample, with a Cauchy distribution on the other hand the mean of a sample of N observations is practically useless because it is no more accurate than a single observation (Fisher 1921). The situation for the variance, or standard deviation squared, is even worse, for the variance of the distribution (15) is infinite.

These properties, and another which we shall need, are easily established by the method of the characteristic function. Suppose the function $P(x)$ specifying the distribution of x can be written

$$P(x)=\frac{1}{2\pi}\int_{-\infty}^{\infty}p(t)\exp(-ixt)\,dt, \quad . \quad . \quad . \quad . \quad (16)$$

then $p(t)$ is the Fourier transform of $P(x)$, apart from a factor $\sqrt{(2\pi)}$, and is called the characteristic function of x. If y is another variate, independent from the first, with a distribution

$$Q(y)=\frac{1}{2\pi}\int_{-\infty}^{\infty} q(t)\exp(-iyt)\,dt, \quad . \quad . \quad . \quad . \quad (17)$$

then the convolution theorem for Fourier transforms shows that the distribution of $x+y=z$ is given in terms of $p(t)$ and $q(t)$ by

$$R(z)=\int_{-\infty}^{\infty} P(z-x)Q(x)\,dx=\frac{1}{2\pi}\int_{-\infty}^{\infty} p(t)q(t)\exp(-izt)\,dt\,;$$

thus we merely have to multiply the characteristic functions together, in order to get the characteristic function of $x+y$.

For the Cauchy distribution (15), the characteristic function is

$$\exp(iXt-S|t|).$$

A short calculation shows that the weighted sum $Ax+By$ of two independent variates x and y each obeying the law (15) has the characteristic function

$$\exp\{i(A+B)t-(|A|+|B|)S|t|\}. \quad . \quad . \quad . \quad . \quad (18)$$

It follows that $Ax+By$ is distributed in a Cauchy distribution, centred at $(A+B)X$, and with spread $(|A|+|B|)S$.

We make two applications of this. First, the argument just given can be extended to N observations $x, y \ldots$ instead of two ; and taking the weighting coefficients $A, B, \ldots$ to be each equal to $1/N$, we find that the mean of a sample of N observations has exactly the same distribution (and the same spread) as one single observation—as stated earlier.

Secondly, if we have a nucleus with spin I, the coherent scattering amplitude a which is observed depends on the scattering lengths (a_+a_-) for the two spin channels as follows :

$$a=\frac{I+1}{2I+1}a_+ + \frac{I}{2I+1}a_-, \quad . \quad . \quad . \quad . \quad . \quad . \quad (19)$$

and is in effect a weighted mean. Now if a_+ and a_- follow a Cauchy distribution we see that a obeys identically the same distribution law. This argument can be extended to apply to an element that is a mixture of isotopes ; for statistical purposes, the observed value, which is a weighted mean of perhaps half a dozen scattering lengths, can be treated just as if it were an observation on a pure single isotope.

This is most important, for it enables us to use all the data instead of keeping to the few known cases of scattering by a definite isotope in a definite spin-state. (The suggestion that ^{51}V has a very small cross section because of its non-zero spin, which permits a destructive interference effect (Ford and Bohm 1950), can only be partly correct. Although destructive interference no doubt occurs, the resultant coherent scattering is just as likely to be small for a nucleus with spin $I=0$ as for an odd-mass one.)

4.3. *Value of the Spread Parameter S*

The data used consist of the coherent scattering amplitude of elements, or if possible of individual isotopes, with $A \geqslant 12$. Many of them come from the work of Shull and Wollan (1951), but the figures have been brought up to date with the help of the compilation edited by Hughes (1953) which contains many new and revised values. Most of the data are also accessible in Hughes' book (1952).

The statistical variate $a-R$ which is to be studied is found by subtracting the nominal nuclear radius

$$R=r_0A^{1/3}+C \quad . \quad . \quad . \quad . \quad . \quad . \quad . \quad . \quad (20)$$

from the scattering length. The constant C will be omitted for simplicity in this section and the next, as it can always be easily allowed for afterwards if desired ; the question of its value will be taken up again in §4.5. The values $r_0=14$ and $r_0=12$ (in units of 10^{-14} cm) have both been tried, but the exact value used turns out to be of little importance at this stage : the trend of a with increasing mass A is scarcely perceptible compared with the random fluctuations, and it is sufficient to remove this trend approximately in order to deduce S. (The use of $r_0=14$ yields in fact practically the same value of S, but of course gives a smaller median value of $a-R$.)

The kind of method used for estimating the standard deviation of a Gaussian distribution is useless here, and indeed no sufficient statistic is known (Koopman 1936). But a good estimate of the spread parameter S can be obtained from the interquartile distance. The 25% points of the distribution are separated by an amount which can be used as an estimate of $2S$, subject to a small correction for bias. The efficiency of this estimate is $8/\pi^2$ and its probable error is only 11% more than the theoretical least possible. In this way it is found that

$$\left.\begin{aligned} \text{Spread } S &= 16{\cdot}9 \pm 2 \\ \text{Central value } X &= \ 7 \ \pm 2 \end{aligned}\right\}, \quad . \quad . \quad . \quad . \quad . \quad (21)$$

in units of 10^{-14} cm. The complete distribution is given in Appendix II.

If the value of S is interpreted (13) on the sharp boundary hypothesis, as giving $1/K$, it leads (8 *b*) to a value of the well-depth $W=7{\cdot}2$ Mev, which is too small by at least a factor 4. This discrepancy cannot be accounted for by, for instance, a fluctuation in R due to shell effects, which could not be large enough to affect S appreciably or to explain the outlying values of $a-R$.

It must be concluded that the sharp boundary hypothesis fails to explain even very low-energy reactions. Though it may be useful for a rough picture of bound states, it is too crude an approximation to be of any value in discussing scattering or reactions.

4.4. *Boundary Not Assumed Sharp*

We now come to what is the main task before us, namely to examine the consequences of the lack of sharpness of the boundary of the nucleus.

Expressed in terms of the potential $V(r)$, we have to deal with a gradual transition from the value $-W$ inside the nucleus to zero outside it, instead of an abrupt one. A similar mathematical problem arises in optics and radio, in connection with the failure of the Fresnel formulae for partial reflection when the boundary between two media is no longer sharp. In the extreme case of a very gradual transition from one value of the refractive index to the other, there is no partial reflection and the wave propagation can be described mathematically by the phase-integral or *WKB* method, which is practically equivalent to a ray-theory. But in the present problem, as we shall see, the phase-integral method is not applicable.

It will be convenient to distinguish an ' internal region ' in which $V(r)$ is nearly constant ($=-W$), an ' external region ', in which $V(r)$ is zero or nearly zero, and a ' boundary region ', in which the transition between these two conditions takes place, and which takes the place of the sharp boundary of § 4.1. The ' tail ' of the potential $V(r)$ in the outermost part of the transition region decreases like

$$\exp\{-(r-R)/b\}, \quad . \quad . \quad . \quad . \quad . \quad . \quad . \quad (22)$$

as we have seen (§ 3.2), where b is a constant depending either on the distribution of density at the edge of the nucleus or on the range of nuclear forces, whichever has the more gradual decay.

The conditions for the phase-integral or *WKB* method to be applicable require that the ' local wave-number ' does not vary much when r changes by one ' local wavelength ', and when the neutron energy E is very small this condition is certainly not fulfilled in the outer part of the transition region, since the local wavelength is large compared with b. It is therefore necessary to solve the wave equation in some other way. But it is just in this region that we can be fairly certain that $V(r)$ behaves like an exponential ; and we may anticipate that the constant b in this exponential plays a dominant part in determining what the neutron waves will do.

4.4.1. *First Type of Profile*

A convenient shape to choose, which admits of an analytical solution, is the form

$$V(r)=-\tfrac{1}{2}W\{1-\tanh[(r-R)/2b]\}. \quad . \quad . \quad . \quad . \quad . \quad (23)$$

As before, we write the limiting values of the propagation constant for large and for small r as k and K, given by

$$k=(1/\hbar)\sqrt{(2ME)}, \quad . \quad . \quad . \quad . \quad . \quad . \quad . \quad (24)$$

which is small for neutrons of low energy E ($E<1$ ev say), and K given by (8 b) which is practically constant for small energies E.

If we define $\exp[(r-R)/b]=\zeta$, so that $r=R+b\log\zeta$, the wave equation, which is

$$\frac{d^2\chi}{dr^2}+\left\{\frac{K^2+k^2}{2}-\frac{K^2-k^2}{2}\tanh\frac{r-R}{2b}\right\}\chi=0 \quad . \quad . \quad . \quad (25)$$

transforms into a differential equation in ζ with three regular singularities ; in terms of $F=\zeta^{-\alpha}\chi$ (α=a constant), it becomes

$$\zeta(1+\zeta)\frac{d^2F}{d\zeta^2}+(1+2\alpha)(1+\zeta)\frac{dF}{d\zeta}+\left\{k^2b^2+\alpha^2+\frac{K^2b^2+\alpha^2}{\zeta}\right\}F=0 \quad . \quad (26)$$

which can be recognized as a hypergeometric equation provided that α is chosen to make $K^2b^2+\alpha^2=0$. Two solutions for the wave function are obtained in this way, in terms of hypergeometric functions :

$$\vec{\chi}_i=\zeta^{iKb}\,.\,F(iKb+ikb,\ iKb-ikb\ ;\ 1+2iKb\ ;\ -\zeta), \quad . \quad . \quad . \quad (27\,a)$$

$$\overleftarrow{\chi}_i=\zeta^{-iKb}\,.\,F(-iKb+ikb,\ -iKb-ikb\ ;\ 1-2iKb\ ;\ -\zeta). \quad . \quad (27\,b)$$

These represent progressive waves inside the nucleus, since they are approximately $\exp[\pm iK(r-R)]$ respectively when r is small. Another pair of solutions can be obtained by noticing that (25) is unchanged if we interchange K and k, and change the sign of $r-R$.

$$\overleftarrow{\chi}_0=\zeta^{-ikb}\,.\,F(iKb+ikb,\ -iKb+ikb\ ;\ 1+2ikb\ ;\ -1/\zeta), \quad . \quad (28\,a)$$

$$\vec{\chi}_0=\zeta^{+ikb}\,.\,F(iKb-ikb,\ -iKb-ikb\ ;\ 1-2ikb\ ;\ -1/\zeta). \quad . \quad (28\,b)$$

These solutions represent progressive waves outside the nucleus, the first approaching the boundary and the second receding from it.

The series converge and all four solutions are valid for all $\zeta>0$ and thus for all real r ; in particular throughout the transition region (though, of course, the centre of the nucleus is not really infinitely distant, and they have no physical meaning for $r<0$; the criterion for the existence of an 'interior region' at all is $\zeta_{r=0}\ll 1$ which fails for the lightest nuclei, to which the present theory is in any case not applicable ; as will be seen later, $\zeta_{r=0}$ is normally of the order of 10^{-3} to 10^{-5}).

The connection between the two kinds of solution (27) and (28) can be found by the contour integral method given in Whittaker and Watson (1952), where however there is an error in the final result. The correct relation is

$$\frac{F(a,b\ ;\ c\ ;\ -\zeta)}{\Gamma(c)}=\frac{\Gamma(b-a)}{\Gamma(b)\Gamma(c-a)}\,\zeta^{-a}\,.\,F(a,\ 1-c+a\ ;\ 1-b+a\ ;\ -1/\zeta)$$
$$+\frac{\Gamma(a-b)}{\Gamma(a)\Gamma(c-b)}\,\zeta^{-b}\,.\,F(b,\ 1-c+b\ ;\ 1-a+b\ ;\ -1/\zeta). \quad . \quad . \quad . \quad . \quad (29)$$

This gives

$$\frac{\vec{\chi}_i}{\Gamma(1+2iKb)}=\frac{\Gamma(-2ikb)\,.\,\overleftarrow{\chi}_0}{\Gamma(iKb-ikb)\Gamma(1+iKb-ikb)}+\frac{\Gamma(2ikb)\,.\,\vec{\chi}_0}{\Gamma(iKb+ikb)\Gamma(1+iKb+ikb)} \quad . \quad . \quad . \quad . \quad (30\,a)$$

and a second formula can be obtained by changing the sign of K in (30 a), or equally well by taking the complex conjugate remembering that this will interchange $\overleftarrow{\chi}_0$ and $\vec{\chi}_0$.

The connection formula can conveniently be written in terms of the asymptotic forms of the χ's in the interior and exterior regions, as follows :

$$\underset{\text{(interior)}}{\exp[iK(r-R)]}\rightleftarrows\rho_1\exp(i\phi_1)\underset{\text{(exterior)}}{\exp[ik(r-R)]}-\rho_2\exp(i\phi_2)\exp[-ik(r-R)] \quad . \quad . \quad . \quad . \quad (31)$$

in which ρ_1, ρ_2, ϕ_1, ϕ_2 are real constants which can be found from (30 a).

It is assumed as before that there are stationary waves, with random phases, set up in the interior region of the nucleus, and the next task is to obtain the distribution of phase-shifts in the external region, which will yield the distribution of Fermi scattering lengths. Multiplying (31) by $\exp(iKR+i\beta)$ and taking the imaginary part,

$$\underset{\text{(interior)}}{\sin(Kr+\beta)} \rightleftarrows (\rho_1+\rho_2)\cos\theta\sin[kr-kR+\tfrac{1}{2}(\phi_1-\phi_2)]$$
$$-(\rho_1-\rho_2)\sin\theta\cos[kr-kR+\tfrac{1}{2}(\phi_1-\phi_2),\ \underset{\text{(exterior)}}{}$$
. . . (32)

in which θ denotes $-\beta-KR-\frac{1}{2}(\phi_1+\phi_2)$, and is random for the set of nuclei under consideration. The phase-shift δ is determined by the fact that the right-hand side of (32) is a multiple of $\sin(kr+\delta)$, i.e. of

$$\cos(\Delta-\delta)\sin(kr+\Delta)-\sin(\Delta-\delta)\cos(kr+\Delta),$$

and so
$$\delta=-kR+\tfrac{1}{2}(\phi_1-\phi_2)-\tan^{-1}\left(\frac{\rho_1-\rho_2}{\rho_1+\rho_2}\tan\theta\right). \quad . \quad . \quad . \quad . \quad (33)$$

We are concerned with the long wavelength limit for slow incident particles, $k\to 0$. Inserting the values of ρ_1 etc. from (30 *a*), it is found that

$$\frac{\rho_1-\rho_2}{\rho_1+\rho_2}=\frac{\tanh\pi kb}{\tanh\pi Kb}, \quad . \quad . \quad . \quad . \quad . \quad . \quad (34)$$

and
$$\phi_1-\phi_2=-4kb[\mathrm{Re}\,\psi(1+iKb)-\psi(1)]+O(k^3b^3), \quad . \quad . \quad (35)$$

in which $\psi(x)$ denotes the logarithmic derivative of the gamma function, $\Gamma'(x)/\Gamma(x)$ (Appendix III). Hence we find for the scattering length

$$a=\lim_{k\to 0}(-\delta/k)=R+Y+S\tan\theta, \quad . \quad . \quad . \quad . \quad . \quad (36)$$

where
$$Y=2b[\mathrm{Re}\,\psi(1+iKb)-\psi(1)], \quad . \quad . \quad . \quad . \quad . \quad . \quad (37)$$
$$S=\pi b/\tanh\pi Kb, \quad . \quad . \quad . \quad . \quad . \quad . \quad . \quad . \quad . \quad . \quad (38)$$

and θ is randomly distributed.

In the limiting case $b\to 0$ we recover the sharp boundary formula ($S=1/K$). If Kb is not small, we have an increased spread S, and the mean point of reflection is displaced outwards slightly (by Y). If πKb is large, >5 say, we have
$$S\simeq\pi b, \quad . \quad . \quad . \quad . \quad . \quad . \quad . \quad . \quad . \quad (39)$$

independent of K. The asymptotic form of Y for large Kb is

$$2b[\log Kb+\gamma+\tfrac{1}{12}(Kb)^{-2}], \quad . \quad . \quad . \quad . \quad . \quad . \quad (40)$$

where $\gamma=0{\cdot}577\ldots$

The analysis of the experimental material which was given in §§4.1–4.3 still holds good as a determination of the quantities S and Y, provided only that b is not so large that the transition region reaches as far as the centre of the nucleus.

4.4.2. *A Second Type of Profile*

In order to test how far the results depend on the shape (24) of the $V(r)$ profile, several forms were tried with the standard exponential

behaviour (22) as $r \to \infty$; of these, the one that gave the most extreme results was

$$V(r) = \frac{-W}{\{1+\exp[(r-R)/2b]\}^2}. \quad . \quad . \quad . \quad . \quad . \quad (41)$$

This curve approaches its asymptotic form rather slowly, e.g. when V has fallen to 1 MeV, the asymptotic formula (22) is still out by 40%. It also approaches $-W$ rather slowly inside the nucleus.

Writing $r = R + 2b \log \xi$, so that ξ^2 is equal to the ζ used previously, the wave equation which is

$$\frac{d^2\chi}{dr^2} + \left\{k^2 + \frac{K^2-k^2}{(\xi+1)^2}\right\}\chi = 0, \quad . \quad . \quad . \quad . \quad . \quad (42)$$

can again be solved in terms of hypergeometric functions. The details are somewhat more complicated than before, and being of little interest are omitted. A typical solution is

$$\vec{\chi}_i = \xi^{2iKb}(1+\xi)^{\frac{1}{2}+i\eta} F(2iKb+2ikb+\tfrac{1}{2}+i\eta,$$
$$2iKb-2ikb+\tfrac{1}{2}+i\eta\,;\ 1+4iKb\,;\ -\xi), \quad . \quad . \quad . \quad (43)$$

which is $\sim \exp[iK(r-R)]$ in the interior region where ξ is small. Here

$$\eta = \sqrt{(4K^2b^2 - \tfrac{1}{4})}. \quad . \quad . \quad . \quad . \quad . \quad . \quad . \quad (44)$$

The connection formula analogous to (30 a) can again be written in the form (31) but with different coefficients ρ_1. ρ_2, ϕ_1, ϕ_2. Their values are not required individually; the combinations in which they are wanted have the following values:

$$\frac{\rho_1}{\rho_2} = \sqrt{\frac{\cosh(2\pi Kb+\pi\eta+2\pi kb)\cosh(2\pi Kb-\pi\eta+2\pi kb)}{\cosh(2\pi Kb+\pi\eta-2\pi kb)\cosh(2\pi Kb-\pi\eta-2\pi kb)}}, \quad . \quad . \quad (45)$$

$$\frac{\rho_1-\rho_2}{\rho_1+\rho_2} = \tanh\left(\frac{1}{2}\log\frac{\rho_1}{\rho_2}\right) = \pi kb[\tanh(2\pi Kb+\pi\eta)+\tanh(2\pi Kb-\pi\eta)]+O(k^3),$$
$$. \quad . \quad . \quad . \quad (46)$$

$$\phi_1-\phi_2 = -4kb\,\mathrm{Re}[\psi(\tfrac{1}{2}+2iKb+i\eta)+\psi(\tfrac{1}{2}+2iKb-i\eta)-2\psi(1)]+O(k^3). \quad (47)$$

It follows from (46) and (33) that

$$S = \lim_{k\to 0}\frac{1}{k}\frac{\rho_1-\rho_2}{\rho_1+\rho_2} = 2\pi b\,\frac{\sinh 4\pi Kb}{\cosh 4\pi Kb+\cosh 2\pi\eta}, \quad . \quad . \quad . \quad (48)$$

where $\eta = \sqrt{(4K^2b^2-\frac{1}{4})}$.

In the limit of an abrupt transition, when $b \to 0$, η becomes imaginary and $\cosh 2\pi\eta \to -1$; we then recover the original result for a sharp boundary, $S \to 1/K$, as we ought to. At the opposite extreme, if πKb is large, we have approximately

$$S = \pi b(1+\pi/16Kb+\ldots) \quad . \quad . \quad . \quad . \quad . \quad . \quad . \quad (49)$$

and

$$Y = 2b[\log Kb+\gamma+O(1/K^2b^2)] \quad . \quad . \quad . \quad . \quad . \quad (50)$$

(compare (39) and (40)).

4.4.3. *Conclusions about Profile*

These calculations with specific shapes of profile confirm what was expected, namely: (i) S is not sensitive to the value of K and of the wavelength inside the nucleus, if that is short enough; (ii) S depends strongly on the value of b, i.e. on the nature of $V(r)$ in the outer part of the boundary region; (iii) S is not sensitive to the variation of $V(r)$ in the inner part of the boundary region. Further, we have to a good approximation

$$S=\pi b, \quad . \quad . \quad . \quad . \quad . \quad . \quad . \quad . \quad . \quad (51)$$

if the tail is exponential. The formulae (40) and (50) for Y may be interpreted by saying that the mean effective point of reflection is approximately the point at which $V(r)$ would have the value

$$\frac{\exp(-2\gamma)\hbar^2}{2Mb^2}$$

if the asymptotic formula (22) were exact, and is not sensitive to the value W of the potential in the interior.

The value (21) of S deduced from neutron experiments implies

$$b=(5{\cdot}4\pm0{\cdot}7)\times10^{-14}\text{ cm}. \quad . \quad . \quad . \quad . \quad . \quad . \quad (52)$$

Comparing this result with the theoretical values in § 3.2, it is evident that the data are inconsistent with the assumption of two-body forces following the Yukawa law if the constants are to agree with the low energy neutron–proton scattering. The result is consistent with the assumption that the nuclear attraction is of a 'short-tailed' type, such as the Gaussian, and that V falls off at the same rate as would be expected from the theoretical falling-off of the density of nuclear matter at the edge of the nucleus.

4.5. *Numerical Value of the Radius*

It is necessary now to distinguish between the various definitions of radius which have occurred in the preceding discussions. (i) The neutron scattering experiments yield a central value, X, of $a-r_0A^{1/3}$, so that for any one nucleus

$$a=r_0A^{1/3}+X+S\tan\theta,$$

where the term $S\tan\theta$ is equally likely to be positive or negative. The data do not suffice to determine r_0 as well as S, because the effect of any reasonable changes in the choice of r_0 on the goodness of fit is completely masked by the larger statistical fluctuations $S\tan\theta$. The following values (expressed in units of 10^{-14} cm) were found :—

Value of r_0 assumed	S	X
12	16·9	+7
14	16·4	−2

(ii) In the theoretical considerations of §4.4, a profile of $V(r)$ was adopted, drawn on a fixed scale for all nuclei, but shifted outwards in passing from lighter to heavier nuclei. It was tacitly assumed that some arbitrarily chosen reference point on the profile is situated at a distance from the centre of the nucleus

$$r=r_0A^{1/3}+C. \quad . \quad . \quad . \quad . \quad . \quad . \quad . \quad . \quad (53)$$

If this reference point is chosen to be the point at which the asymptotic expression $$-V(r)\propto \exp(-r/b),$$ if extrapolated backwards into the nucleus, would reach the value $W(=42$ Mev) of the effective potential in the interior, then with C defined in this way the X found from the experiments can be identified with the $C+Y$ of the theory. (The extrapolated potential need not, of course, and probably will not, resemble the actual V.)

Inserting numerical values, the theoretical calculation gives

$$X=C+4{\cdot}9 \quad . \quad . \quad . \quad . \quad . \quad . \quad . \quad . \quad (54)$$

for the first profile, and not very different values for other forms. Thus the reference point is given by

$$12A^{1/3}+2, \quad . \quad . \quad . \quad . \quad . \quad . \quad . \quad (55\,a)$$

or

$$14A^{1/3}-7, \quad . \quad . \quad . \quad . \quad . \quad . \quad . \quad (55\,b)$$

equally well. If we wish to have $C=0$, we can take

$$r_0=12{\cdot}4\times10^{-14}. \quad . \quad . \quad . \quad . \quad . \quad . \quad . \quad (56)$$

The definition of R just given, namely as the distance at which the potential, if extrapolated exponentially, would reach $-W$, makes it depend on the choice of W (here taken as 42 Mev). This dependence is practically compensated by the dependence (40), (50) of Y on the choice of W, so that the distance at which the potential reaches, say, 1 Mev is not sensitive to changes in the value assumed for this rather more hypothetical quantity.

What the results really depend on is only the last few per cent of the decrease of $|V|$ from the full well-depth to zero.

§5. Reactions Involving Protons

5.1. *The Central Field*

The effective central field $V(r)$ which has been the subject of the preceding discussion is that which determines the motion of neutrons in and near the nucleus, in a zero-order approximation. There is now strong evidence for the hypothesis that the nuclear forces are charge-independent.

Accepting charge-independence, if the effective central field $V(r)$ has any validity at all, then it must be the same for protons as for neutrons except for the addition of an electrostatic term.

In the peripheral region which is of interest in discussing the potential barrier in proton reactions, the electrostatic field is practically the same

as if it were due to a charge Ze at the centre. The part of $V(r)$ which is due to nuclear forces can probably be represented quite well by its asymptotic form (22), so that the form of the barrier is

$$V(r)=Ze^2/r-W\exp[-(r-R)/b]. \quad . \quad . \quad . \quad . \quad . \quad (57)$$

The effect on the penetrability of a potential barrier that is produced by the rounding off of its inner edge by the nuclear-forces term is difficult to treat analytically, and it is impossible to give simple formulae which are both general and accurate. Even with a sharp inner boundary the proper wave-theory calculation is troublesome, and physicists have had to wait till 1950 for exact tables (Bloch, Hull, Broyles, Bouricius, Freeman and Breit 1951).

As it is desirable to have some preliminary orientation about the implications of the present theory, we shall treat two limiting cases in a rough approximation : the case of high barriers and short wavelength, by the phase-integral method, and the case of protons which are only slightly impeded by the barrier.

Only the case of s-wave protons ($l=0$) will be considered here.

5.2. *Energy Well Below the Top of the Barrier*

The question which will be examined in this section is as follows. If the potential barrier is high, and the *WKB* phase-integral method is applicable, at what radius ought the integration to be stopped if the customary pure $1/r$ potential is used, in order to give the same result as a calculation with the rounded-off potential (57) ?

As the integral on which the penetrability depends,

$$\int\sqrt{\{Ze^2/r-E-C^2\exp[-(r-\rho)/b]\}}\,dr, \quad . \quad . \quad . \quad (58)$$

is intractable, we shall replace the hyperbola $Ze^2/r-E$ by an exponential curve touching it at $r=\rho$; ρ is chosen to be the value of r at which the integrand vanishes, i.e. the inner edge of the barrier, and C adjusted accordingly. The integrand is only changed appreciably in places (far from ρ) where the nuclear forces term is negligible. So the *correction* to the integral caused by the presence of the nuclear-forces term is calculated rather accurately.

Thus the integral becomes

$$\int\sqrt{\{C^2\exp[-\beta(r-\rho)/b]-C^2\exp[-(r-\rho)/b]\}}\,dr, \quad . \quad . \quad (59)$$

where
$$C^2=(Ze^2/\rho)-E, \quad . \quad . \quad . \quad . \quad . \quad . \quad . \quad . \quad . \quad (60)$$

and
$$\beta=\frac{Ze^2b}{\rho^2C^2}=\frac{b/\rho}{1-(E\rho/Ze^2)}, \quad . \quad . \quad . \quad . \quad . \quad . \quad (61)$$

which will normally be a fraction such as $\frac{1}{5}$ to $\frac{1}{8}$. Putting $\beta=2\gamma/(1+2\gamma)$, and introducing a variable t by

$$r-\rho=-b(1+2\gamma)\log t, \quad . \quad . \quad . \quad . \quad . \quad . \quad (62)$$

the integral (59) becomes

$$Cb(1+2\gamma)\int_0^1 t^{\gamma-1}(1-t)^{1/2}\,dt=Cb(1+2\gamma)\frac{\Gamma(\gamma)\Gamma(\frac{3}{2})}{\Gamma(\gamma+\frac{3}{2})}. \quad . \quad . \quad . \quad (63)$$

If the nuclear-forces term had been omitted from the beginning of the calculation, the result would be that the factor $(1-t)^{1/2}$ in (63) would drop out. If we wish to obtain the same value by stopping the integration at a suitable value r_1 of r (an ' equivalent radius of the nuclear surface '), it is required to find t_1 so that

$$\int_0^{t_1} t^{\gamma-1}\,dt=\int_0^1 t^{\gamma-1}(1-t)^{1/2}\,dt,$$

which gives the relation

$$t_1{}^{\gamma}=\frac{\Gamma(1+\gamma)\Gamma(\frac{3}{2})}{\Gamma(\frac{3}{2}+\gamma)}. \quad . \quad . \quad . \quad . \quad . \quad . \quad . \quad (64)$$

After a little calculation we find, using (62)

$$r_1=\rho+2b\{1-\log 2+\gamma(1-2\log 2+\tfrac{1}{12}\pi^2)+O(\gamma^2)\}=\rho+0{\cdot}62b \quad . \quad (65)$$

approximately. Using b from (52), and calculating ρ defined in this section from (57) and (56), (65) gives the equivalent radius to be used in the usual penetrability formulae.

5.3. *The Top of the Coulomb Barrier*

The present analysis indicates that the top of the Coulomb barrier is lower and further out from the nucleus than it is usually assumed to be. In considering the escape of energetic protons it is of interest to know how high the barrier is. A few approximate formulae will be presented here to save the labour of finding the maximum of (57) graphically or by trial and error.

For this purpose we define yet another nominal radius R_1, the radius at which the nuclear-forces term assumes a specified value W_1 which is chosen to be 0·3 MeV. Thus the potential for s-protons is

$$V(r)=\frac{Ze^2}{r}-W_1\exp{(R_1-r)/b}. \quad . \quad . \quad . \quad . \quad . \quad (66)$$

The exact condition for a maximum is

$$r/R_1=1+(b/R_1)\log{(W_1R_1{}^2/Ze^2b)}+(2b/R_1)\log{(r/R_1)}, \quad . \quad (67)$$

which is arranged so as to permit rapid solution by successive approximation. To a close approximation the height of the barrier is

$$Ze^2\left\{\frac{1}{R_1+bL}-\frac{b}{R_1{}^2}\right\}, \quad . \quad . \quad . \quad . \quad . \quad . \quad (68)$$

and the position of the maximum is

$$r=R_1+bL/[1-(2b/R_1)], \quad . \quad . \quad . \quad . \quad . \quad . \quad (69)$$

where L denotes the natural logarithm in the middle term of (67). The formulae (68) and (69) have been so devised as to approximate to the

maximum of (66) to a higher order than might appear from their form, and we believe the error is always less than that arising from the uncertainty in the values of the constants b and R.

The most important result of including the nuclear-force term in the potential (66) is to lower the height of the barrier by a substantial amount, usually about 40%. This can be seen by making a much cruder approximation : using 10^{-14} cm and 1 MeV as units, (68) gives roughly

$$\frac{Ze^2}{12{\cdot}4A^{1/3}+Cb}=Z\frac{1{\cdot}2}{A^{1/3}+3}, \quad . \quad . \quad . \quad . \quad . \quad . \quad . \quad (70)$$

as compared with the customary rough approximation

$$Z/A^{1/3} \quad . \quad . \quad . \quad . \quad . \quad . \quad . \quad . \quad . \quad . \quad (71)$$

(Devons 1949, p.15). The reduction in the nuclear radii adopted, which is responsible for the factor 1·2, is much more than offset by the effect of the constant b, which is associated with the nuclear-forces potential. This decrease in the calculated height of the barrier, drastic though it may seem, is perhaps really a conservative estimate : for it is difficult to see how b could be any smaller than 6×10^{-14} cm, and if the Yukawa force deduced from the two-body experiments could be accepted it would have to be much greater (§ 3.2).

5.4. *Energy Near the Top of the Barrier*

In this section an approximate expression will be given for the penetrability, in the case in which the energy E of the proton is nearly equal to the height of the barrier.

The barrier specified by (57) or (66) has a smoothly rounded top. Let the maximum be $V_m=V(R_m)$, situated at $r=R_m$, and expand in a Taylor series as far as the fourth order in $(r-R_m)$:

$$V(r)=V_m+0-c_2(r-R_m)^2+c_3(r-R_m)^3+ \quad . \quad . \quad . \quad (72)$$

At any particular energy V less than V_m, the barrier extends from $r_1(V)$ to $r_2(V)$, say, which is a distance given by

$$r_2-r_1=2\left[\frac{V_m-V}{c_2}\right]^{1/2}+\text{terms in } (V_m-V)^{3/2} \text{ etc.} \quad . \quad . \quad (73)$$

The integral (58) needed in a phase-integral calculation may be equally well written with V as independent variable :

$$\int_{r_1(E)}^{r_2(E)}\sqrt{[V(r)-E]}\,dr=\int_E^{V_m}\frac{r_2(V)-r_1(V)}{2\sqrt{(V-E)}}\,dV \quad . \quad . \quad . \quad . \quad . \quad . \quad (74)$$

$$=c_2^{-1/2}\int_E^{V_m}(V_m-V)^{1/2}(V-E)^{-1/2}\,dV+\text{etc.}$$

$$=\frac{\pi}{2}\frac{V_m-E}{\sqrt{c_2}}+O[(V_m-E)^2]. \quad . \quad . \quad . \quad . \quad . \quad (75)$$

Dividing by the appropriate factor (5), the absolute value of the phase-integral is approximately

$$G=\frac{\pi\sqrt{(2M)}}{2\hbar\sqrt{c_2}}(V_m-E) \quad . \quad . \quad . \quad . \quad . \quad . \quad (76)$$

if E is not too far below V_m. When the WKB approximation is applicable, the penetration factor is

$$\exp(-2G). \quad . \quad . \quad . \quad . \quad . \quad . \quad . \quad . \quad (77)$$

This is only valid if G is not too small. If the energy E is nearly equal to V_m, the WKB method fails, but since the important part of the potential curve is parabolic the theory of the parabolic cylinder functions may be used, which is known to give the result

$$\frac{1}{1+\exp(2G)} \quad . \quad . \quad . \quad . \quad . \quad . \quad . \quad . \quad (78)$$

for the transmission coefficient. This agrees well enough with (77) whenever the latter is applicable, and can be regarded as including it as a limiting case.

In applying (78) and (76), we need the value of the coefficient c_2 in (72), which depends on the curvature of the potential curve (66) at its summit. Its value is approximately

$$c_2=-\tfrac{1}{2}V''(R_m)\doteq\frac{Ze^2}{2b[R_1+b(L+1)]^2}. \quad . \quad . \quad . \quad . \quad (79)$$

It should be borne in mind that these formulae, (78) and (76), are likely to be quite inaccurate when E is several MeV less than the barrier height V_m; but in this region the approximation of § 5.2 is available.

5.5. *Photo-Disintegration*

The greatest changes in theoretical predictions, resulting from the revision of our ideas on potential barriers, are for protons with energies near the top of the barrier. With the heavier nuclei, the barrier deduced in the conventional way from the assumption of a sharp nuclear boundary would be much higher and would greatly impede the emission of such protons. The theoretical expectations for (γ, p) reactions are therefore substantially changed.

An approximate theory of (γ, p) and (γ, n) reactions, based on the assumption of compound-nucleus formation and on the idea of the temperature of the residual nucleus, was given by Weisskopf and Ewing (1940). Ever since the publication of Hirzel and Wäffler's results, there has been much discussion of the apparent disagreement between theory and experiment. Hirzel and Wäffler (1947) found that the (γ, p) cross section for the ten nuclei they studied was less than the (γ, n) cross section by a factor of usually about 30, whereas the theoretical factor was in most cases of the order of 10^4. Several explanations have been proposed: some authors have sought to retain the thermodynamic theory of Weisskopf and Ewing with a drastic revision of the parameters involved, and others have

suggested that most of the protons are directly ejected without compound-nucleus formation, and do not have the energy distribution implied by the evaporation theory. While this question can undoubtedly be settled by observing the energy distribution or the angular distribution of the protons, the experimental results at present available seem to be conflicting. Preliminary calculations with the potential (57), using the approximate method of § 5.4, indicate that the direct ejection mechanism need not be invoked at all to explain Hirzel and Wäffler's results, and at any rate plays a much smaller part than has been supposed.

§ 6. Conclusions

The observed values of the scattering-lengths of the various nuclei for slow neutrons are found to imply that the nuclear forces exerted on a neutron, when it is just outside the nominal surface of the nucleus, decrease according to a certain exponential. The Yukawa force deduced from two-nucleon experiments at low energies, however, would require a more gradual decrease of the force (a less steep-sided potential well), and there would be many more cases of negative scattering length than are actually observed.

The ' radius ' is a somewhat ill-defined concept, but the density of matter inside a heavy nucleus can be described by an equivalent sharp radius, and the present results are in harmony with the rather low values which have been found with fast electrons and with mesonic x-rays.

The approximate shape and height of the Gamow barrier affecting the emission of protons has been calculated, and the height is found to be much lower than is usually supposed. In many cases, however, the penetrability of the barrier is the same as it would be for a sharp nuclear boundary with a rather large value of the radius.

APPENDIX I

This appendix is concerned with a Fermi distribution at zero temperature, with all states occupied up to a certain maximum momentum p_0, and its purpose is to estimate the greatest value of a specified component of momentum, and by how much it will fall short of p_0.

Consider a large box, containing a very large number N of neutrons, moving in a potential $-W$ inside and O outside. Consider a part of the surface, which may be taken to be the xy-plane ($z=0$). The momenta of the neutrons below it (p_x, p_y, $|p_z|$) occupy a hemisphere in momentum space. There are $\frac{1}{2}N$ pairs of neutrons in $\frac{2}{3}\pi {p_0}^3$ of momentum space.

We wish to know the largest value of p_z in a second approximation. The mean number of pairs with z-component of momentum lying within certain limits is

$$\frac{3N}{4{p_0}^3}({p_0}^2 - |p_z|^2) \,.\, d|p_z|.$$

After a short calculation we find that the probability that the numerically highest z-component of momentum $|p_z|$ is $p_0(1-\epsilon)$ is equal to

$$\tfrac{3}{2}N\epsilon \exp(-\tfrac{3}{4}N\epsilon^2)\, d\epsilon,$$

and the highest individual value of $|p_z|$ is therefore on the average

$$p_0[1-\sqrt{(\pi/3N)}].$$

The highest individual *resultant* momentum p differs from p_0 by $p_0 O(1/N)$, which may be neglected in comparison with $p_0/\sqrt{N}$.

The constant κ which determines the rate of decay of the corresponding wave function outside the box, viz.

$$\psi \propto \exp(-\kappa z + i(p_x x + p_y y)/\hbar),$$

is given by

$$\frac{\hbar^2\kappa^2}{2M} = W - \frac{{p_0}^2}{2M} + \left(\frac{4\pi}{3N}\right)^{1/2} \frac{{p_0}^2}{2M}.$$

The first two terms represent the binding energy. The third term is the required correction, which is of the order of 10 MeV for $A=100$.

APPENDIX II

The following table gives the values of $a-1.2A^{1/3}$ arranged in order of magnitude, where a is the scattering length in units of 10^{-14} cm.

^{58}Ni	+97	Pb	+25	Mo	+12	^{54}Fe	−4	W	−21
^{14}N	65	Pt	25	Zn	10	Sb	−5	^{57}Fe	−24
Hg	62	^{146}Nd	24	Zr	9	K	−6	^{44}Ca	−24
^{45}Sc	59	^{19}F	23	^{40}Ca	8	S	−7	^{144}Nd	−35
Cl	59	^{139}La	21	^{197}Au	7	^{127}I	−8	^{51}V	−49
^{56}Fe	+55	Mg	+19	Pd	+6	Ba	−9	Ti	−77
Nd*	51	Tl	18	Sr	4	Cr	−10	^{55}Mn	−83
Se	38	^{154}Sm	16	^{103}Rh	4	^{133}Cs	−12	^{152}Sm	−109
^{12}C	38	Br	16	Si	3	A	−14	^{62}Ni	−134
Ge	34	^{209}Bi	15	Rb	2	^{109}Ag	−14		
^{13}C	+32	^{93}Nb	+15	^{181}Ta	+2	^{140}Ce	−16		
^{16}O	28	^{142}Nd	15	Sn	+2	^{60}Ni	−18		
Cu	27	Er	13	^{23}Na	+1	^{142}Ce	−18		
^{232}Th	26	^{75}As	12	^{27}Al	−1	^{59}Co	−19		
^{107}Ag	26	^{31}P	12	Te	−2	^{141}Pr	−19		

The entry for Nd which is marked with an asterisk refers to the mixture of Nd (143, 145, 148, 150) which is responsible for that part of the scattering length of natural neodymium which remains when the known contributions of Nd (142, 144, 146) have been allowed for.

APPENDIX III

The function $\psi(1+iy)$ has apparently not been tabulated in the range we require (which is just beyond the range of Hartree and Johnston's (1948) table). We have calculated the following values, which cover the range that is needed in §4.5.

y	Re $\psi(1+iy)$	y	Re $\psi(1+iy)$	y	Re $\psi(1+iy)$
0·0	−0·5772	0·5	−0·3289	1·0	+0·0947
0·1	−0·5653	0·6	−0·2442	1·1	+0·1722
0·2	−0·5307	0·7	−0·1573	1·2	+0·2459
0·3	−0·4768	0·8	−0·0709	1·3	+0·3158
0·4	−0·4079	0·9	+0·0135	1·4	+0·3820

References

Bitter, F., and Feshbach, H., 1953, *Phys. Rev.*, **92**, 837.

Blatt, J. M., and Weisskopf, V. F., 1952, *Theoretical Nuclear Physics* (New York : Wiley).

Bloch, I., Hull, M. M., Broyles, A. A., Bouricius, W. G., Freeman, B. E., and Breit, G., 1951, *Rev. Mod. Phys.*, **23**, 147.

Cassels, J. M., 1950, *Rep. Prog. Nuc. Phys.*, **1**, 185.

Condon, E. U., and Shortley, G. H., 1935, *The Theory of Atomic Spectra* (Cambridge : University Press).

Devons, S., 1949, *Excited States of Nuclei* (Cambridge : University Press).

Fermi, E., and Marshall, L., 1947, *Phys. Rev.*, **71**, 666.

Feshbach, H., Peaslee, D. C., and Weisskopf, V. F., 1947, *Phys. Rev.*, **71**, 145.

Feshbach, H., Porter, C. E., and Weisskopf, V. F., 1953, *Phys. Rev.*, **90**, 166.

Fisher, Sir Ronald A., 1921, *Phil. Trans. Roy. Soc.* A, **222**, 309.

Fitch, V. L., and Rainwater, J., 1953, *Phys. Rev.*, **92**, 789.

Ford, K. W., and Bohm, D., 1950, *Phys. Rev.*, **79**, 745.

Hartree, D. R., and Johnston, S., 1948, *Quart. J. Mech. Appl. Math.*, **1**, 29.

Hirzel, O., and Wäffler, H., 1947, *Helv. Phys. Acta*, **20**, 373, 403.

Hughes, D. J., 1952, *Pile Neutron Research* ; 1953 (Editor), *Neutron Cross Sections* (AECU.2040 issued 1952 and two supplements) (U.S. : Dept. of Commerce).

Inglis, D. R., 1953, *Rev. Mod. Phys.*, **25**, 390.

Kapur, P. L., and Peierls, R. E., 1938, *Proc. Roy. Soc.* A, **166**, 277.

Koehler, W. C., and Wollan, E. O., 1953, *Phys. Rev.*, **91**, 597.

Koopman, B. O., 1936, *Trans. Amer. Math. Soc.*, **39**, 399.

Lane, A. M., 1953, *Proc. Phys. Soc.* A, **66**, 982, 983.

Lane, A. M., and Thomas, R. G., 1954, *Rev. Mod. Phys.* (in the press).

Salpeter, E. E., 1951, *Phys. Rev.*, **82**, 60.

Shull, C. G., and Wollan, E. O., 1951, *Phys. Rev.*, **81**, 527.

Weisskopf, V. F., and Ewing, D. H., 1940, *Phys. Rev.*, **57**, 472.

Whittaker, Sir Edmund, and Watson, G. N., 1952, *Modern Analysis*, p. 289.

Wigner, E. P., and Feenberg, E., 1941, *Rep. Prog. Phys.*, **8**, 302 (London : Physical Society).

Wigner, E. P., and Eisenbud, L., 1947, *Phys. Rev.*, **72**, 29.

Wilson, R. R., 1952, *Phys. Rev.*, **88**, 350.

LV. *A Property of 'Repeating' Secular Determinants*

By H. O. Pritchard and F. H. Sumner
Department of Chemistry, University of Manchester*

[Received January 7, 1954]

Summary

A special type of secular determinant is encountered in the molecular orbital treatment of second-order hyperconjugation in normal paraffin molecules. For such a determinant, the sum of the positive roots is a linear function of the number of rows in the determinant, to an accuracy which is usually better than one part in 10^5.

In the molecular orbital theory of second-order hyperconjugation, it is usual to treat the ethane molecule in the form $H_3{\equiv}C{-}C{\equiv}H_3$ (see e.g. Crawford 1949). The valency electrons in the CH_3 group are treated in like manner to those in the $C{\equiv}N$ group ; thus the three hydrogen atoms in the methyl group may be imagined to compose a pseudo atom whose orbitals are made up by grouping the three H-atom 1s orbitals. The theoretical treatment of π-hyperconjugation in ethane then becomes analogous to the treatment of π-conjugation in cyanogen.

One method of extending this kind of treatment to higher paraffins is to assume that the CH_2 groups may be treated similarly ; thus, the normal paraffin molecule $n\text{–}C_kH_{2k+2}$ may be described by the structure

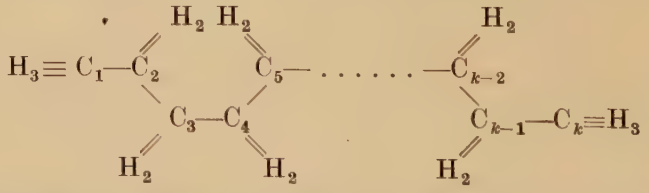

with conjugation between the pseudo atoms H_2 and H_3 through the carbon chain. The secular determinant representing this molecule may be simplified by putting both the Coulomb terms (α's) and the resonance integrals (**H**'s) in terms of the resonance integral (β) for a C—C bond length of 1·54 Å, viz. :

$$\mathbf{H}_{C-C}=\beta\ ;\ \mathbf{H}_{C=H_s}=s\beta\ ;\ \mathbf{H}_{C\equiv H_s}=t\beta\ ;$$
$$\alpha_C=0\ ;\qquad \alpha_{H_s}=r\beta\ ;\qquad \alpha_{H_s}=u\beta.$$

---

* Communicated by the Authors.

The secular determinant then becomes

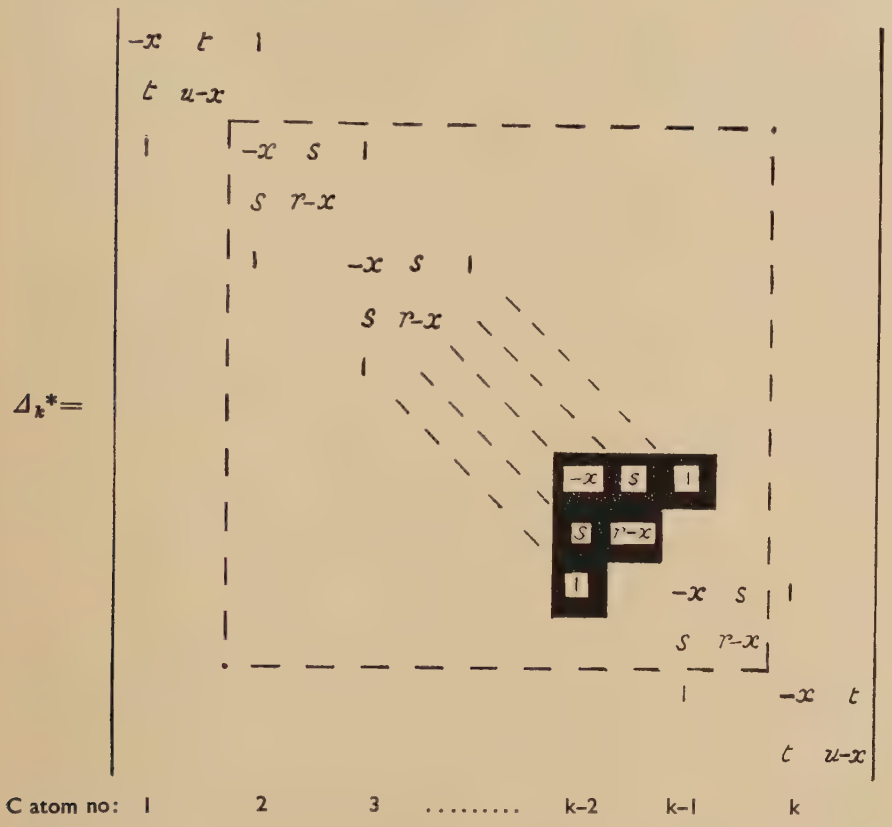

The first two rows and columns and the last two correspond to the CH_3 groups and the rest of the determinant Δ_{k-2} (enclosed in the – – – – box) represents the CH_2 groups ; increasing the chain length of the molecule merely adds another element such as the one shaded to this central portion of Δ_k^*.

Values of r, s, t and u were assigned, allowing for overlap (see Coulson and Crawford 1953) as follows: $r=-0{\cdot}43$, $s=3{\cdot}98$, $t=3{\cdot}35$, $u=-0{\cdot}65$, and the determinant Δ_k^* was solved for the series of molecules from ethane to n-hexane using the Manchester University Electronic Computer ; the techniques involved will be described by us in due course. It was found that from propane upwards, the sum of the positive roots for n–C_kH_{2k+2} was proportional to k with an accuracy of about 1 in 10^6 ; for ethane, the sum of the roots deviated from this regularity by about 1 part in 10^4. A relationship of this sort was not foreseen, but the conditions under which it holds may be established by the following analysis.

If we put $\quad P=x^2-rx-s^2, \quad Q=r-x,$

$\quad R=x^2-ux-t^2, \quad S=u-x,$

the general determinant Δ_k^* may be represented by the difference formula

$$\Delta_k^* = R^2\Delta_{k-2} - 2RSQ\Delta_{k-3} + S^2Q^2\Delta_{k-4} \quad . \quad . \quad . \quad . \quad (1)$$

where the determinants Δ_{k-2}, etc. are functions of r, s and x only; furthermore, these simpler determinants are related to each other by the formula

$$\Delta_k = P\Delta_{k-1} - Q^2\Delta_{k-2}. \quad . \quad . \quad . \quad . \quad . \quad . \quad . \quad (2)$$

This being so, it should be possible to represent Δ_k, etc. by λ^k, etc. in eqn. (2), which leads to the quadratic relationship

$$\lambda^2 - P\lambda + Q^2 = 0. \quad . \quad . \quad . \quad . \quad . \quad . \quad . \quad (3)$$

There are two roots, λ_1 and λ_2, so that

$$\Delta_k = A\lambda_1^k + B\lambda_2^k \quad . \quad . \quad . \quad . \quad . \quad . \quad . \quad (4)$$

where A and B are defined by the conditions that $\Delta_0 = 1$ and $\Delta_1 = P$. The values of λ_1, λ_2, A and B that satisfy these relationships are

$$\lambda_1 = \tfrac{1}{2}(P + \sqrt{(P^2 - 4Q^2)}), \quad . \quad . \quad . \quad . \quad . \quad . \quad (4\,a)$$

$$\lambda_2 = \tfrac{1}{2}(P - \sqrt{(P^2 - 4Q^2)}), \quad . \quad . \quad . \quad . \quad . \quad . \quad (4\,b)$$

$$A = \lambda_1(P^2 - 4Q^2)^{-1/2}, \quad . \quad . \quad . \quad . \quad . \quad . \quad . \quad (4\,c)$$

$$B = -\lambda_2(P^2 - 4Q^2)^{-1/2}. \quad . \quad . \quad . \quad . \quad . \quad . \quad . \quad (4\,d)$$

Therefore, eqn. (1) becomes

$$\Delta_k^* = R^2(A\lambda_1^{k-2} + B\lambda_2^{k-2}) - 2RSQ(A\lambda_1^{k-3} + B\lambda_2^{k-3}) + S^2Q^2(A\lambda_1^{k-4} + B\lambda_2^{k-4})$$

$$= \frac{\lambda_1^{k-3}(R\lambda_1 - SQ)^2 - \lambda_2^{k-3}(R\lambda_2 - SQ)^2}{\sqrt{(P^2 - 4Q^2)}}. \quad . \quad . \quad . \quad . \quad . \quad . \quad . \quad . \quad (5)$$

The roots $x_1, x_2, \ldots x_j, \ldots x_{2k}$ of this determinant are the orbital energy levels; the first k roots are positive, and their sum may be expressed (see Coulson and Longuet-Higgins 1947) in contour integral form as

$$\sum_{j=1}^{j=k} x_j = \epsilon_k = \tfrac{1}{2}\Sigma\alpha + \frac{1}{2\pi}\int_{-i\infty}^{i\infty}\left(x\frac{d}{dx}\log\Delta_k^* - k\right)dx. \quad . \quad . \quad . \quad (6)$$

This equation can only reduce to the form

$$\epsilon_k = mk + c \quad . \quad . \quad . \quad . \quad . \quad . \quad . \quad . \quad . \quad (7)$$

if $\log\Delta_k^*$ is a linear function of k, and this is so only if one of the terms in the numerator of eqn. (5) may be neglected, viz.:

$$\lambda_1^{k-3}(R\lambda_1 - SQ)^2 >>> \lambda_2^{k-3}(R\lambda_2 - SQ)^2. \quad . \quad . \quad . \quad . \quad (8)$$

Then eqn. (6) reduces to

$$\epsilon_k = \tfrac{1}{2}\{2u + (k-2)r\} + \frac{1}{2\pi}\int_{-i\infty}^{i\infty}\left\{(k-3)x\frac{d}{dx}\log\lambda_1 + 2x\frac{d}{dx}\log(R\lambda_1 - SQ) - \frac{x}{2}\cdot\frac{d}{dx}\log(P^2 - 4Q^2) - k\right\}dx.$$

The number k only occurs linearly in the integrand, and so this expression must integrate to the form of eqn. (7) if the inequality (8) is valid over the range of integration which is from $x = -i\infty$ to $x = i\infty$.

The final stages of the analysis are most readily completed by specific reference to the problem of π-hyperconjugation in n-C_kH_{2k+2} molecules. The ratios λ_1/λ_2 and $[(R\lambda_1-SQ)/(R\lambda_2-SQ)]^2$ can be calculated in terms of r, s, t, u and x from eqns. (4 *a*) and (4 *b*) by substituting the appropriate expressions for P, Q, R and S. Using the numerical values of r, s, t and u already discussed, it is possible to show graphically that the minimum value of $|\lambda_1/\lambda_2|$ is about $10^{1\cdot80}$ and the minimum value of

$$\left|\left(\frac{R\lambda_1-SQ}{R\lambda_2-SQ}\right)^2\right|$$

is about $10^{4\cdot85}$ over the whole range of $-i\infty \leqslant x \leqslant i\infty$. Thus, we would expect the order of magnitude of the deviation from eqn. (7) to be not more than ~ 1 in $10^{\{4\cdot85+1\cdot80(k-3)\}}$; in table 1 we compare this estimate with the observed deviation from the expression

$$\epsilon_k = 3\cdot8326305k - 1\cdot5113809.$$

The precision of the calculations decreases with increasing k, due to rounding off errors, but is better than 1 in 10^7 for $k=6$; the precision is estimated from the difference between

$$\sum_{j=1}^{j=2k} x_j$$

and the sum of the diagonal elements of the determinant Δ_k^*, which is the figure listed in the ' precision ' column of the table. It is seen that our analysis reproduces fairly well the variation in order of magnitude of the deviations, and shows that for $k \geqslant 5$, any deviation is too small to be detected. It does not, however, predict the change in sign of the deviation for $k=2$, although it is a rather dubious procedure to apply the analysis to this case.

Table 1

k	ϵ_k (in β units)	Precision	deviation from $\epsilon_k = mk+c$	
			observed	estimated
2	6·154 658 4	10^{-10}	1 in 10^4 †	1 in $10^{3\cdot05}$
3	9·986 493 5	3×10^{-8}	1 in 5×10^5	1 in $10^{4\cdot85}$
4	13·819 136 7	2×10^{-8}	1 in 3×10^6	1 in $10^{6\cdot65}$
5	17·651 771 6	1×10^{-6}	zero	1 in $10^{8\cdot45}$
6	21·484 402 1	3×10^{-6}	zero	1 in $10^{10\cdot25}$

† This deviation is of the opposite sign to those for $k=3$ and $k=4$.

There are obvious extensions of this treatment, for example, to n-paraffin free radicals, and to substituted conjugated polyenes, which may be represented by this same type of determinant. Furthermore,

it may be possible to extend the argument to more complicated cases, such as the methyl benzenes or the methyl ethylenes, where there is a constant increment in hyperconjugation energy for each methyl group added to the system (Coulson and Crawford 1953). The molecular model considered in this paper gives a particularly unfavourable description of π-hyperconjugation ; a much fairer description of these molecules would be achieved by putting $r=u=-0{\cdot}65$ and $s=t=3{\cdot}35$, leading to the simplification that $\Delta_k{}^*=\Delta_k$, $P=R$ and $Q=S$, in which case the linear relationship between ϵ_k and k is obeyed even more closely. This means that the reason for deviations from additive bond energies in these molecules cannot be sought in terms of the theory of π-hyperconjugation.

In conclusion, we wish to thank Dr. H. A. Skinner for calling our attention to the problem of calculating hyperconjugation energies. Our thanks are also due to the Manchester University Computing Machine Laboratory for the use of their facilities, and we are especially indebted to Mr. R. A. Brooker and Dr. A. M. Turing, F.R.S., of that laboratory, who suggested to us the method of analysis presented here. One of us (F. H. S.) wishes to acknowledge the award of a D.S.I.R. maintenance grant.

References

Coulson, C. A., and Crawford, V. A., 1953, *J. Chem. Soc.*, 2052.

Coulson, C. A., and Longuet-Higgins, H. C., 1947, *Proc. Roy. Soc.* A, **191**, 39.

Crawford, V. A., 1949, *Quarterly Reviews*, **3**, 226.

LVI. *Systematic Wind Measurements at Altitudes of* 80–100 km *Using Radio Echoes from Meteor Trails*

By J. S. Greenhow
Jodrell Bank Experimental Station*

[Received January 30, 1954]

Abstract

A method for the systematic measurement of winds at altitudes of 80–100 km is described. Wind drifts of ionized meteor trails cause small changes in range of the radio echoes, and these are measured using a coherent pulse doppler technique. The method is able to resolve mean hourly wind speeds and directions on any day. Observations during September and October 1953, have shown that both semi-diurnal and diurnal wind components exist, corresponding to clockwise rotations of the wind vectors. The amplitudes and phases of these components are variable. There is also a prevailing wind which blows towards the east in September, and towards the west in October. The presence of a positive wind gradient of approximately 2·7 m sec^{-1} km^{-1} between altitudes of 78 and 98 km has also been established.

Large irregularities in the wind have been observed, and although at times the short period variation in wind velocity is as low as 25%, at other times variations of 360° in direction, and several hundred per cent in speed are observed over intervals of a few minutes.

§ 1. Introduction

Atmospheric winds with velocities of the order of 100 m/sec, at altitudes of 80–100 km, were first measured from the movements of long duration visual meteor trails and noctilucent clouds (Olivier 1942, Störmer 1937). These phenomena are rare and systematic wind observations were not possible until the evolution of radio techniques. Two principal radio echo methods are now available for the study of upper atmosphere winds. At low frequencies (2–6 Mc/s) the time displacements of echo fading patterns obtained at spaced stations, after reflection from the ionosphere, enable uniform drift velocities to be determined (Mitra 1949, Salzberg and Greenstone 1951, Phillips 1952).

This method is somewhat handicapped owing to the absence of a regular E region at night, and also because the exact height of the measurements is uncertain. It is also possible that the movements of the fading patterns may be due to an electrodynamical effect, and not to a true motion of air molecules.

* Communicated by Professor A. C. B. Lovell.

These uncertainties do not apply to the investigation of winds by observation of the radio echoes from ionized meteor trails, at frequencies of 30–70 Mc/s (Greenhow 1950, 1952 a, b, Manning, Villard and Peterson 1950, Robertson, Liddy and Elford 1953). Changes in range of the echoes are attributed to drifts of the columns of ionization in the presence of winds. It is unlikely that these drifts are due to any effect other than a true wind motion of air molecules, since we are dealing with extremely well defined echoing sources in which the electron density may be several orders of magnitude greater than that in the surrounding ionosphere. At frequencies of the order of 30–40 Mc/s, which are commonly used for meteor observations, echoes are generally obtained only when the radius of the reflecting column is less than $\lambda/2\pi$ (1·5 metres). The electrons, which are responsible for the radio echoes, are prevented from separating from the positive ions in a direction perpendicular to the trail by strong electrostatic forces. This is the direction in which echoes are obtained. Collisions between the ionized matter and surrounding air molecules thus cause movements of the trail as a whole, and drifts in range of over a kilometre may be observed in echoes of several seconds duration.

As radio echoes are obtainable from sporadic meteors at all times of the day or night, they provide an excellent tool for a detailed investigation of winds in the upper atmosphere. This paper describes a continuous recording technique for the systematic observations of winds in the meteor region, from which a daily hour by hour survey of the wind speed and direction can be obtained. Some preliminary results for the months of September and October 1953 are also presented, in order to demonstrate the ability of the method to resolve periodic and prevailing wind components from a single days observations.

§ 2. Technique

Hitherto two principal methods have been used for the measurement of winds from observations of meteor echoes. Changes in echo range have been measured by Greenhow (1952) by direct observation of a high resolution range amplitude display. This method requires echoes with durations of several seconds in order that the change in range can be measured. Because of the low rate of such echoes, integration of continuous observations over a month or so would be required for systematic wind measurements. By using continuous wave measuring techniques smaller range changes can be observed, and hence echoes of short duration can be used for the wind measurements (Manning, Villard and Petersen 1950). The rate of wind measurement is thereby increased, but C.W. methods are unsuitable for continuous automatic recording at a high level of sensitivity because of their susceptibility to unwanted short range interfering signals. With pulsed techniques these unwanted signals may be removed by receiver suppression, together with the direct transmitted ground wave and irregular ground echoes. The presence of a ground wave

in a continuous wave transmission makes it necessary to use spaced transmitting and receiving stations. This complicates the use of beamed aerials for direction finding.

Because of the regular pulse spacing and wider receiver bandwidth, pulsed systems are able to distinguish positively between very small short duration meteor echoes and much larger unwanted interference signals. This results in a higher effective sensitivity than is possible using a comparable C.W. system. Using a continuous wave transmitter with a mean

Fig. 1

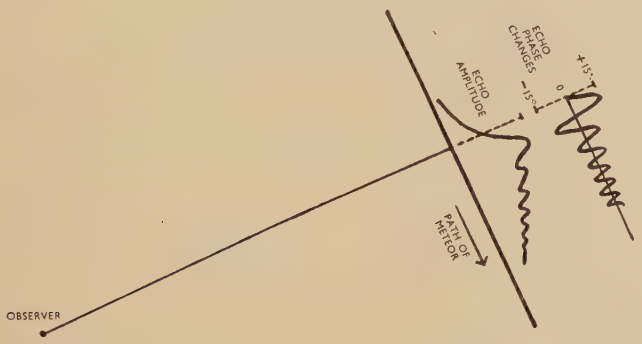

Diagram showing fluctuations in echo amplitude and phase during trail formation, exclusive of phase changes due to wind drift of the trail as a whole.

Fig. 2

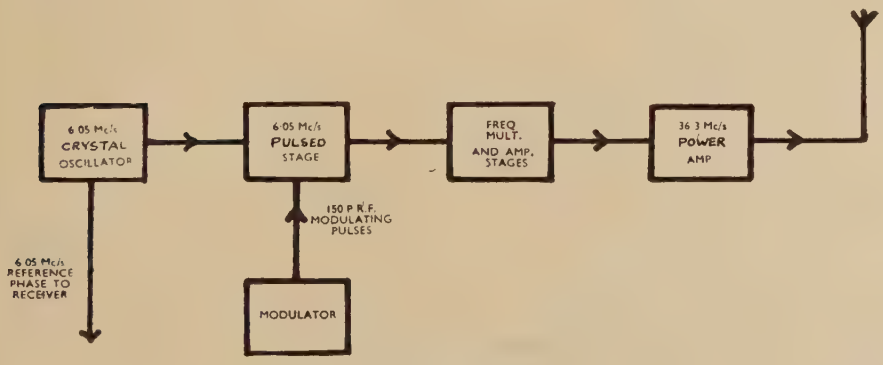

Transmitter block diagram.

power of a few hundred watts Elford and Robertson (1953) obtain about 50 usable echoes daily, and they find it necessary to integrate a month's continuous observations for a satisfactory wind determination. With a coherent pulse transmitter of similar mean power—giving the same overall sensitivity—it is possible to obtain over 3 000 usable echoes each day. A good wind determination can thus be made from one hours observatoins. This coherent pulse technique, which combines all the advantages of

simple pulsed systems with the ability of continuous wave systems to measure echo phase, is described below.

(*a*) *Transmitter*

A block diagram of the transmitter is shown in fig. 2. The fundamental frequency is generated by a 6·05 Mc/s crystal oscillator, which is pulse modulated at a very low power level, the resultant signal being amplified and frequency multiplied to a 36·3 Mc/s. The 36·3 Mc/s power output stages give a peak power of 100 kw with a pulse length of 20 μsec, at a pulse repetition frequency of 150 c/s. The signal frequency thus appears only in the form of short pulses at the transmitter output, although the oscillation is fixed in phase relative to the 6·05 Mc/s reference signal.

Fig. 3

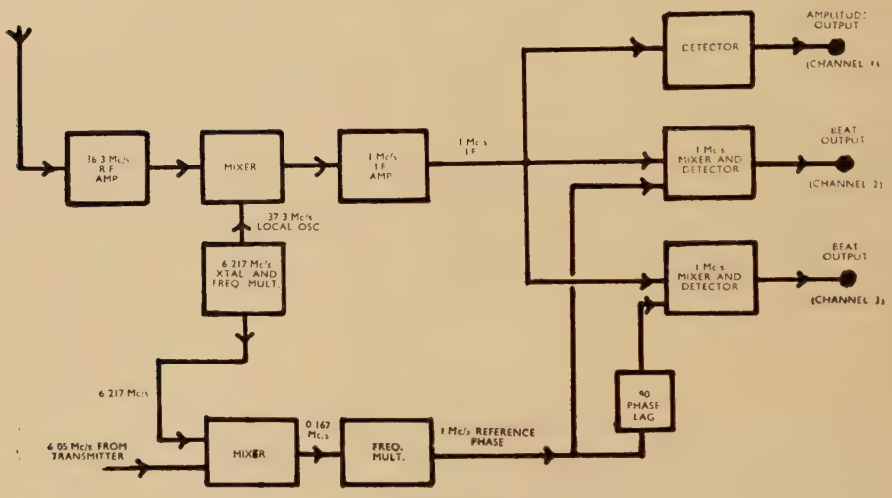

Receiver block diagram.

(*b*) *Receiver*

The receiver is a conventional superheterodyne, with 36·3 Mc/s R.F. mixer, and 1 Mc/s I.F. amplifiers. A block diagram is given in fig. 3. The 37·3 Mc/s local oscillation is derived from a 6·217 Mc/s crystal oscillator, by frequency multiplication. At the last I.F. stage the receiver output splits into three channels. One is used for simple echo amplitude and range measurements, while the other two are beat channels in which the echo signal is combined with reference signals from the transmitter for phase determinations. These reference signals are produced by mixing the 6·05 Mc/s fundamental transmitter frequency, and the 6·217 Mc/s basic local oscillation, to give a difference frequency of 0·167 Mc/s. When frequency multiplied this gives a 1 Mc/s signal of constant phase, coherent

with the 1 Mc/s I.F. in the receiver. In this way the reference signals are accurately controllable in amplitude and phase.

As discussed by Manning and his co-workers (Manning, Villard and Peterson 1952) a single beat frequency channel does not indicate whether the drift in echo range is towards or away from the observing station. This ambiguity is removed by using two beat channels in which the reference signals are 90° out of phase. Thus the beat in echo amplitude in channel 3 either leads or lags behind that in channel 2, depending upon the sense of the drift (Plate 15).

(*c*) *Aerial System*

The measurement of the range drifts give only the radial components of wind velocity. In order to determine the absolute wind speed and direction it is therefore necessary to observe a large number of echoes at various azimuths and elevations. In order to simplify the analysis—a major consideration when dealing with thousands of echoes a day—a beamed aerial is directed alternately in two directions at right angles for periods of ten minutes. In this way average perpendicular components of wind velocity are obtained, and these are combined to give the resultant wind speed and direction. The aerial is a six director Yagi half a wave-length above the ground, horizontally polarized, and the polar diagram is such that an echo has a 50% probability of lying on an azimuth within $\pm 12°$ of the aerial direction.

(*d*) *Photographic Recorder*

The photographic recorder contains four six inch cathode ray tubes, which display the outputs of the three receiver channels (Plates 15 and 16). The oscillographs are normally blacked out, the camera being operated without a shutter. The signal from the amplitude channel of the receiver is passed through circuits which discriminate against unwanted interference, and on the reception of an echo of predetermined amplitude, a time base of 0·3 sec duration is triggered. This is applied as an X-deflection to oscillographs B, C, and D, and at the same time a square wave bright-up pulse of the same duration is applied to all four tubes.

The output of receiver channel ' 1 ' is displayed on cathode ray tube ' B ' to show the simple amplitude variations in signal strength, without reference to phase. The two beat channels are displayed on tubes C and D, and show the phase variations throughout the echo. Tube A has a strobed range amplitude display, with 50 and 200 km markers. The date, time and aerial azimuth are also photographed. Various pulse bright up signals are applied to the cathode ray tubes. In particular 50 c/s pulses are displayed to assist in measuring time intervals, and in identifying corresponding pulses in the three channels.

On the conclusion of the time base sweep the tubes are again blacked out, and the camera winds on in preparation for the next echo. Each

frame occupies 4·5 mm of standard 35 mm recording film, and 6 400 frames (roughly one days observation), are obtained on a 100 ft. roll.

§ 3. Method of Analysis for Radial Wind Components

(*a*) *Large Phase Changes*

If an echo persists long enough to drift through more than $\lambda/2$, at least one complete beat cycle is produced, and the analysis is very simple. For example, in frame 1, Plate 15, one fluctuation takes place in 21 pulses at 150 P.R.F. (0·14 sec). This corresponds to a drift in range of 4·13 m at 36·3 Mc/s, giving 29·5 m/sec as the radial component of wind velocity. The beat in channel 3 leads that in channel 2, which in this case corresponds to a drift towards the observing station.

(*b*) *Small Phase Changes*

When the phase change is less than 360° during the echo lifetime (or in some cases 180°), the change in phase cannot be observed directly since the complete beat cycle is not recorded. The procedure adopted in this case is as follows. If the time variation of echo amplitude is given by $A(t)$, then the signal in channel 3 is given by $A(t)\sin\phi$ (where ϕ is some arbitrary phase angle), and the signal in channel 2 by $A(t)\cos\phi$. The variation of $\tan\phi$ throughout the echo is then obtained by division of the amplitudes of corresponding pulses in channels 3 and 2. Frame 5, Plate 15, is an example of this type of echo. The ratio of amplitudes between corresponding pulses in channels 3 and 2 changes from -8 $+4$ to $0/-3$ units, between the points X and Y (60 milli-sec). This corresponds to a phase shift of 116° towards the observer, and a radial velocity of 22 m/sec.

(*c*) *Errors in Phase Measurement*

Phase changes occur due to diffraction effects (Davies and Ellyett 1949), and in order to avoid confusion between these and the phase changes due to wind drifts, the latter are only measured after the first maximum of the diffraction pattern. This restricts the oscillations in phase to within $\pm 15°$ (fig. 1). In general the pulse repetition frequency is too low to resolve the small fluctuations due to diffraction, and it is sufficient to take the point of maximum initial echo amplitude as the first diffraction maximum (points ' F ', Plate 15).

As discussed by Greenhow (1952), most meteor trails behave as uniform cylindrical reflectors for only the first 0·2 to 1·0 sec after their formation (at 36 Mc/s). These are the echoes used in the wind analysis. The small percentage of long duration echoes generally show large fluctuations in amplitude and phase, even in the absence of a reference signal. These large fluctuations occur when multiple reflecting centres are present—such as would be caused when the linear column of ionization is distorted by irregular winds. In the presence of a reference phase the beats in

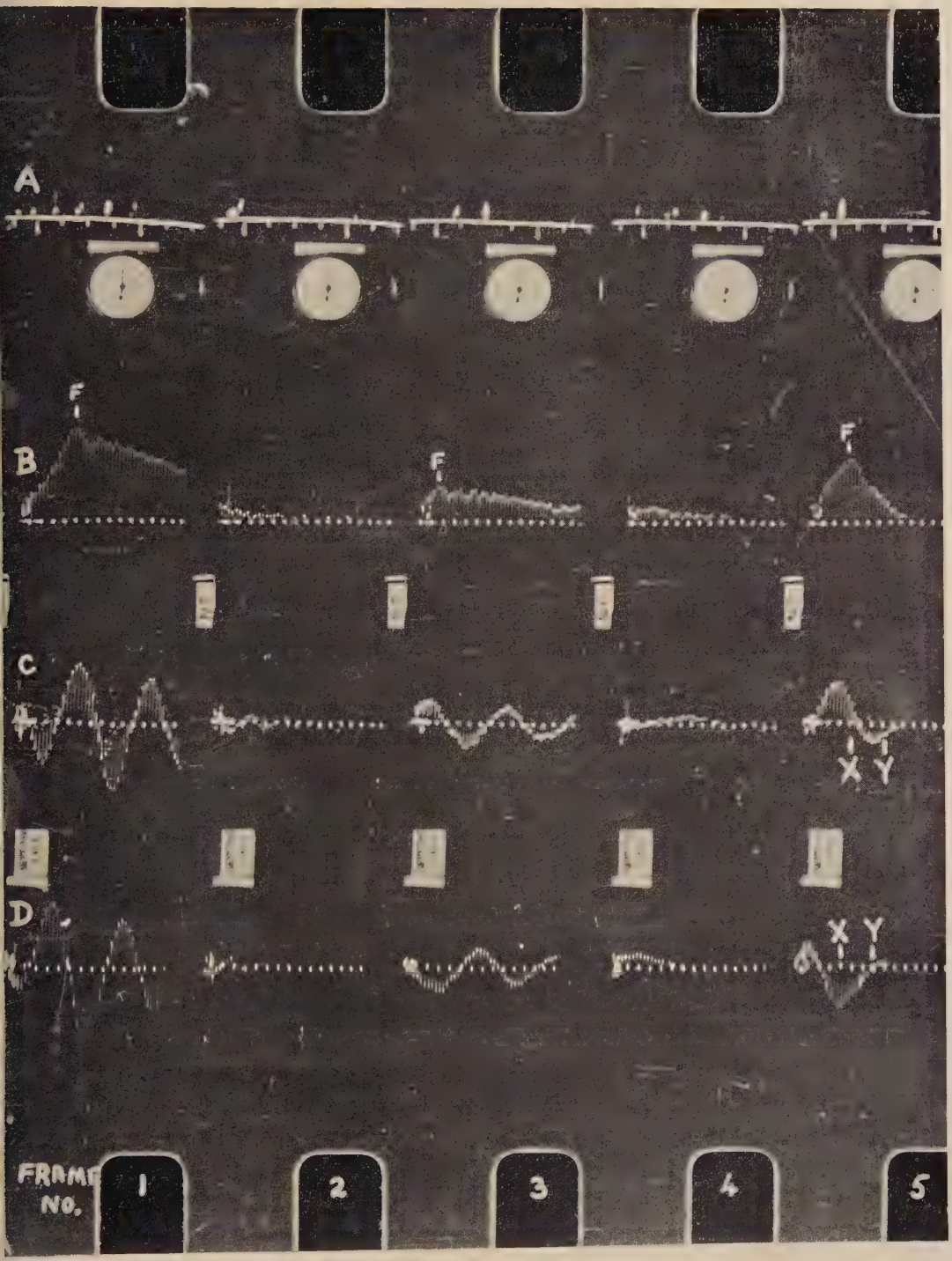

Section of a film record obtained during wind observations. A, B, C and D are four cathode ray tubes on which echo range amplitude and phase variations are recorded.

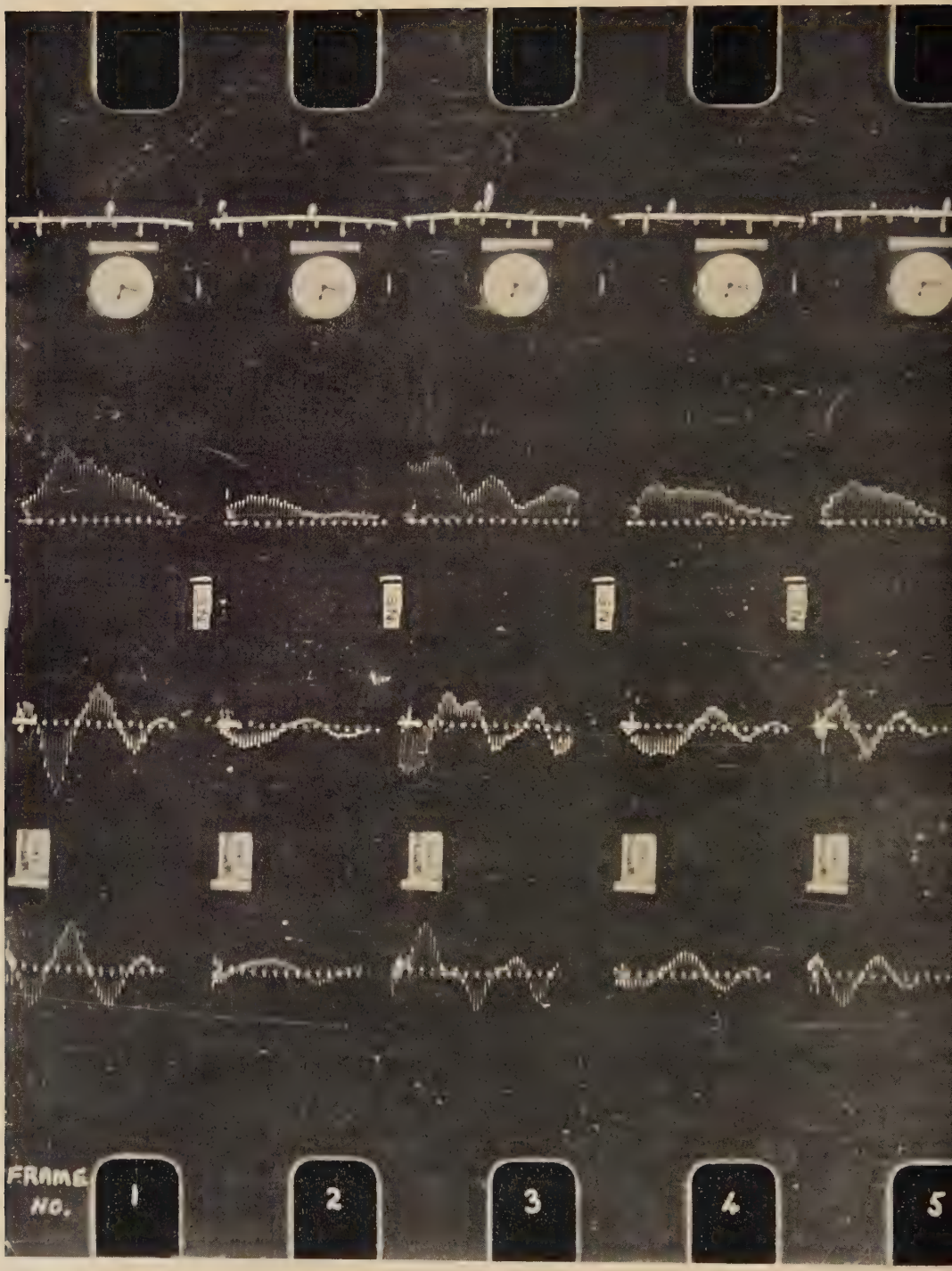

Section of a film record obtained during wind observations. Frame 3 illustrates part of a long duration echo, showing the irregular variations in amplitude and phase associated with multiple reflecting centres in a distorted trail.

amplitude become very complex, and these echoes cannot be used for wind measurements. A section of such a long duration echo is illustrated in frame 3, Plate 16.

§ 4. Results

(*a*) *Systematic Wind Measurements*

(i) *Qualitative Discussion of Results*

Continuous wind observations have been carried out on a number of days during September and October 1953. It has been possible to measure average wind speeds and directions over hourly intervals on any day, as the usable echo rate is seldom less than 50 per hour at the time of lowest activity in the evening. At other times rates of several hundred per hour are obtained. Diurnal variations in observed and usable echo rates are given in table 1. Approximately 8 500 echoes are recorded daily, of which 3 500 can be used for wind measurements.

Table 1. Diurnal Variations in Observed and Usable Echo Rates for September 16–17–18, 1953

Time	Sept. 16–17		Sept. 17–18	
	Observed	Usable	Observed	Usable
00–02	830	366	827	358
02–04	1134	517	1176	266
04–06	1406	470	1330	387
06–08	1336	456	1237	563
08–10	1170	450	1010	332
10–12	910	464	951	415
12–14	654	255	514	248
14–16	510	180	301	161
16–18	396	136	348	107
18–20	289	133	402	172
20–22	283	154	271	149
22–24	560	220	554	265
Total	8478	3801	8921	3423

As an example of the results obtained the mean wind vectors, specifying speed and direction, have been plotted in fig. 4 for a 24-hour period during September 17–18, 1953. At about midday the wind velocity is very low. The velocity then increases towards the North, swings round through East and South, falling again to a very low value near midnight. This cycle repeats itself in the succeeding 12 hours. The tip of the

Fig. 4

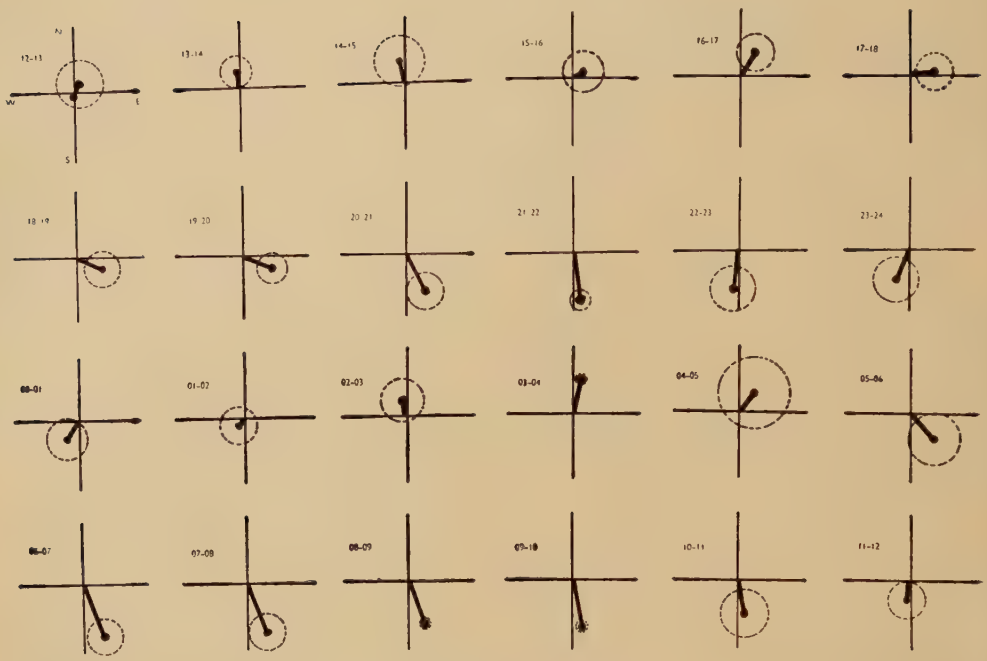

Mean hourly wind vectors. Sept. 17–18, 1953. Scale : Distance from origin to tip of axis=80 metres/sec. Winds blow towards directions indicated. Dotted circles represent the spread in observed velocities.

Fig. 5

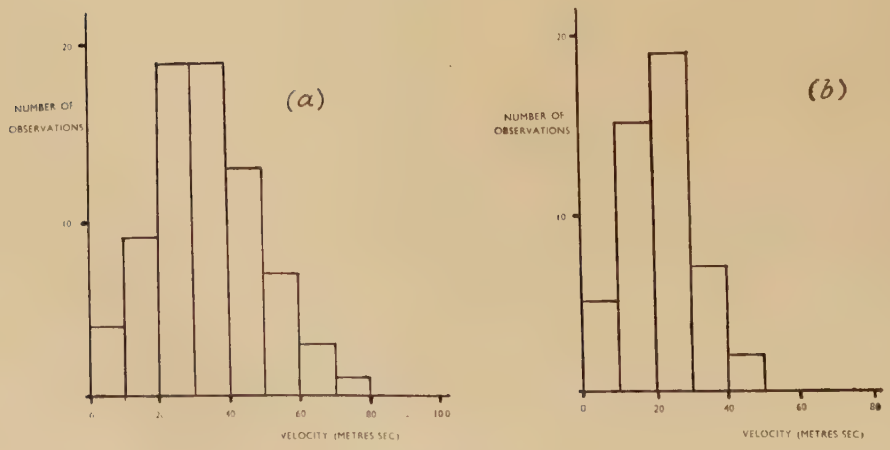

Frequency distribution of mean hourly wind velocities.
(*a*) September. (*b*) October.

velocity vector is almost always East of the North–South line, and velocity components towards the West are very small. Hence there appears to be a prevailing wind in an Easterly direction in addition to a semi-diurnal wind. This causes the tip of the wind vector to rotate about some point displaced from the origin. This behaviour is repeated very closely on all the days in September. In October the semi-diurnal oscillation is again present, but the prevailing wind reverses to a westerly direction, and a large diurnal periodic component also appears. Distributions of mean hourly wind velocities for September and October are given in fig. 5. The most probable velocity is of the order of 30 m/sec, while the highest observed value is 80 m/sec. The wind speeds measured in September are significantly higher than those observed during October. Although plots such as those in fig. 4 give a good pictorial representation of the wind speed and direction at any time, they are not of great value if quantitative measurements of the various wind components are required. For such measurements it is necessary to carry out a harmonic analysis of perpendicular wind components as described below.

(ii) *Harmonic Analysis of Wind Components*

North–South and East–West components of velocity for five days in September and October are shown figs. 6 and 7. Winds towards the North and East are taken as positive. Marked semi-diurnal oscillations are present in both directions in each period of 12 hours. The oscillations in the North–South direction lead those in the East–West direction, corresponding to a clockwise rotation of the wind vector. A diurnal oscillation is also present in October, and this component has the effect of varying the amplitudes of the semi-diurnal oscillations.

Table 2. Results of Harmonic Analysis for Prevailing Wind Components. Amplitudes are in metres/sec. Winds Blow towards Directions Indicated

Date (1953)	North–South	East–West	Resultant amplitude	Direction of resultant
Sept. 7– 8	$+2\pm2$	$+21\pm3$	21 ± 3	$080°\pm10°$
Sept. 16–17	-12 ± 2	$+12\pm2$	17 ± 2	$140°\pm10°$
Sept. 17–18	-14 ± 3	$+11\pm1$	18 ± 3	$140°\pm10°$
Oct. 16–17	$+5\pm2$	-5 ± 2	7 ± 2	$310°\pm20°$
Oct. 17–18	0 ± 2	-8 ± 2	8 ± 3	$270°\pm20°$

A harmonic analysis has been carried out on the N–S and E–W components for each day separately. The results are given in tables 2, 3 and 4, and plotted in polar form in fig. 8. Only three terms are significant. One represents a constant displacement due to a prevailing wind. The velocity of this component varies between 7 and 21 m/sec,

Fig. 6

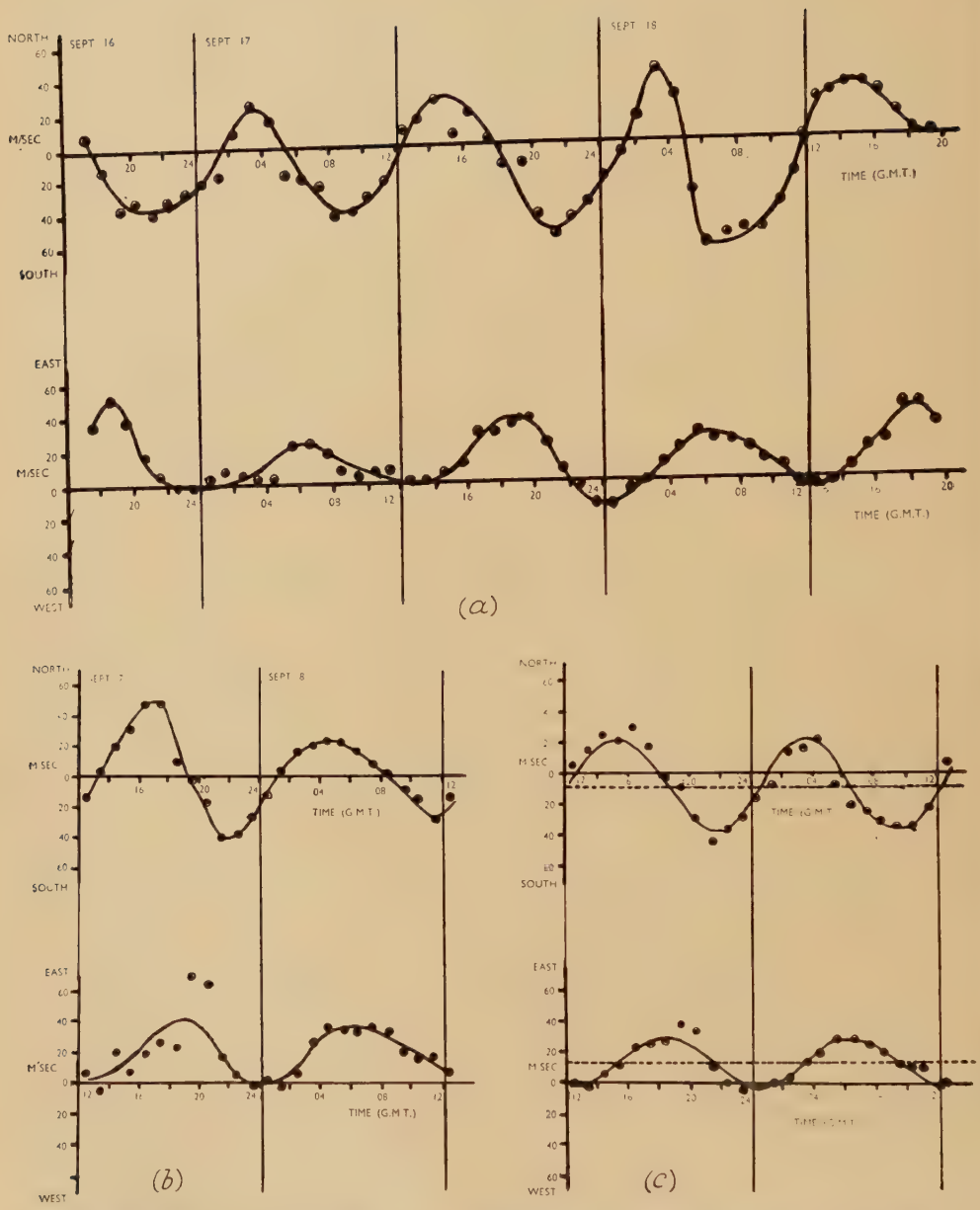

Components of wind velocity, September 1953. Ordinate: Velocity (metres/sec). Abscissa: Local time (G.M.T.). (*a*) North–South and East–West wind components. Sept. 16–17–18, 1953. (*b*) North–South and East–West wind components. Sept. 7–8, 1953. (*c*) North–South and East–West wind components. Average for Sept. 7–8, 16–17–18, 1953. Constant and semi-diurnal terms of the harmonic analysis are shown.

on the five days, while the direction varies between East and South–East in September, to West in October. Very large semi-diurnal components of magnitude 20–40 m/sec are present on all the days in September. These correspond to a wind vector rotating in a clockwise direction,

Fig. 7

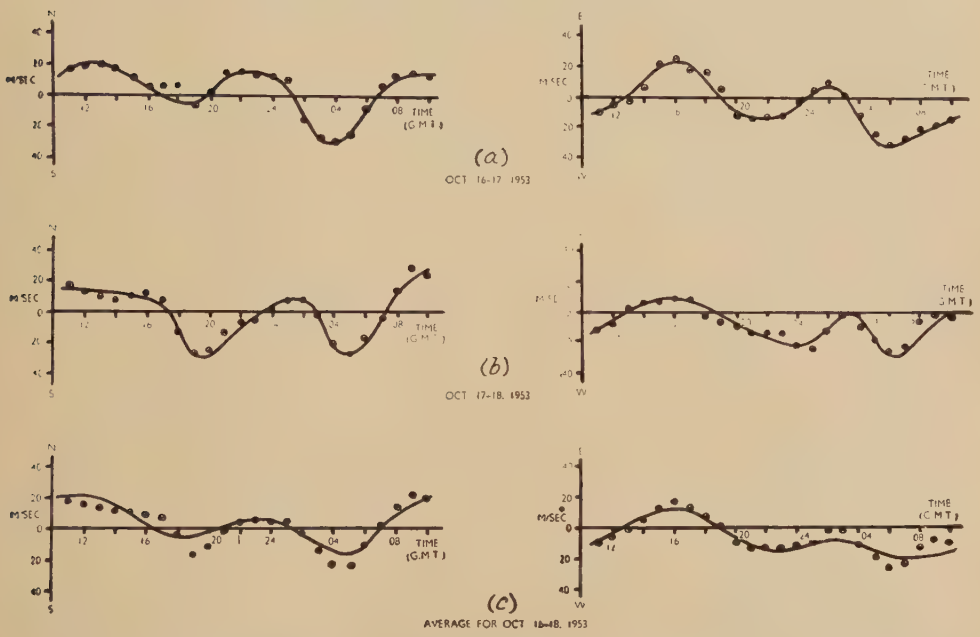

North–South and East–West components of wind velocity, October, 1953. (*a*) Oct. 16–17, 1953. (*b*) Oct. 17–18, 1953. (*c*) Average for Oct. 16–18, 1953. Smoothed curves are drawn through the points for individual days. The continuous lines for the average day represent the constant, diurnal and semidiurnal terms of the harmonic analysis. Ordinate: Component of wind velocity (metres/sec). Abscissa: Local time (G.M.T.).

Table 3. Results of Harmonic Analysis for 12 hour Periodic Wind Components. Amplitudes are in metres/sec. Local Times are Given

Date (1953)	North–South	East–West	Time of northerly velocity vector	Time of easterly velocity vector
Sept. 7– 8	31 ± 3	21 ± 3	0400 ± 0015	0730 ± 0015
Sept. 16–17	28 ± 2	14 ± 2	0330 ± 0015	0630 ± 0015
Sept. 17–18	41 ± 5	20 ± 2	0330 ± 0015	0600 ± 0015
Oct. 16–17	15 ± 2	13 ± 2	0000 ± 0030	0230 ± 0030
Oct. 17–18	12 ± 4	7 ± 2	0000 ± 0030	0300 ± 0100

blowing towards the north at 0340±0010 hrs. and 1540±0010 hrs. The semi-diurnal oscillation is markedly elliptical, with the major axis, which appears to lie in the N–S direction, about twice as great as the minor axis. The amplitude of the semi-diurnal component also appears to vary considerably from day to day, although the phase remains fairly constant. In October, however, the phase of the semi-diurnal oscillation is markedly different, the time of northerly velocity being 0000±0030 hrs. and 1200±0030 hrs. The amplitude of this component (~12 m/sec) is also reduced to about one third of the September value.

Table 4. Results of Harmonic Analysis for 24-hour Periodic Wind Components. Amplitudes are in metres/sec. Local Times are Given. The Figures in Italics on Sept. 7–8, 17–18, represent Maximum-values for the Diurnal Components on These Days

Date (1953)	North–South	East–West	Time of northerly velocity vector	Time of easterly velocity vector
Sept. 7– 8	*7±3*	*1±4*	*1230±0300*	*1830±——*
Sept. 16–17	6±2	7±2	1100±0200	1930±0200
Sept. 17–18	*9±4*	*5±2*	*0900±0300*	*2030±0200*
Oct. 16–17	13±2	15±3	1130±0100	2000±0100
Oct. 17–18	12±2	10±3	0900±0100	1700±0100

Harmonic analysis of the October results also showed the presence of a diurnal component of the same amplitude as the semi-diurnal wind. The wind vector again rotates in a clockwise sense, being directed towards the north at 1015±0100 hrs. The diurnal component in September is very small (~5 m/sec), and is not significant on all three days. The values given in italics serve to indicate the maximum value of such a component if it is present. The phase appears to agree with the October measurements.

The amplitudes and phases of these periodic winds thus vary considerably. On the basis of an atmospheric resonance theory, the variations in the amplitude and phase of the semi-diurnal component would indicate a variation in the properties of the atmosphere, producing a small variation in the 12 hour resonant period. The presence of a 24 hour periodic wind, however, would require explanation. It is possible that the reversal in direction of the prevailing wind is due to a seasonal change in atmospheric temperature between summer and winter.

(*b*) *Inclination of Wind to the Horizontal*

In the above analysis it has been assumed that the wind motions are horizontal (Manning, Villard and Peterson 1950, Elford and Robertson 1953). The validity of this assumption has been checked by observing

Fig. 8

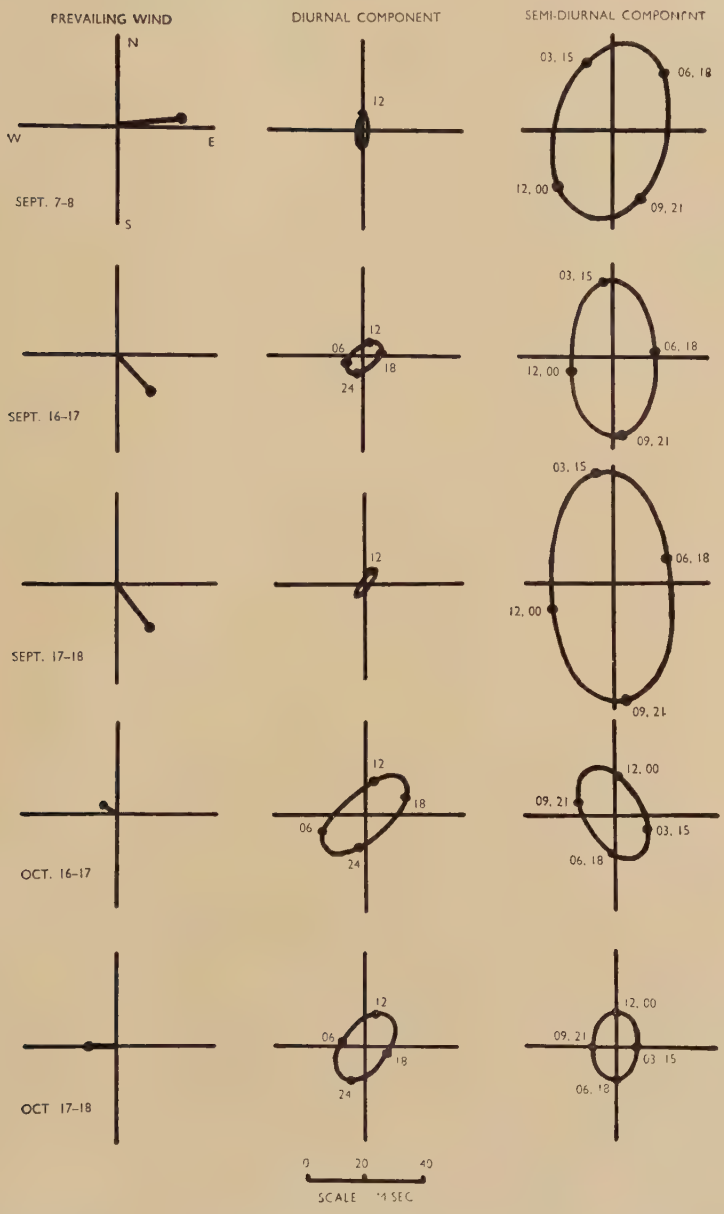

Results of analysis of wind measurements for prevailing, diurnal, and semi-diurnal wind components. Sept.–Oct. 1953.

radial components of velocity at a fixed azimuth, but varying elevations. If V_r is the radial wind velocity observed at an elevation θ, then for a horizontal wind, V_r should be proportional to $\cos\theta$. As the majority of meteor echoes are obtained from a narrow band of heights between 90 and 95 km, the elevation of an echoing point approximates to $\theta=\sin^{-1}(92{\cdot}5/R)$ where R is the range in kilometres. In fig. 9 $V_r/\cos\theta$ is plotted as a function of θ for a large number of meteors observed at a given azimuth. Times were selected when the wind was blowing in the direction of the aerial beam, so for a horizontal wind V, $V_r/\cos\theta$ should be constant and equal to V. Figure 9 shows that the wind is horizontal to within a few degrees. Similar results are obtained at other times and for different aerial positions. In analysing the records for horizontal wind components, elevation corrections are applied to the radial components obtained as in § 3 from a knowledge of echo range.

Fig.

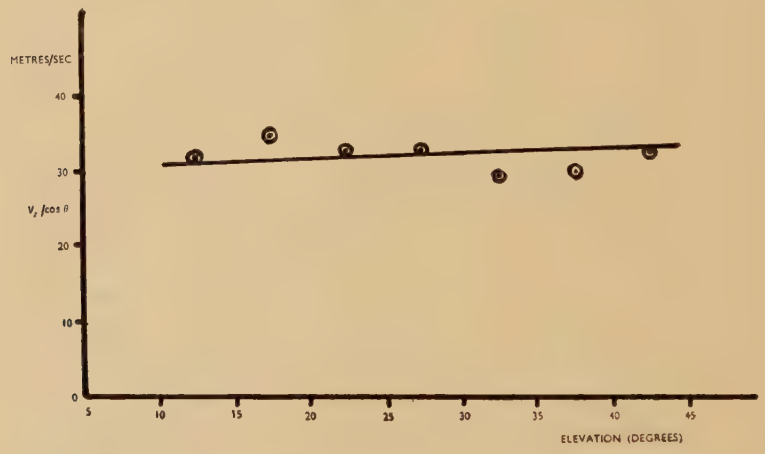

Variation of radial wind components (V_r), with elevation (θ).

(c) *Variation of Wind Velocity with Height*

(i) *Measurement of Height*

In view of the large number of results obtained during a wind run all direct methods of measuring heights of reflection are unsuitable, since the analysis of a single days observation might occupy several months. For this reason echo duration, which depends directly upon the atmospheric pressure at the height of reflection, has been used to give a measure of the meteor height. At a given wavelength this duration is governed almost entirely by diffusion of the ionized matter, and for most trails the echo amplitude A at time t after the passage of the meteor is given by

$$A=A_0 \exp(-16\pi^2 Dt/\lambda^2) \text{ (Herlofson 1948)} \quad . \quad . \quad . \quad . \quad . \quad (1)$$

where A_0 is the initial amplitude, and D the appropriate diffusion coefficient.

Since D is approximately inversely proportional to the pressure, the rate of decay of echo amplitude can thus be used to determine the actual heights of occurrence of the ionized columns. At a frequency of 36 Mc/s the appropriate diffusion coefficients between 80 and 100 km are such that the echo durations to half initial amplitude lie between 0·02 and 0·5 sec.

For the very densely ionized trails from bright visual meteors eqn. (1) ceases to hold, since the echo durations also depend upon the linear electron densities in the columns (Greenhow 1952, Kaiser and Closs 1952). Such echoes, which may have durations of many seconds, cannot be used for direct height determinations, but they constitute only a small fraction of the total number of echoes observed.

A preliminary experiment was made in order to calibrate echo duration in terms of height, and for this purpose the split beam method devised by Clegg and Davidson (1950) was used. A discussion of these results forms the subject of another paper (Greenhow and Neufeld, in pub.), but the direct height duration calibration obtained during these experiments is shown in fig. 11.

(ii) *Variation of Wind Speed and Direction with Height*

As most meteor echoes occur in a fairly narrow band of heights, the division of the observations into several reasonably spaced height groups can only be made when the echo rate is very high. Figure 10 (*a*) shows the

Fig. 10

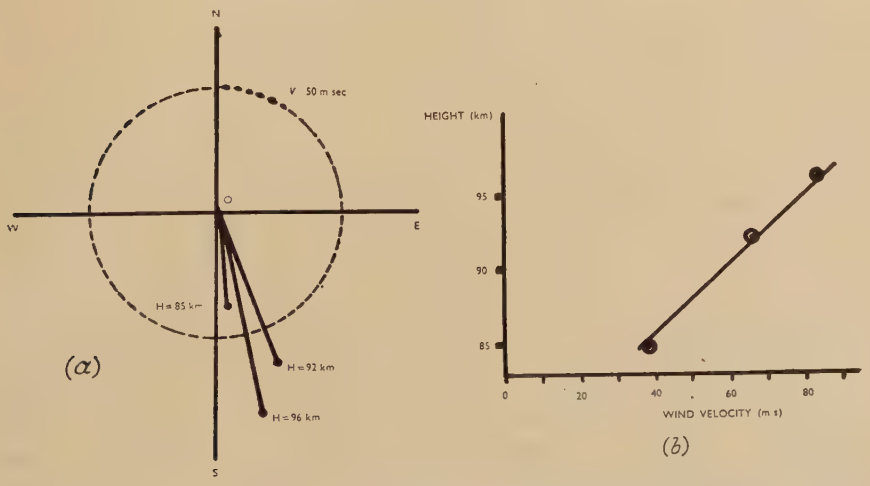

Variation of wind velocity with height. 0600–0900 hrs. Sept. 18, 1953. (*a*) Vector presentation. (*b*) Velocity–Height relation (wind gradient $\sim 4{\cdot}2$ m sec^{-1} km^{-1}).

results obtained between 0600 and 0900 hrs. on Sept. 18, for height groups centred about 85, 92 and 96 km. Although the wind direction does not vary significantly, the wind speed increases with height. The variation of wind speed with height is shown separately in fig. 10 (*b*)

from which it appears that during this time interval there was a positive wind gradient of approximately 4·2 m $sec^{-1}km^{-1}$.

(iii) *Average Variation of Wind Speed with Height*

Since the wind direction varies with time, the type of analysis carried out in the previous section cannot be extended to greater height ranges by integrating over larger time intervals. However, an average measure of the variation of wind speed with height, irrespective of direction, can be determined by averaging together all the individual drift velocities obtained over several days. Nearly equal numbers of meteors are observed in two directions at right angles, hence the average wind speed obtained in each height group is approximately 0·7 of the true wind speed. The average variation of wind speed with height, for three days during September, 1953, is shown in fig. 11. The speed varies between 14 m/sec

Fig. 11

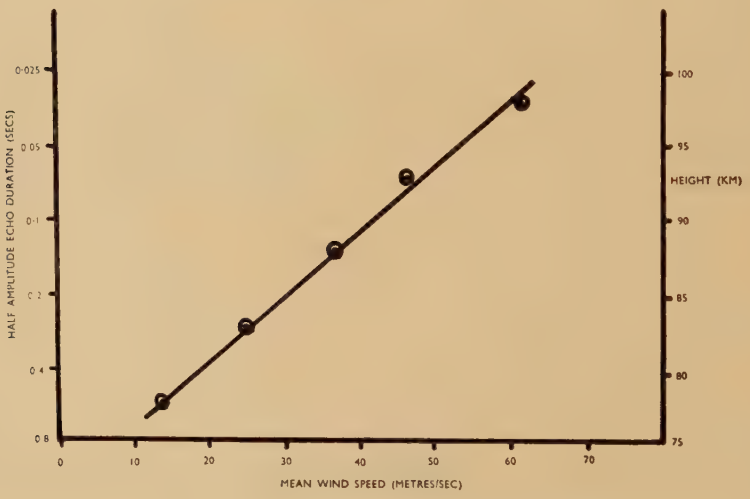

Variation of mean wind speed with height.

at a height of 78 km to over 60 m/sec at a height of 98 km. This represents an average positive wind gradient of 2·3 m $sec^{-1}km^{-1}$. These results may be compared with the measurements of Elford and Robertson (1953) who found a positive wind gradient of 3·6 m $sec^{-1}km^{-1}$ between heights of 92 and 98 km.

(iv) *Diurnal Variation of Meteor Heights*

The diurnal variation of geocentric meteor velocities causes a diurnal variation in meteor heights. For those used in the wind analysis the variation amounts to approximately $92{\cdot}5 \pm 2{\cdot}5$ km. Hence the vertical wind gradient discussed in (ii) and (iii) above will introduce a spurious diurnal component into the wind velocity if all the echoes are included in

the hourly wind measurements. A correction to the results has been made to allow for this variation by normalizing the heights to 90 km, and using the data in fig. 11. The velocity correction amounts to approximately $\pm 10\%$ over the 24 hours.

(*d*) *Irregularities in the Wind*

The resultant wind vectors shown in fig. 4 were determined by combining perpendicular components of velocity. These components are the averages of a large number of individual meteor drift velocities observed in North–easterly and North–westerly directions. For a uniform wind a spread in drift velocities will be observed in any aerial position because of the finite beamwidth ($\delta V \sim \pm 20\%$), errors in the measurement of velocity ($\delta V \sim \pm 15\%$), and the variation of velocity with height ($\delta V \sim \pm 8\%$). Theoretical velocity distributions can therefore be computed for a wind of given velocity and direction. Any observed increase over these theoretical distributions then represents a true variation in the actual wind speed and direction.

A number of observed velocity distributions are shown in figs. 12 (*a*) and (*b*), together with the theoretical distributions calculated from the mean wind vectors. In fig. 12 (*a*) the observed distributions follow closely the theoretical curves for a uniform wind speed of 63 m/sec, towards azimuth 160°. In this case the irregularities in wind velocity were small. In fig. 12 (*b*) on the other hand, although the average velocity is only 8 m/sec towards azimuth 007°, individual velocities between +40 and −40 m/sec are observed. Such large irregularities in velocity do not appear to be due to any regular change of wind direction with height, but rather to completely variable winds.

The velocity spreads for the 24-hour vector plots in fig. 4, calculated from the excess widths of the individual velocity distributions, are shown as dotted circles. The circles are such that at any time the instantaneous wind vector has a 50% probability of lying anywhere within the circle.

Wind gradients considerably greater than the mean gradient of 2·7 m/sec/km have been measured by Greenhow (1952) from the amplitude fluctuations in long duration echoes. Winds with velocities differing by 10 to 50 m/sec over height differences of 5 to 10 km were commonly observed. Such wind variations are evident in the present work on occasions when velocity distributions similar to those in fig. 12 (*b*) are obtained.

§ 5. Comparison of Results with Other Observations

(*a*) *Meteor Observations*

Some of the earliest upper atmospheric wind measurements were made from observations of long enduring visual meteor trails, and noctilucent clouds. These phenomena however, occur too infrequently for systematic observations to be made, and the wind directions measured

by different observers are somewhat conflicting. On the other hand the wind speeds measured in this way are of the same order as those obtained using radio methods. In view of the variations in wind velocity discussed in the previous section, the differences in directions observed by visual means are not surprising.

Fig. 12

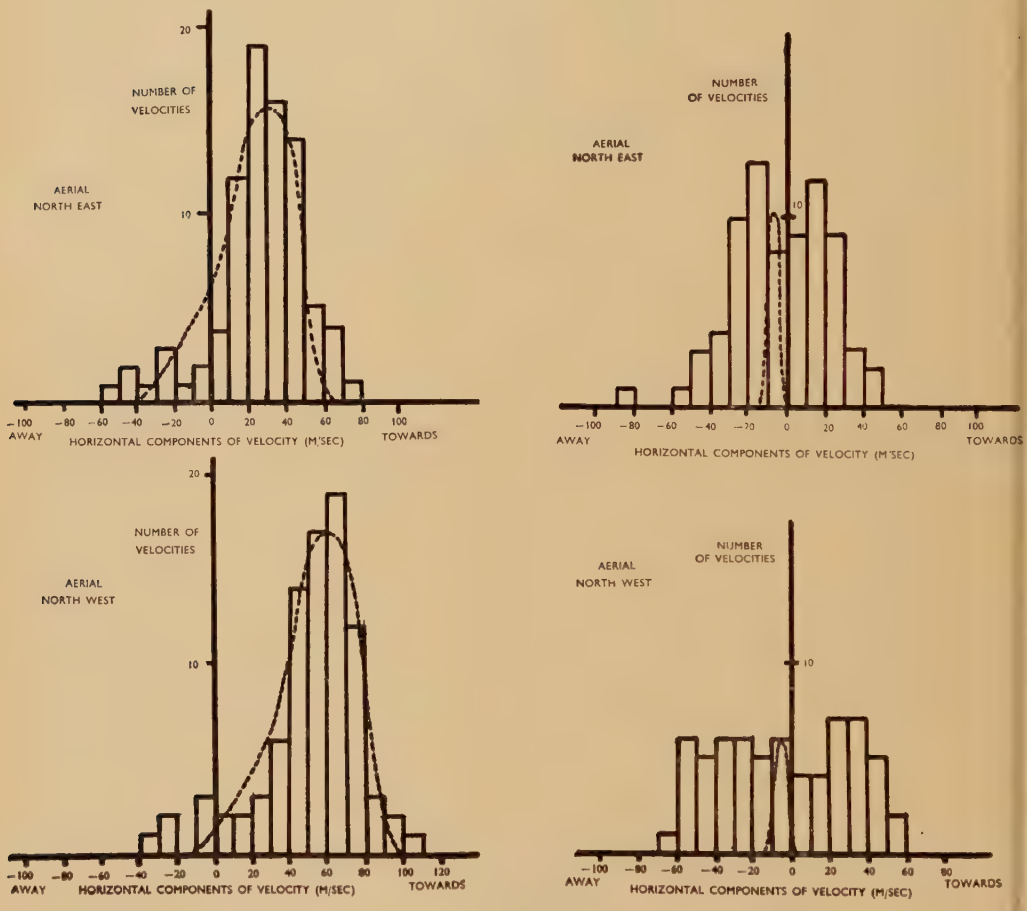

(*a*) (*b*)

(*a*) Velocity distributions observed between 0800–0900 hrs. Sept. 18, 1953. Theoretical distributions are shown for a uniform wind of 63 m/sec towards azimuth 160°. (*b*) Velocity distributions observed between 1200 and 1300 hrs. Sept. 17, 1953. Theoretical distributions are shown for a uniform wind of 8 m/sec towards azimuth 007°.

Wind data from the radio observation of meteors is now accumulating. In a northern latitude similar to that of Jodrell Bank, Manning, Villard and Peterson (1950) have measured the average wind velocity for the

period 3–6 a.m. (local time), on a number of occasions during the summer. They found the predominant direction to be between North–East and North with speeds of approximately 30 m/sec. These results are in general agreement with the September observations discussed previously (fig. 4).

On a number of nights during December, Greenhow (1952) found the wind direction to be roughly southerly before midnight, reversing to a northerly direction after 0200 hrs. This behaviour is also in agreement with the presence of the periodic winds described in § 4.

Working in the southern hemisphere, Elford and Robertson (1953) have measured winds in the meteor region using an apparatus of somewhat lower resolving power, so that detailed hourly and daily comparisons cannot be made. However, as a result of integrating continuous monthly observations, these workers have also shown that periodic and prevailing winds are present around the 90 km level. It is interesting to observe that their periodic components rotate in an anti-clockwise direction—that is counter to the one discussed in this paper. This is in agreement with tidal theory, as the directions of rotation should differ in the northern and southern hemispheres. The directions of the prevailing winds at comparable times (October), are also in opposite quadrants in the two hemispheres. On the other hand the phases of their periodic winds—semi-diurnal and diurnal due North at $0 \pm 1\frac{1}{2}$ hrs. and 18 ± 2 hrs. respectively—are not in agreement with those observed in northern latitudes. The phases might be expected to differ by 180° in the two hemispheres.

(*b*) *Ionospheric Sounding Methods*

Using the ionospheric echo fading technique, a number of workers have measured winds in the lower E–region, although the exact height of the measurements is not specified (e.g. Mitra 1949, Salzberg and Greenstone 1951, Phillips 1952). The observations by Phillips at a site within 200 km of Jodrell Bank are typical of the results obtained by this method. His observations do not show the regular characteristics of those obtained using meteor echo techniques, and smooth daily periodic variations in velocity are generally not recorded. However, an average over a period of several months shows the presence of a 12 hour periodic wind with an amplitude of 15 m/sec. The phase of this component (towards the North at 0300 hrs.), is in good agreement with the phase of the semi-diurnal component for September observed at Jodrell Bank. Most of the observed ionospheric wind velocities lie between 50 and 150 m/sec. The existence of the positive wind gradient found in the meteor observations, thus indicates that these measurements refer to altitudes greater than 100 km.

Acknowledgments

The work described in this paper has been carried out at the Jodrell Bank Experimental Station of the University of Manchester, under the direction of Professor A. C. B. Lovell. The author is particularly indebted

to Mr. E. L. Neufeld for his invaluable assistance in analysing the records, and to Mr. S. Evans for the use of his height finding apparatus in the height-duration calibration. He also wishes to thank the Department of Scientific and Industrial Research for the grant of a Senior Research Award.

References

Clegg, J. A., and Davidson, I.A., 1950, *Phil. Mag.*, **41**, 77.
Davies, J. G., and Ellyett, C. D., 1949, *Phil. Mag.*, **40**, 614.
Elford, W. G., and Robertson, D. S., 1953, *J. Atmos. Terr. Phys.*, **4**, 271.
Greenhow, J. S., 1950, *Phil. Mag.*, **41**, 682; 1952 a, *J. Atmos. Terr. Phys.*, **2**, 282; 1952 b, *Proc. Phys. Soc.* B, **65**, 169.
Herlofson, N., 1948, *Phys. Soc. Rep. Prog. Phys.*, **11**, 444.
Kaiser, T. R., and Closs, R. L., 1952, *Phil. Mag.*, **43**, 1.
Manning, L. A., Villard, O. G., and Peterson, A. M., 1950, *Proc. Inst. Radio Engrs.*, **38**, 877; 1952, *J. Geophys. Res.*, **57**, 387.
Mitra, S. N., 1949, *Proc. Inst. Elect. Engrs.* (Part III), **96**, 441.
Olivier, C. P., 1942, *Proc. Amer. Phys. Soc.*, **85**, 93.
Phillips, G. J., 1952, *J. Atmos. Terr. Phys.*, **2**, 141.
Robertson, D. S., Liddy, D. T., and Elford, W. G., 1953, *J. Atmos. Terr. Phys.*, **4**, 255.
Salzberg, C. D., and Greenstone, R., 1951, *J. Geophys. Res.*, **56**, 521.
Störmer, C., 1937, *Astrophysica Norvegica*, No. 5.

LVII. *Anomalous Electron-Scattering in Metals*

By D. K. C. MacDonald and W. B. Pearson
Physics Division, National Research Council, Ottawa*

[Received March 1, 1954]

Abstract

A semi-theoretical equation was proposed previously to account qualitatively for the thermoelectric power of metals and alloys, particularly at low temperatures. The consequences of this equation are now examined quantitatively in relation to experimental data on alloys of copper.

In the continuing absence of a satisfactory fundamental theory to account for the well-known minimum of electrical resistance in certain metals at low temperatures (e.g. de Haas, de Boer and van den Berg 1933, Mendoza and Thomas 1951, 1952, MacDonald 1952, 1953) and the thermoelectric experiments of the authors (MacDonald and Pearson 1953, 1954) which appear undoubtedly associated, it has seemed worthwhile to us to attempt to correlate the results semi-empirically.

The quantum theory of metals (e.g. Mott and Jones 1936) yields the expression

$$S=-\frac{\pi^2k^2T}{3e\zeta}\left(\frac{d\log\rho(E)}{d\log E}\right)_{E=\zeta}, \quad \ldots\ldots \quad (1)$$

for the absolute thermoelectric power. Our experiments on the 'simplest' metals have already shown that the theory is certainly inadequate in its prediction of a simple linear temperature dependence at low temperatures. (This is further confirmed by our most recent experimental work on potassium which appears to display a constant S between 2°K and ~9°K.) However, writing the resistance as $\rho_{\text{total}}=\rho_{\text{therm}}+\rho_{\text{res}}+\rho_{\text{anom}}$ (where ρ_{anom} represents the anomalous component yielding the resistance-minimum) we found that the factor $\left(\frac{d\log\rho(E)}{d\log E}\right)$ provided a reasonable qualitative correlation between the resistive and thermoelectric behaviour and therefore suggested (MacDonald and Pearson 1953) that we write in place of (1)

$$S=F_i(T)\left(\frac{d\log\rho(E)}{d\log E}\right)_{E=\zeta} \quad \ldots\ldots \quad (2)$$

where $F_i(T)$ is some function (as yet undetermined) of temperature and of those parameters characteristic of the pure metal.

Let us now examine this proposed relationship more quantitatively. Consider relatively dilute alloys of copper, with measurements at a

---

* Communicated by the Authors.

sufficiently low* and constant temperature (T_0 say) that we may neglect ρ_{therm}, and hence

$$S=C\left\{\frac{\rho_{\text{res}}}{\rho_{\text{res}}+\rho_{\text{anom}}}\left(\frac{d\log\rho_{\text{res}}}{d\log E}\right)+\frac{\rho_{\text{anom}}}{\rho_{\text{res}}+\rho_{\text{anom}}}\left(\frac{d\log\rho_{\text{anom}}}{d\log E}\right)\right\}$$
$$(C=F_{\text{cu}}(T_0)) \qquad \ldots\ldots\ldots \quad (3)$$

Now in general the overall magnitude of the resistance-minimum anomaly is not more than several per cent of the apparent residual resistance and it therefore seems reasonable to write

$$S\doteq C\left\{\frac{d\log\rho_{\text{res}}}{d\log E}+\frac{\rho_{\text{anom}}}{\rho_{\text{res}}}\left(\frac{d\log\rho_{\text{anom}}}{d\log E}\right)\right\}$$
$$=A+B(\rho_{\text{anom}}/\rho_{\text{res}}). \qquad \ldots\ldots\ldots \quad (4)$$

Thus, if (2) is correct, S should vary linearly as $\rho_{\text{anom}}/\rho_{\text{res}}$. We now assume that we may take $\{\rho_{4\cdot2^\circ\text{K}}-\rho_{\text{min}}\}$ as a proportional measure of ρ_{anom}. Thus we write $\rho_{\text{anom}}=\lambda(\rho_{4\cdot2^\circ\text{K}}-\rho_{\text{min}})$ where λ will be assumed independent of concentration but will, of course, be a function of temperature; however, for this discussion of measurements at a fixed temperature λ will be a constant throughout for a given impurity. Then figs. 1 and 2, comparing S and $(1/\lambda)\rho_{\text{anom}}$ ρ_{res} for alloys of tin in copper, each plotted against ρ_{res} as abscissa, show immediately their very strong similarity. If, however, we take the more stringent course of plotting S directly against $(1/\lambda)\rho_{\text{anom}}/\rho_{\text{res}}$ as in figs. 3 and 4 for tin and bismuth alloys in copper, the situation is somewhat less certain. The results for the tin alloys suggest rather strongly *two* linear branches for the equation; the bismuth data show a single quite pleasing straight-line plot over a rather wide range of ρ_{res}, but on the other hand results for such alloys are not available extending appreciably into the 'saturation' range of the resistive-minimum, in contrast to those for the tin alloys.

If one accepts that the evidence is in favour of retaining (4), (with its antecedent (2)), one can then readily explain the *two* lines of the tin alloy data by assuming that the energy-dependence of the anomalous 'scattering' (i.e. $d\log\rho_{\text{anom}}/d\log E$) changes rather abruptly as the resistance-minimum saturates—i.e. at the 'cusp' on fig. 2. This hypothesis would indeed seem quite reasonable in view of the very saturation of the process which is clearly rather sharp.

It is evident for both these sets of data (and particularly so for the tin alloys) that

$$\lambda\frac{d\log\rho_{\text{anom}}}{d\log E}\gg\frac{d\log\rho_{\text{res}}}{d\log E},$$

and it therefore appears that the mechanism of ρ_{anom} must indeed be *highly* energy-dependent† if (4) be granted. For bismuth,

$$\lambda\frac{d\log\rho_{\text{anom}}}{d\log E}\approx 30\frac{d\log\rho_{\text{res}}}{d\log E}.$$

* One is limited, however, by the accuracy of measurement, since by the Third Law S must vanish as $T\to 0$.

† It appears very probable that for copper $\lambda_{15^\circ\text{K}}$ must be less than unity.

In figs. 1 and 2 we have chosen ρ_{res} as abscissa rather than the more obvious impurity-concentration, say x, since we have found that causes such as selective evaporation during annealing may cause the *nominal* value of x to deviate very considerably from that in fact present in the final specimen ; ρ_{res} consequently provides a much more reliable direct measure of the *effective* value of x. From fig. 5 where $(1/\lambda)\rho_{anom}$ is plotted

Fig. 1

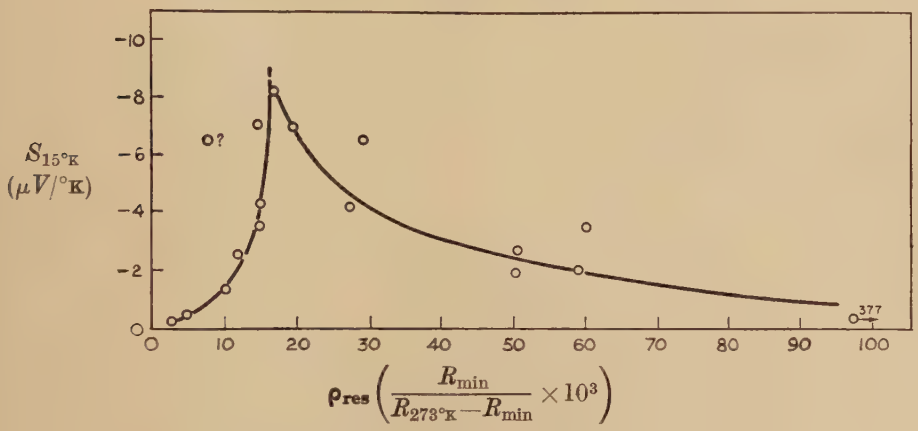

Thermoelectric power (at 15°K) of alloys of tin in copper.

Fig. 2

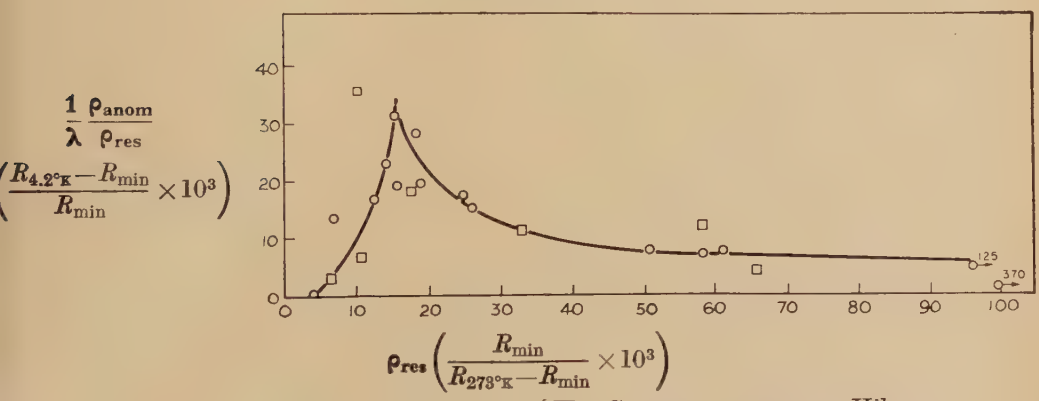

$\frac{1}{\lambda}\rho_{anom}/\rho_{res}$ for alloys of tin in copper { □ : Copper spec. pure ex Hilger ; ○ : Electrolytic Copper ex J.T.H.

against ρ_{res} for various alloys, we are led to suggest that an expression for ρ_{anom} may be of the general type

$$\frac{1}{\lambda}\rho_{anom} = \frac{A\rho_{res}^2}{1+B\rho_{res}^2}, \quad \ldots\ldots\ldots \quad (5a)$$

i.e.

$$\rho_{anom} = \lambda\frac{A\rho_{res}^2}{1+B\rho_{res}^2}, \quad \ldots\ldots\ldots \quad (5b)$$

where A is a 'universal' constant for a given parent metal, and B

Fig. 3

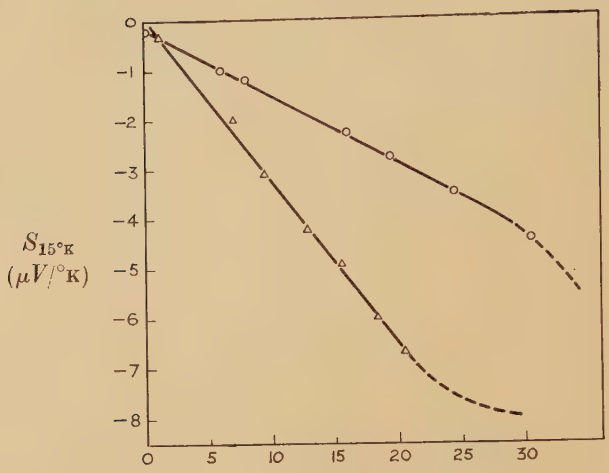

Variation of S with $\frac{1}{\lambda}\rho_{anom}/\rho_{res}$ for alloys of tin in copper.

——○—— : $\rho_{res} < 16\times10^{-3}$
——△—— : $\rho_{res} > 16\times10^{-3}$

Fig. 4

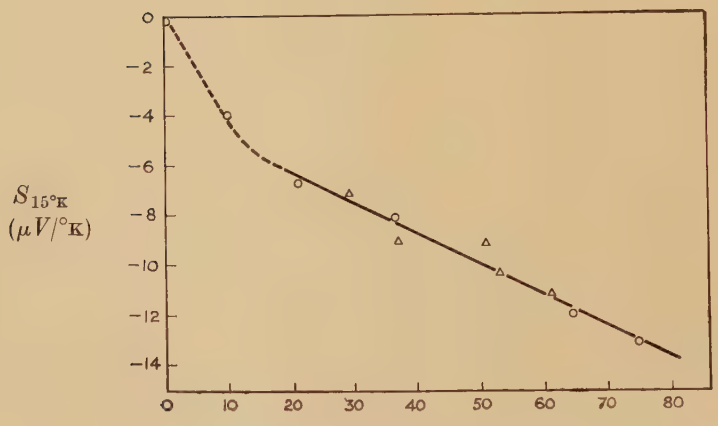

Variation of S with $\frac{1}{\lambda}\rho_{anom}/\rho_{res}$ for alloys of bismuth in copper.

——○—— : 0·006% Bi(wt.)
——△—— : 0·05% Bi(wt.)

} Varying amounts of Bi in solid solution obtained by quenching from appropriate temperatures.

depends on the specific type of impurity atom. An impurity atom such as bismuth in copper productive of a large minimum and 'saturating' only at relatively high values of ρ_{res} would then have a small ratio B/A, while for nickel and silver in copper producing no observable minimum (MacDonald 1952) we must assume $B/A \gg 1$.

Fig. 5

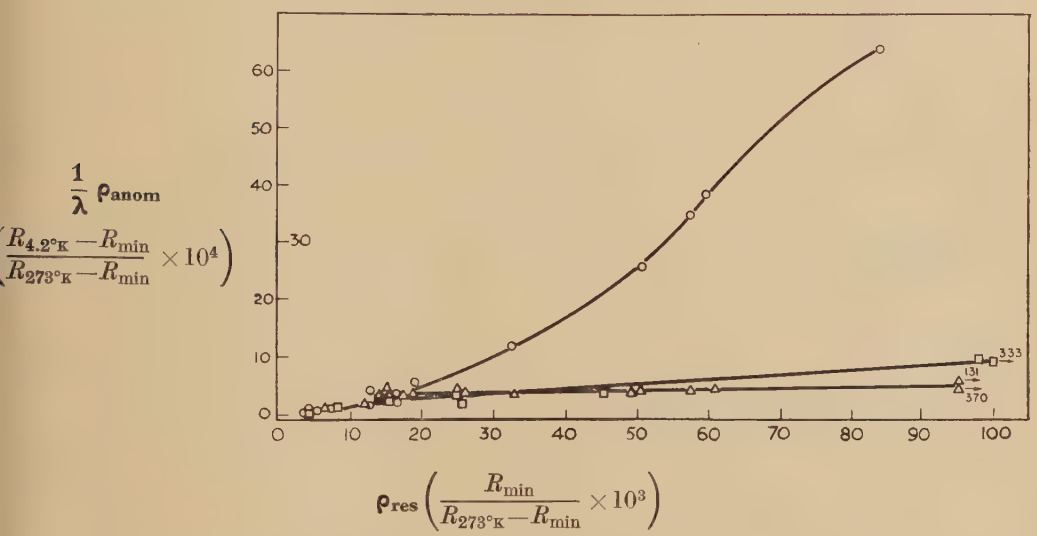

Anomalous low temperature resistance of copper alloys.

——△——: Sn in Cu
——□——: Ga in Cu
——○——: Bi in Cu

We are tempted to suggest that the incorrect prediction of temperature dependence of eqn. (1) may find its source in the inadequacy of the Boltzmann equation as used in present theory to describe electron-transport in a metal under a thermal gradient. For, on the one hand, it is a basic assumption that electron–electron collisions may be ignored (cf. Lorentz: "... we shall suppose the collisions with the metallic atoms to preponderate; the number of these encounters will be taken so far to exceed that of the collisions between electrons mutually, that these latter may be altogether neglected ...") while, on the other hand, a temperature-gradient is introduced by assuming specifically that we may write

$$\frac{\partial f}{dx} \doteq \frac{df_0}{dT}\cdot\frac{dT}{dx},$$

(where f_0 is the Fermi distribution function). This assumption—even as a first approximation—that we may characterize the electron-distribution under a thermal gradient by a single thermodynamic temperature appears to us incompatible with the previous assumption. Indeed one would

rather have thought that in order to introduce a statistical thermodynamic distribution in this way it would be necessary to assume that electron–electron collisions were always sufficiently active to maintain effective internal thermal equilibrium amongst the conduction electrons in spite of the electron-lattice perturbation.

We are inclined to believe that this inadequacy may also be the source—at least in part—of the notable discrepancies between theory and experiment (cf. e.g. Wilson 1953, pp. 289, 290) in thermal conductivity in metals.

Acknowledgment

We are indebted to Dr. J. S. Dugdale for helpful comments.

References

de Haas, W., de Boer, J., and van den Berg, G. J., 1933, *Physica*, **1**, 1115.
MacDonald, D. K. C., 1952, *Phys. Rev.*, **88**, 148 ; 1953, *Physica*, **19**, 841.
MacDonald, D. K. C., and Pearson, W. B., 1953, *Proc. Roy. Soc.* A, **219**, 373 ; 1954, *Ibid.*, **221**, 534.
Mendoza, E., and Thomas, J. G., 1951, *Phil. Mag.*, **42**, 291 ; 1952, *Ibid.*, **43**, 900.
Mott, N. F., and Jones, H., 1936, *Theory of Properties of Metals and Alloys* (Oxford : Clarendon Press).
Wilson, A. H., 1953, *Theory of Metals*, 2nd ed. (Cambridge : University Press).

LVIII. *The Effects of Finite Size and Decentring of the Source in an Angular Correlation Experiment*

By Ernst Breitenberger
Cavendish Laboratory, Cambridge*

[Received February 18, 1954]

Summary

In a first approximation any extended source behaves like a point source situated at the 'centre of gravity' of the given activity distribution. The first-order errors caused by bad centring of a point source are rather large and exhibit a strong angular dependence. They can be minimized by a randomized block design when it is impossible to avoid them altogether owing to technical reasons.

Numerical formulae are given for the rapid estimation of first- and second-order errors. The relations between source decentring and angular resolution of the detectors are examined. The approximation method used in this study can be adapted to other problems (e.g. angular distributions, scattering experiments).

§ 1. Introduction

In a typical angular correlation experiment two particles (or quanta) emitted from a source in quick succession are observed by means of two detectors in coincidence, with the purpose of determining the correlation function $W(\omega)$, i.e. the probability that the directions of propagation of the two rays form an angle ω with each other. $W(\omega)$ is inferred from the way in which the coincidence rate depends on the position of the detectors relative to the source, and is then compared with theory. Theoretical correlation functions have been calculated explicitly for almost any case amenable to experiment (see Biedenharn and Rose 1953). One gathers from the numerical tables that often the alternatives to be considered in the interpretation of an experiment do not differ very much; sometimes they even fill a continuous range, e.g. when a mixed transition is involved. Such cases require extreme experimental care, the smallest systematic errors being capable of falsifying the results very seriously. The technical difficulties and their disturbing effects are borne out in recent work on correlations with mixed γ-rays (Aeppli, Frauenfelder and Walter 1951, Klema and McGowan 1952, 1953, Steffen and Zobel 1952, Steffen 1953 a, b, c) which are of particular interest because they can yield valuable direct information

* Communicated by Professor O. R. Frisch, F.R.S.

about nuclear matrix elements. Both the measurement of ω and of the coincidence rate are in general subject to uncertainties, the one for geometrical, the other for statistical reasons. A high standard of accuracy clearly necessitates the application of sound statistical significance tests,* reliable corrections for the finite angular resolution of the detectors, and last not least, a critical consideration of all errors that may be caused by the finite extension and uncertain position of the source.

The latter subject has received only scant attention (Walter, Huber and Zünti 1950, Deutsch 1951) despite its obvious importance. In the present note it will be discussed by means of a simple approximation method which leads to several useful results concerning the nature and magnitude of the possible errors and suggests how to deal with them when they cannot be avoided owing to some technical reason.

We shall assume that the correlation function is expanded in Legendre polynomials

$$W(\omega)=\Sigma a_n P_n(\cos\omega), \qquad (1)$$

with $a_0=1$ and the normalization $P_n(1)=1$, as usual.† Self-absorption in the source and all scattering effects will be neglected. At the beginning the detectors are regarded as infinitely small and freely movable on the unit sphere about the centre of the apparatus, which serves as coordinate origin. We specify the position of the two sensitive surface elements $d\Omega_1$, $d\Omega_2$ by the unit vectors $\mathbf{r}_1$ and $\mathbf{r}_2$ and denote the angle between these by ω, as above. Extended detectors will be considered at the end.

§ 2. The Decentred Point Source

In the simplest case to be discussed the source has effectively the size of a point but is located off the centre.

Call the vector of source displacement $\mathbf{d}$ and set $\mathbf{r}_1-\mathbf{d}=\mathbf{r}_1'$ and $\mathbf{r}_2-\mathbf{d}=\mathbf{r}_2'$. The two detectors subtend solid angles $d\Omega_1'$ and $d\Omega_2'$ at the decentred source and are seen from there under the angle ω' between $\mathbf{r}_1'$ and $\mathbf{r}_2'$. The observed coincidence count will be proportional to

$$W(\omega')\,d\Omega_1'\,d\Omega_2', \qquad (2)$$

and the problem is to express this in terms of the known $d\Omega_1$, $d\Omega_2$, ω and $\mathbf{d}$.

For ω' one has immediately

$$\cos\omega'=\frac{\mathbf{r}_1'\mathbf{r}_2'}{|\mathbf{r}_1'||\mathbf{r}_2'|}=\frac{\mathbf{r}_1\mathbf{r}_2-(\mathbf{r}_1+\mathbf{r}_2)\mathbf{d}+\mathbf{d}^2}{\sqrt{(1-2\mathbf{r}_1\mathbf{d}+\mathbf{d}^2)}\,\sqrt{(1-2\mathbf{r}_2\mathbf{d}+\mathbf{d}^2)}}. \qquad (3)$$

* The great numerical labour involved in the least squares computations can sometimes be lessened by the use of mathematical short cuts (e.g. Hayes and Vickers 1951, Price 1954).

† The parity of n will not be restricted to even values because several of the following developments may be found useful in other problems where odd terms occur (e.g. angular distributions, scattering experiments with a large scatterer).

Abbreviating $\cos(\mathbf{r}_1, \mathbf{d})=u$, $\cos(\mathbf{r}_2, \mathbf{d})=v$, $|\mathbf{d}|=d$ and using the well-known expansion $(1-2zt+t^2)^{-1/2}=\Sigma P_n(z)t^n$ (which converges uniformly for all $|t|<1$ and all z) this becomes

$$\cos\omega' = [\cos\omega-(u+v)d+d^2][1+ud+(3u^2-1)d^2/2+\ldots][1+vd+\ldots]$$
$$= \cos\omega-(u+v)d+\cos\omega(u+v)d+O(d^2).$$

In practice $d \ll 1$; so one can neglect the terms of higher order, and obtains the first approximation

$$\cos\omega' = \cos\omega+(\cos\omega-1)(\mathbf{r}_1+\mathbf{r}_2)\mathbf{d}. \quad . \quad . \quad . \quad . \quad (4)$$

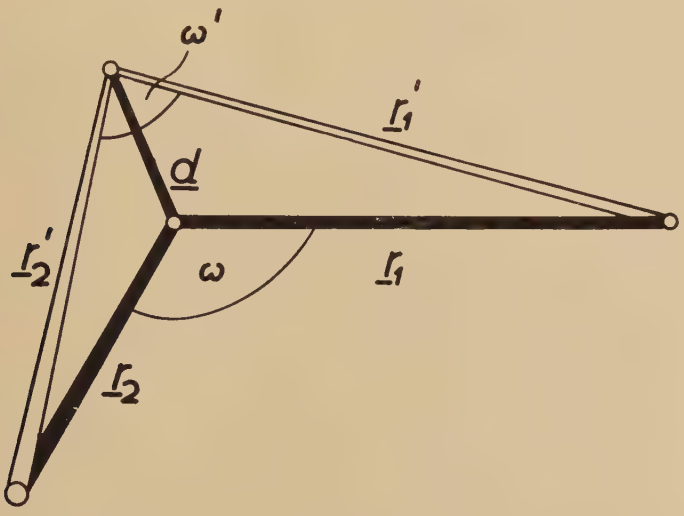

In a similar way one finds for the solid angle

$$d\Omega_1' = d\Omega_1 \frac{1}{|\mathbf{r}_1'|^2} \frac{\mathbf{r}_1\mathbf{r}_1'}{|\mathbf{r}_1'|} = d\Omega_1[1+2ud+O(d^2)],$$

and the first-order approximation is

$$d\Omega_1' = (1+2\mathbf{r}_1\mathbf{d})\, d\Omega_1. \quad . \quad . \quad . \quad . \quad . \quad . \quad (5)$$

An analogous formula holds for $d\Omega_2'$.

Next we evaluate $P_n(\cos\omega')$ from the Taylor development

$$P_n(x+h) = P_n(x)+hP_n'(x)+O(h^2)$$

which can be safely used since it is finite, P_n being a polynomial of degree n. With (4) comes, again in the first-order approximation,

$$P_n(\cos\omega') = P_n(\cos\omega)+P_n'(\cos\omega)(\cos\omega-1)(\mathbf{r}_1+\mathbf{r}_2)\mathbf{d}. \quad . \quad . \quad (6)$$

The factor of the form $P_n'(x)(x-1)$ in the second member on the right can be simplified further with the help of various recurrence formulae. The result is

$$P_n'(x)(x-1) = nP_n(x)+(-1)^n \sum_{\nu=0}^{n-1} (-1)^\nu(2\nu+1)P_\nu(x), \quad . \quad . \quad (7)$$

and shows clearly that source decentring completely distorts the

correlation by transforming each term of (1) into a whole series of Legendre polynomials. In fact the situation is even a little worse because (7), when substituted into (6), must be multiplied with $(\mathbf{r}_1+\mathbf{r}_2)\mathbf{d}$ which again depends on ω and thus aggravates the distortion suggested by (7) alone.

The individual terms of which (2) consists are now obtained by combining (5), the analogous formula for $d\Omega_2'$, and (6). Retaining only terms of the first order in d,

$$P_n(\cos\omega')\,d\Omega_1'\,d\Omega_2' = \{P_n(\cos\omega)+[2P_n(\cos\omega)+P_n'(\cos\omega)(\cos\omega-1)] \times(\mathbf{r}_1+\mathbf{r}_2)\mathbf{d}\}\,d\Omega_1\,d\Omega_2. \quad . \; . \; . \quad (8)$$

With this formula one can build up the complete expression (2), and calculate the total first-order counting error, for any given correlation function (1). The accuracy of a high-precision experiment should always be checked by such a calculation, taking account of the source displacements which are likely to arise in the given apparatus. The total error has the general property that it must vanish at $\omega=180°$ because $\mathbf{r}_1+\mathbf{r}_2$ vanishes there. Discussion of a few specific examples (which the reader can easily carry out for himself) shows however that away from 180° it can exhibit almost any sort of behaviour owing to the complicated interplay between the errors in the individual members of (1). Sometimes it is highly symmetrical about $\omega=90°$ and thus will mainly falsify the correlation coefficients ; in other cases it may be rather unsymmetric and then will mainly simulate odd terms in the correlation function which impair the goodness of the least squares fit. In this complex situation it is quite imperative to check on every particular case.

Numerically, the error is in general surprisingly large. An example : correlation function $1-P_3(\cos\omega)$, counters at $\omega=90°$, $d=0{\cdot}02$ and $\mathbf{d}$ directed along the bisector of $\mathbf{r}_1$ and $\mathbf{r}_2$. Here the decentring causes a counting error of 10% ! The example has not been constructed so as to be pathological, but so that the reader can easily verify it.

In the planning of an experiment one often wants to know approximately how large the decentring errors can be, e.g. to see whether they would remain well hidden beneath the sampling errors in the coincidence counts for which a level may have been set by other considerations. An estimation formula for this purpose is readily derived. Suppose that all directions of source displacement are equally likely to occur and that in each direction the length of $\mathbf{d}$ has the same probability distribution. Then the expectation value of $|(\mathbf{r}_1+\mathbf{r}_2)\mathbf{d}|$ is $\bar{d}\cos(\omega/2)$; inserting this into (8) and applying various recurrence formulae one finds that the expectation value of the first-order error in a P_n-term is nowhere greater than

$$(2+n)\bar{d} \quad . \; . \; . \; . \; . \; . \; . \; . \; . \quad (9)$$

in absolute magnitude ; here the n is due to the distortion effect (7) and the 2 to the solid angle effects (5).

§ 3. The Extended Source

The decentred point source can also serve to represent a volume element of a more extended source. Hence the treatment of a finite source size requires only that (8) be multiplied with the volume density ρ of the activity, integrated over the active volume, and divided by $\int \rho \, dV$ to normalize to unit source strength. It is seen that this operation simply replaces $\mathbf{d}$ in (8) by

$$\int \rho \mathbf{d} \, dV \Big/ \int \rho \, dV = \mathbf{d}_0, \qquad \ldots\ldots \quad (10)$$

which is just the vector leading from the centre to the ' centre of gravity ' of the activity distribution.

Thus in the first approximation any extended source behaves as if the whole activity was concentrated in its centre of gravity.

§ 4. The Extended Decentred Source

Frequently the location of this centre of gravity is not known accurately enough to place it precisely at the centre of the apparatus and then the decentring errors as discussed for a point source must be expected to occur.

As a specific example, take a source which has been prepared by the evaporation of a drop of carrier-free solution on a thin backing. The activity distribution will be of about 6 mm diameter, almost invisible and probably somewhat inhomogeneous (cf. Cook 1953), so that we can hardly guess at its centre of gravity with an error of less than 1 mm. If the unit of length (source-to-counter distance) is 10 cm and the correlation function is $1+0{\cdot}3P_2(\cos\omega)$, we have $\bar{d}=0{\cdot}01$ and find from (9) that the expected decentring error may be as large as 0·032. Thus—roughly speaking—it would be empty magnification to count much more than 1000 coincidences at any angle. Now the total error is composed of three parts : the solid angle effects (5) in either counter (40% each) and the distortion effect (7) (20%). If, as usual, one of the two counters remains fixed relative to the source, its solid angle effect will not cause a counting error but only change an irrelevant scale factor so that the expected error will be smaller than 0·019. Still, this much might be inadmissible.

The remedy proposed by Brady and Deutsch (1950), Walter, Huber and Zünti (1950) and Deutsch (1951) is to divide every coincidence count by the corresponding single count in the movable detector. The latter being proportional to the disturbing solid angle, this procedure leaves us with only the distortion effect (which was not considered by these authors). The adequacy of the resulting improvement will depend on given circumstances. In our example the expectation value of the distortion error is $<0{\cdot}006$ which seems sufficiently small for most purposes. However, in correlations of higher order, or even in second-order

correlations of higher anisotropy than in the example, the distortion effects are appreciable. It must be emphasized again that in any case they exhibit a marked dependence on ω which strains the least squares analysis and makes it difficult to find a very small term of higher order —in direct opposition to the requirements of many experiments on mixed transitions.

Apart from the use of very small and accurately centred sources there appears to be only one *safe* way to avoid these difficulties, namely to repeat the experiment with several sources for the same set of detector positions and to add up the data taken at each one position. It follows from the *linear* dependence of (5), (6) and (8) on $\mathbf{d}$ that the first-order errors from the different sources then cancel provided the position vectors of the different centres of gravity add up to zero. More precisely, if we use s sources the expectation value of any first-order error will be decreased by a factor $1/\sqrt{s}$.

Sometimes such a randomized block design offers additional advantages which fully outweigh its cumbersome complexity. The above example refers to an experiment on the successive conversion electrons from the isomeric transition in ^{80}Br (Breitenberger 1954) where there was no other choice because of both the short half-life of 4·5 hours and the presence of small scattering effects in the source backings. Measuring on eight sources allowed enough data to be accumulated; placing the sources about the axis of rotation of the apparatus like the compartment walls in a capsule of poppy randomized the anisotropy of the scattering effects; dividing the sum of the coincidence counts by the sum of the single counts in one of the detectors removed one solid angle effect and corrected automatically for source decay as well as for counting time. The remaining decentring error was then $<0{\cdot}019/\sqrt{8}=0{\cdot}007$ which seemed entirely satisfactory because all scattering effects had been brought under control at the same time.

§ 5. The Second Approximation

When the calculations are carried to terms in d^2 the formulae become very complicated. Some useful results will be quoted without proof.

The dependence on ω is much more pronounced in the second order than in the first. The second-order effects are always greatest at $\omega=180^\circ$ (where the first-order effects vanish). Numerically, they are usually rather small, but the second-order distortion error increases very rapidly with n so that caution is necessary when correlation coefficients of higher order are to be measured accurately.

Under the conditions that led to (9) the expectation value of the total second-order error in a P_n-term is nowhere greater than

$$4(n+1)^2\overline{d}^2/3 \quad . \quad . \quad . \quad . \quad . \quad . \quad . \quad . \quad . \quad (11)$$

in absolute magnitude. This formula holds for a point source only: extended sources do not behave like point sources in the second

approximation and thus cannot be treated in terms of an equivalent point source.

For a line source of length $2a$ which is perfectly centred and perpendicular to both $\mathbf{r}_1$ and $\mathbf{r}_2$, there is a second-order error of magnitude nowhere greater than

$$(2n^2+2n+3)a^2/3 \quad . \quad . \quad . \quad . \quad . \quad . \quad . \quad (12)$$

in a P_n-term. For a spherical, homogeneous and perfectly centred source of radius a the limit becomes

$$4(n+1)^2a^2/5\,; \quad . \quad . \quad . \quad . \quad . \quad . \quad . \quad (13)$$

if the activity density falls off linearly to zero at $r=a$, replace 4/5 by 8/15. Other source shapes and positions lead to unwieldy formulae.

The limits (11)–(13) are very close near 180° ; the error is negative there for even n and positive for odd n. Setting $n=0$ in the formulae one obtains the contribution from the two solid angle effects ; everything else is distortion effect. It is seen that the latter increases faster than n^2 and far exceeds the combined solid angle effects.

When data from several sources are pooled to minimize the first-order errors the second-order errors do not cancel at the same time. The remaining part can be estimated safely by means of (12) or (13). In the example of § 4 the fan-like arrangement of eight sources is closely similar to a combination of a spherical source with a line source, both of which have $a<0{\cdot}04$, and then the second-order error must be well below 0·005. Note that the presence of this residual second-order effect makes it impracticable to increase the number of sources indefinitely to achieve highest precision.

§ 6. Extended Detectors

The finite angular resolution of *flat* detectors (e.g. thin crystals, counters with an entrance window) is taken into account by integrating (8) with respect to ω over the sensitive detector areas. Under the integration the first term transforms in a way which has been calculated for square counters (Chatterjee and Saha 1953) and circular counters (Breitenberger 1953) of constant sensitivity, and can also be determined semi-empirically (Church and Kraushaar 1952 ; cf. Lawson and Frauenfelder 1953). The next term, which depends on $\mathbf{d}$, would transform in a very complicated manner ; the upper limit for the expected first-order error does however not depend on angle and therefore remains unaltered. The same goes for the second-order error. Hence with flat counters we can correct for angular resolution as if the source was a perfectly centred point, and subsequently estimate the decentring errors as if the counters were infinitely small.

In the case of massive counters, such as thick crystals used for γ-ray detection, the situation is much more complicated due to an additional effect. A decentred point source sees the crystal sideways ; hence the

data are distorted as if the crystal was ' smeared out ' beyond its side faces. Of course it is then impossible to correct for angular resolution as if the crystal had its actual size (e.g. with the formulae given by Rose 1953). A simple and efficient remedy is the use of circular lead diaphragms in front of the crystals (Steffen 1953 b) which act like entrance windows and define a sensitive area as for flat counters. It may also be possible to determine the smearing effect empirically, in a way much as Lawson and Frauenfelder (1953) have done, but using a displaced point source.

Lastly it should be mentioned that none of the preceding conclusions is altered substantially when the two detectors are at unequal distances from the source. If $\mathbf{r}_1$ and $\mathbf{r}_2$ are not unit vectors, factors $1/|\mathbf{r}_1|$ and $1/|\mathbf{r}_2|$ appear in several places in (8); their only effect is a slight change in the formulae for the error limits which can safely be neglected as long as $|\mathbf{r}_1|$ and $|\mathbf{r}_2|$ do not differ by a factor of, say, more than 2.

Acknowledgment

This study was written while the author held a British Council Scholarship.

References

Aeppli, H., Frauenfelder, H., and Walter, M., 1951, *Helv. Phys. Acta*, **24,** 335.

Biedenharn, L. C., and Rose, M. E., 1953, *Rev. Mod. Phys.*, **25,** 729.

Brady, E. L., and Deutsch, M., 1950, *Phys. Rev.*, **78,** 558.

Breitenberger, E., 1953, *Proc. Phys. Soc.* A, **66,** 846; 1954, to be published in *Proc. Phys. Soc.*

Chatterjee, S., and Saha, A. K., 1953, *Z. Physik*, **135,** 141.

Church, E. L., and Kraushaar, J. J., 1952, *Phys. Rev.*, **88,** 419.

Cook, C. S., 1953, *Nucleonics*, **11,** No. 12, 28.

Deutsch, M., 1951, *Rep. Progr. Phys.*, **14,** (London: Physical Society), p. 196.

Hayes, J. G., and Vickers, T., 1951, *Phil. Mag.*, **42,** 1387.

Klema, E. D., and McGowan, F. K., 1952, *Phys. Rev.*, **87,** 524; 1953, *Phys. Rev.*, **92,** 1469.

Lawson, J. S., and Frauenfelder, H., 1953, *Phys. Rev.*, **91,** 649.

Price, P. C., 1954, *Phil. Mag.*, **45,** 237.

Rose, M. E., 1953, *Phys. Rev.*, **91,** 610.

Steffen, R. M., 1953 a, *Phys. Rev.*, **89,** 665; 1953 b, *Ibid.*, **90,** 321; 1953 c, *Ibid.*, **91,** 443.

Steffen, R. M., and Zobel, W., 1952, *Phys. Rev.*, **88,** 170.

Walter, M., Huber, O., and Zünti, W., 1950, *Helv. Phys. Acta*, **23,** 697.

LIX. *Magnetic Viscosity in Precipitation Alloys: FeNiAl, Fe_2NiAl and Alnico*

By J. H. Phillips, R. Street and J. C. Woolley
The University, Nottingham*

[Received January 20, 1954]

Abstract

Investigations on the effects of various heat treatments on magnetic viscosity in FeNiAl, Fe_2NiAl and Alnico are described. The heat treatments adopted were (*a*) quenching at different rates from the solution temperature, (*b*) annealing of water quenched specimens at different temperatures in ranges where precipitation takes place and (*c*) annealing of specimens which have been cooled at different rates from the solution temperature. The results are interpreted in terms of the thermal activation theory of magnetic viscosity, Néel's disperse field theory and Geisler's theory of coherency hardening. It is shown that magnetic viscosity methods can be applied to investigate precipitate and magnetic structures of the order 10^{-17} cm^3 in volume, which are below the limit of resolution of more conventional techniques. Specimens of alnico and Fe_2NiAl were suitably treated to enable magnetic viscosity measurements to be made at temperatures up to 900°K. The results obtained together with those previously reported show that the thermal activation theory is valid at least over the temperature range 90°K to 900°K. The variation of the coercive force of these alloys as a function of temperature is also considered.

§ 1. Introduction

In previous papers (Street and Woolley 1949 and 1950, Street, Woolley and Smith 1952 a and b, which will be referred to below as I, II, III and IV respectively) the phenomenon of magnetic viscosity occurring in alnico, a permanent magnet alloy, was investigated. It has been shown that in a constant applied magnetic field the intensity of magnetization, I, varies as a function of time, t, according to the law

$$I = S_0 \ln t + \text{const.} \quad . \quad . \quad . \quad . \quad . \quad . \quad . \quad (1)$$

where t is measured from the instant the applied field becomes fixed. S_0 is independent of time and varies with applied field (for example, see fig. 9). Within the temperature range 90°K to 500°K, S_0 is linearly related to the absolute temperature, T, of the specimen. This result is

*Communicated by Professor L. F. Bates, F.R.S.

in agreement with a formal theory of magnetic viscosity, given in I and IV, based on the concept of thermal activation of metastable magnetization processes. The theory predicts that

$$S_0 = \bar{\imath} p k T, \qquad \ldots\ldots\ldots \quad (2)$$

where $\bar{\imath}$ is the mean increase, per activation, in the intensity of magnetization of the specimen and $p\,dE$ is the number of metastable states having activation energies between E and $E+dE$. Good agreement is obtained between the theory and the experimental results if it is assumed that p is effectively independent of E. Over the range of temperature mentioned above the experimental result that S_0 is directly proportional to T indicates that $\bar{\imath}p$ is a constant independent of temperature.

Investigations of magnetic viscosity occurring in specimens subjected to variable magnetic fields are described in IV. The results obtained are accounted for in terms of the theory by assuming that the change in activation energy, ΔE, of a metastable state is linearly related to a small change in internal magnetic field, ΔH_i, i.e. $\Delta E = q \,.\, \Delta H_i$ where q is a constant. Experimental methods for the determination of q* have been described and it has been shown that from 90°K to 500°K q is independent of temperature and to a good approximation is constant over wide ranges of applied field. By considering simple models of the magnetization processes it has been found possible (see IV) to relate q to the volume of material which is involved in a single activation. For the alnico specimen considered this volume is of the order 10^{-17} cm^3. This point will be discussed further below.

Alnico is a typical member of a group of permanent magnet materials based on the ternary alloy Fe_2NiAl. Metallurgically Fe_2NiAl is single phase at temperatures of the order 1200°C but at room temperature the equilibrium state is two phase. Thus, if the alloy is quenched rapidly to room temperature from the single phase state at 1200°C, equilibrium is not reached and the material contains an incipient precipitate phase. Precipitation may be increased by maintaining the material at a temperature of about 600°C for varying periods of time, and this is accompanied by changes in the values of the coercivity and other magnetic parameters of the alloy (Hoselitz 1952). There is an optimum heat treatment for Fe_2NiAl and other precipitation permanent magnet alloys, which produces optimum magnetic properties and which, in terms of nucleation theory (Fisher, Hollomon and Turnbull 1948, Hollomon and Turnbull 1953), corresponds to the development of a particular distribution in the size and number of nuclei of the precipitate. Heidenreich and Nesbitt (1952) have investigated by electron microscope methods a permanent magnet material of the alnico type (Alnico V)

* The quantity which is directly calculated from the experimental results is q/kT. For convenience, the measurements of q given below will usually be expressed as this ratio.

subjected to various types of heat treatment. It was shown to be impossible to resolve the precipitate occurring in material subjected to optimum heat treatment but it was estimated by extrapolation methods that the precipitate was in the form of rods of dimensions approximately 75–100 Å by 400 Å long, i.e. a volume of about 3×10^{-18} cm^3. Because of the small differences between the lattice parameters of the matrix and the precipitate in alnico type alloys, structures on this small scale are below the limit of resolution of x-ray techniques ; conventional methods of magnetic investigation, e.g. Bitter figures and Barkhausen discontinuities, are insufficiently sensitive by many orders of magnitude (Bozorth 1951, Bush and Tebble 1948). However, the volumes of material involved in magnetic viscosity in these alloys are of approximately the same order as that derived by Heidenreich and Nesbitt. Consequently, magnetic viscosity investigations were made on three precipitation alloys with the object of examining the magnetization processes in these materials. It was also hoped that the investigations might be useful in the elucidation of the phenomenon of precipitation, especially in the early stages of the process.

§2. Method

The intensity of magnetization of the specimen was measured by a conventional magnetometric method using a flux-gate or saturated core magnetometer placed in the Gauss B position. The system was made accurately linear by introducing a high degree of negative feedback, the field intensity at the flux-gate and hence the intensity of magnetization of the specimen, being measured in terms of the feed-back current. The apparatus and the experimental procedures are described more fully in IV. However, the work described here was greatly facilitated by the incorporation of a high speed recording potentiometer to measure the feed-back current. With this addition the sensitivity of the apparatus was also greatly increased, the maximum sensitivity being about 2×10^{-5} oersted per mm scale deflection.

§3. Specimens

The three types of precipitation alloys investigated were Fe_2NiAl, FeNiAl and alnico of approximate percentage composition Fe, 54 ; Al, 10 ; Ni, 18 ; Co, 12 ; Cu, 6 by weight. The specimens were in the form of cylindrical rods about 30 cm long and 0.6 cm diameter. The rods were left in the rough cast state owing to the mechanical difficulties of producing accurately cylindrical rods of these brittle materials. All heat treatment of the specimens was carried out *in vacuo* to reduce oxidation.

§4. Results

The investigations may be divided into three categories depending on the type of heat treatment. In the first category the specimens were cooled at various rates from the solution temperature of 1250°C. The

influence on magnetic viscosity of the different states of precipitation thus produced was then examined. In the second group of experiments the influence of various annealing treatments was investigated. Before annealing, each specimen was quenched in water after being heated for about 20 minutes at 1250°C. Such rapid cooling effectively retains the single phase state characteristic of the solution temperature. The state is unstable at the subsequent annealing temperature and it was thus possible to follow the changes in magnetic viscosity consequent upon the increasing precipitation of the second phase produced by annealing

Fig. 1

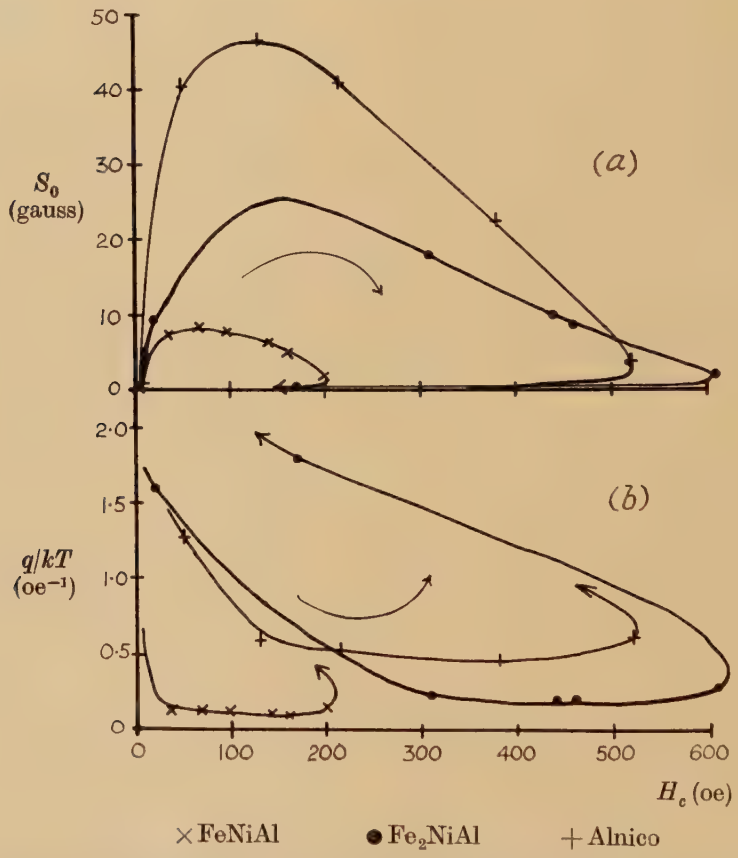

Variation of S_0 and q/kT as functions of H_c for specimens cooled from 1250°C at different rates. The arrows indicate direction of decreasing rate of cooling.

for various periods of time. In the third category, measurements were made on specimens which had been quenched at various rates from 1250°C and then annealed. In these experiments it was therefore possible to investigate the effects associated with the development of the precipitate starting from different initial conditions.

It should be noted that S_0 in eqn. (1) applies to a specimen of zero demagnetization factor, D. As shown in IV if $D \neq 0$ the change of intensity of magnetization is $\Delta I = S \ln t + \text{const.}$ where S is related to S_0 by

$$S_0 = \frac{S(1+D\chi_{rev})}{(1-D(qS/kT))}. \quad \ldots\ldots\ldots \quad (3)$$

χ_{rev} is the reversible magnetic susceptibility at the point of measurement. Where possible, the values of S_0 have been calculated from the observed values of S using eqn. (3).

4.1. *Variable Rates of Cooling from* 1250°C

The methods used for cooling the specimens from 1250°C together with the time required to cool between the limits of 800°C and 600°C are shown in table 1. The results of the measurements of S_0 and q/kT

Fig. 2

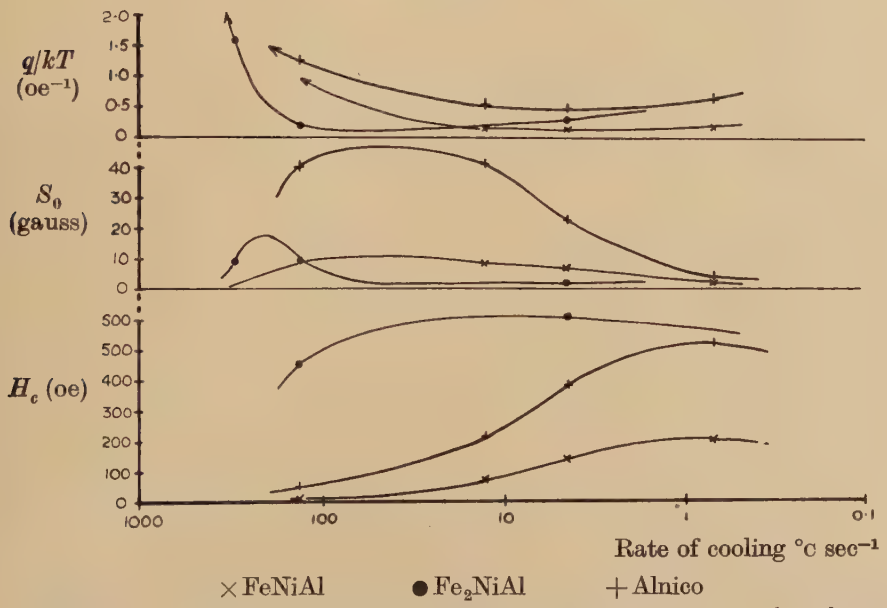

× FeNiAl ● Fe_2NiAl + Alnico

Variation of S_0, q/kT and H_c as functions of the average rate of cooling of specimens between 800°C and 600°C.

Table 1

Method of quenching from 1250°C	Time taken to cool from 800°–600°C
Water	<1 sec
Oil	1·5 ,, (approx.)
Air-blast	15·5 ,,
Air	43 ,,
Kieselgur	285 ,,

as functions of the coercive force, H_c, and S_0, q/kT and H_c as functions of the average rate of cooling between 800°C and 600°C are plotted in figs. 1 and 2 respectively. The higher values of coercive force are not

strictly true values since it was not always possible to apply the technically saturating field (which is usually taken as $5 \times H_c$) since the maximum field given by the solenoid used was 1300 oersted. However, subsidiary experiments to determine how S_0 varied with the maximum field applied during the cycle showed that the general forms of the curves are not seriously in error.

Fig. 3

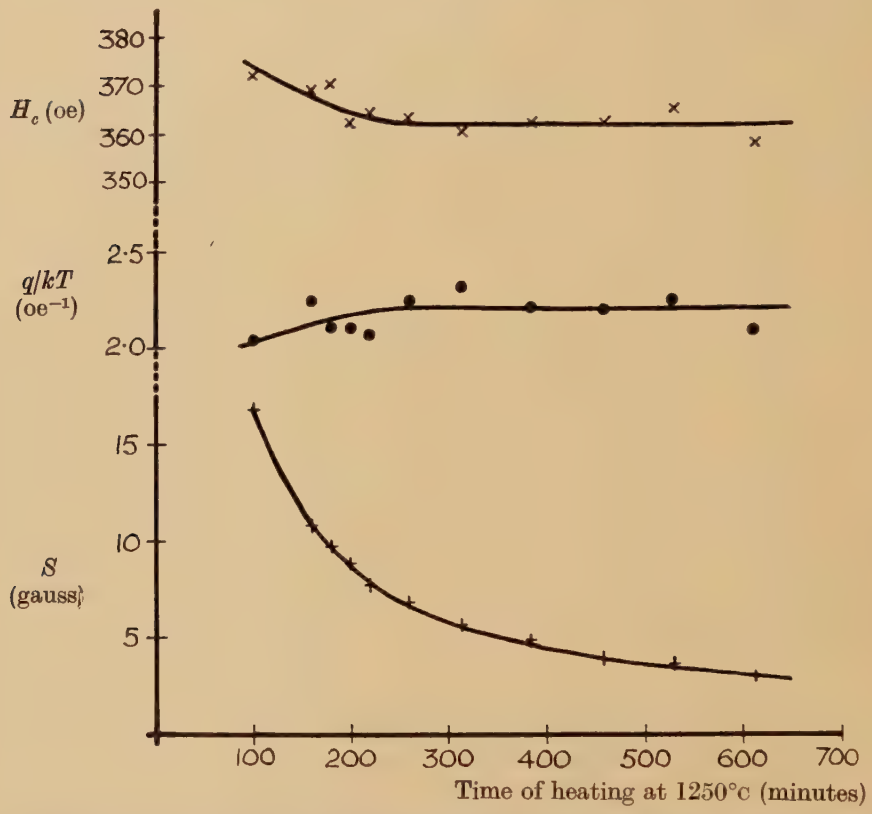

Variation of S, q/kT and H_c as functions of time of heating at 1250°c for an embrittled alnico specimen.

In the case of one specimen of alnico it was found that prolonged heating at and quenching from 1250°c led to a deterioration in its condition due to embrittlement and cracks developed perpendicular to the length of the specimen. The effects of this on the magnetic properties were investigated by repeatedly heating the specimen at 1250°c, cooling in air and then determining q/kT, S and H_c. The results obtained are shown in fig. 3. H_c and q/kT are seen to be substantially independent of the time of heating at 1250°c but S varied markedly. These observations are in complete agreement with the theoretical predictions in IV, which show that q/kT, as well as H_c, are independent of D whereas

S is critically dependent thereon, the progressive development of cracks perpendicular to the axis results in an increasing effective demagnetization factor. It was established that none of the other specimens suffered in this way from embrittlement during the course of the measurements.

Fig. 4

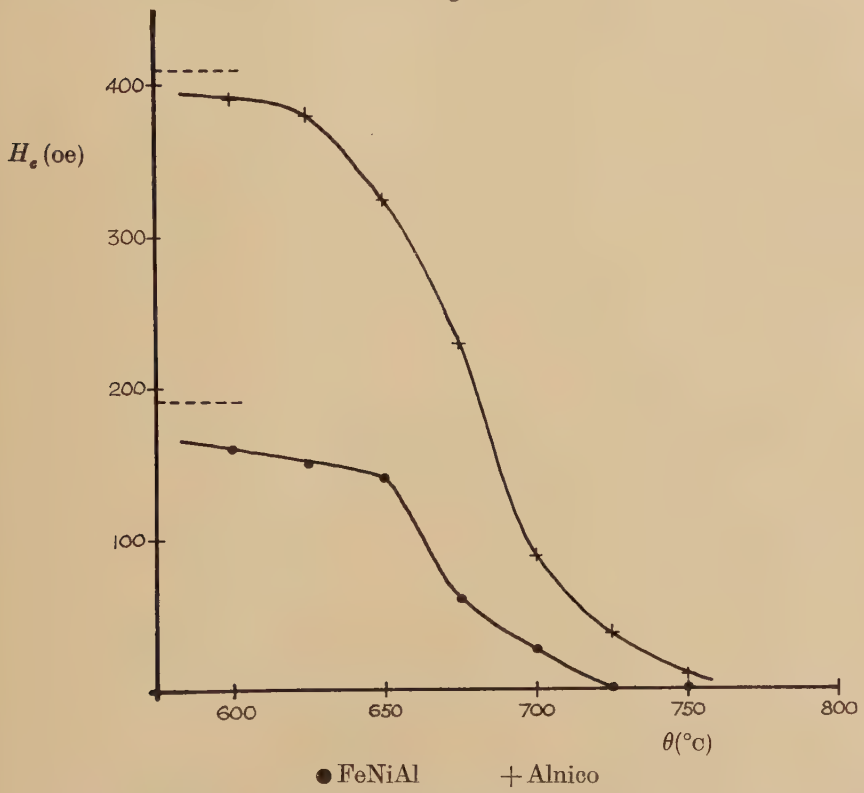

Values of H_c obtained when specimens, cooling in air from 1250°C, are quenched in water at various temperatures, θ. The dotted lines indicate values of H_c obtained on cooling in air to room temperature.

4.2. *Annealing at Different Temperatures*

In this set of experiments the specimens were initially quenched in water after being heated at 1250°C for 20 minutes. They were then annealed at various temperatures for varying periods of time ; suitable temperatures were determined in the following way. A specimen was heated to 1250°C, allowed to cool in air and then quenched in water when the temperature of the specimen reached a predetermined value, θ. The measured values of H_c of specimens of alnico and FeNiAl as a function of θ over the range 800°C–600°C are shown in fig. 4, together with the result for θ=room temperature. It is obvious that most of the metallurgical processes which determine the value of H_c and

other structure sensitive magnetic properties occur within the range 750°C–620°C. The rate of cooling below 620°C has little influence on these processes. Using these results, representative annealing temperatures of 800°C, 715°C and 610°C were chosen. From fig. 4 it is to be expected that the rate of cooling from the annealing temperature to room temperature, after each period of anneal, would only be unimportant for annealing temperatures of 620°C and below. At higher annealing

Fig. 5

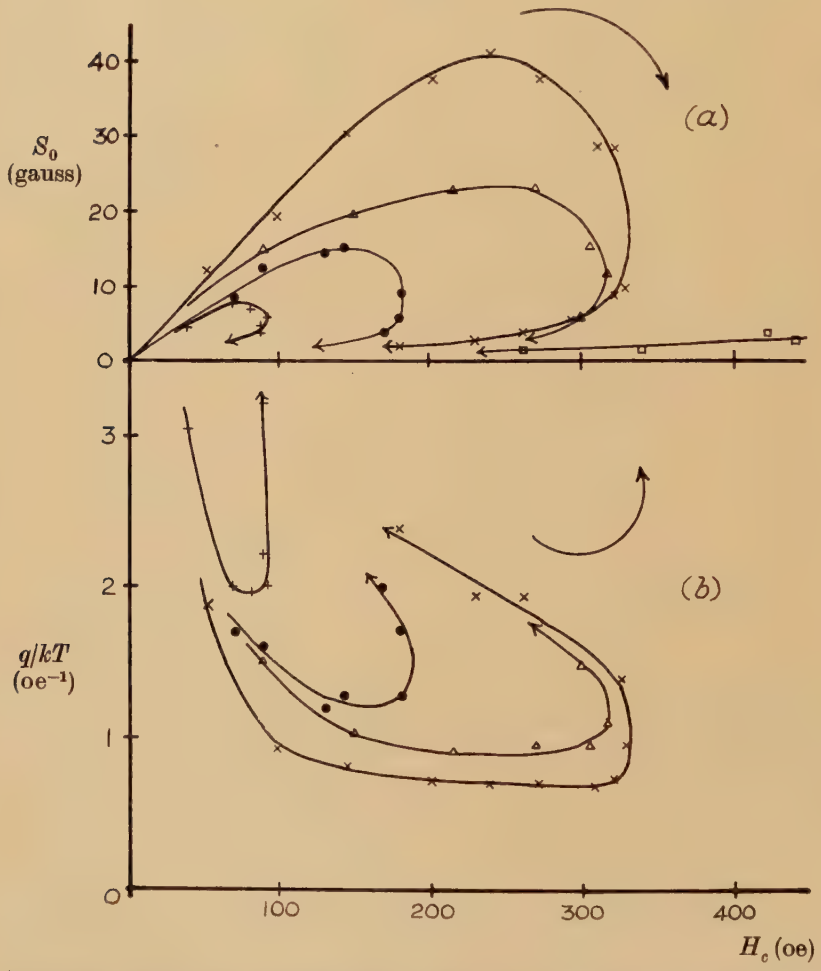

Variation of S_0 and q/kT as functions of H_c for alnico specimens annealed after an initial water quench from 1250°C. The arrows indicate direction of increasing time of anneal.

Symbol	+	●	△	×	□
Temperature of anneal	800°C	715°C	610°C	715°C	800°C
Quench after each annealing period	Water	Water	Water and Air	Air	Air

temperatures the method of cooling to room temperature after each period of anneal is a significant factor in the magnetic development. In figs. 5 and 6 the values of q/kT and S_0 produced by successive annealing of specimens of alnico and FeNiAl are plotted as functions of H_c. Results of two sets of experiments are shown; in one set cooling to

Fig. 6

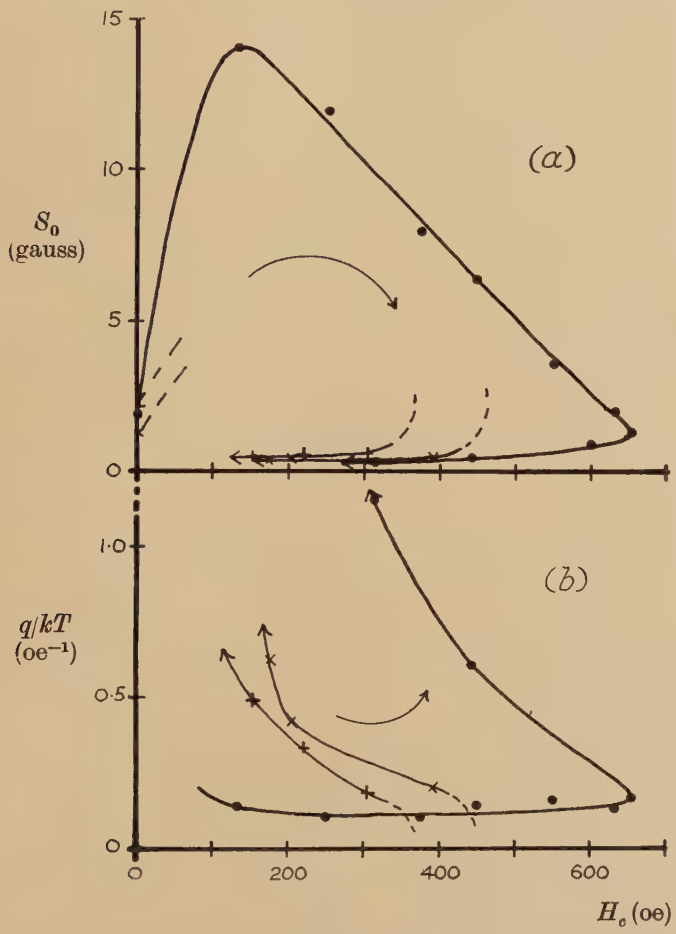

Variation of S_0 and q/kT as functions of H_c for FeNiAl specimen annealed after an initial water quench from 1250°C. The arrows indicate direction of increasing time of anneal.

Symbol	+	●	△
Temperature of anneal	725°C	615°C	725°C
Quench after each annealing period	Water	Water and Air	Air

The intermediate regions for the anneals at 725°C were not obtainable owing to the high reaction rate in FeNiAl. The first points shown correspond to annealing periods of 1 minute only at 725°C.

room temperature, after each annealing period, was achieved by water quenching and in the other by air quenching.

In fig. 7 are shown typical results of values of q/kT, S_0 and H_c plotted as functions of time of anneal at 610°C for an alnico specimen. Comparison with fig. 2 shows that the maximum value of H_c is again reached after the maximum in S_0 and the minimum in q/kT. This was true for all the annealing treatments performed in this group of experiments.

Fig. 7

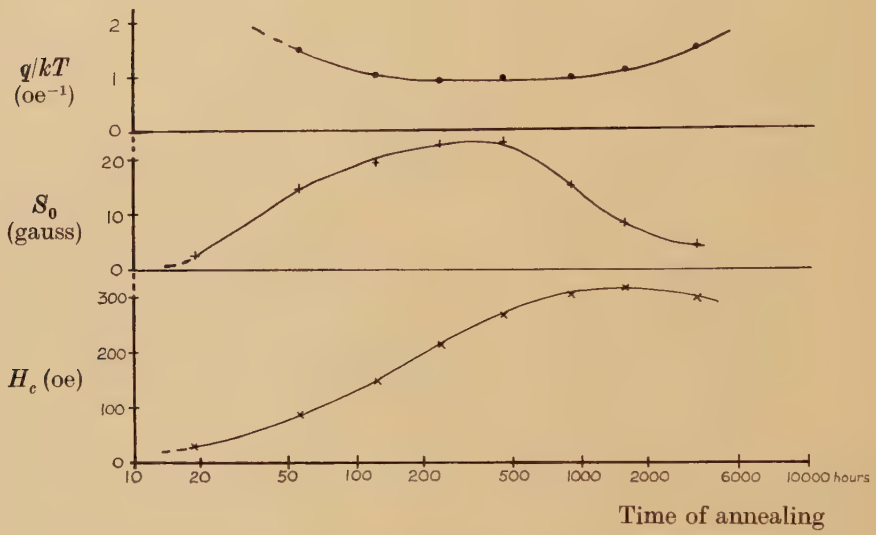

Variation of S_0, q/kT and H_c as functions of time of anneal at 610°C for an alnico specimen initially water quenched from 1250°C. Specimen air cooled after each annealing period.

4.3. *Annealing after Variable Rates of Cooling from the Solution Temperature*

For the experiments described in § 4.2, after water quenching from 1250°C, the specimens were effectively in the single phase state, and subsequent annealing induced precipitation of the second phase. In this section, results are described for annealing treatments on specimens with variable initial states of precipitation produced by the quenching experiments of § 4.1. The most complete investigation was carried out using specimens of alnico treated in this way and then annealed at 715°C for various periods of time, the specimens being air-cooled after each annealing period. The results obtained are shown in fig. 8, and the general pattern of behaviour shown in these graphs was observed in similar experiments at different annealing temperatures and with water cooling as well as air-cooling after each annealing period. It is apparent from fig. 8 that the properties of the specimens after long periods of

annealing are independent of their initial condition, which is presumably a reflection of the fact that whatever the initial state, the final state of precipitation is dependent only on the temperature of anneal.

Fig. 8

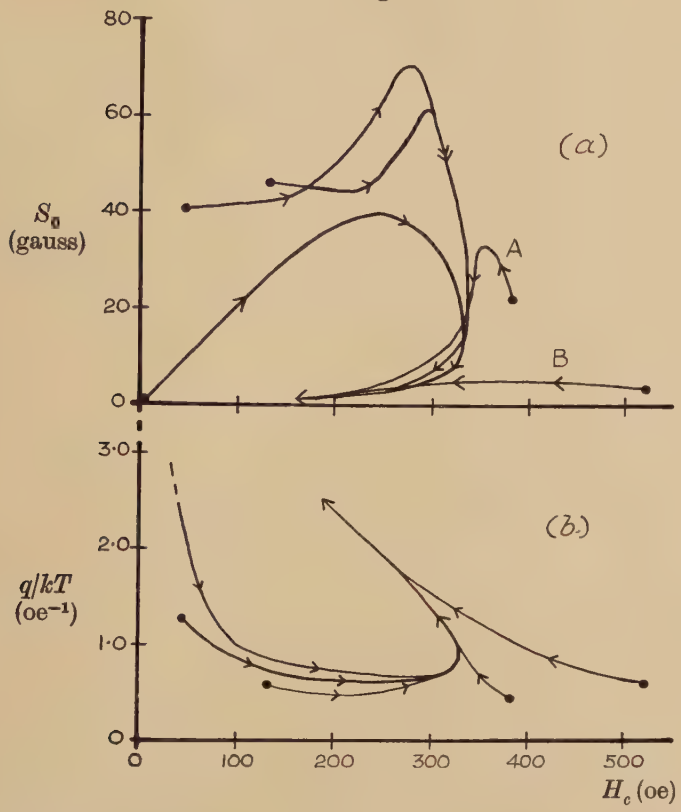

Variation of S_0 and q/kT as functions of H_c for alnico specimens, quenched initially from 1250°C at different rates of cooling, and then annealed at 715°C. Specimens air cooled after each annealing period. The arrows indicate increasing time of anneal. The curves marked A and B are referred to in § 5.

§ 5. Discussion

Before the results presented here can be rationalized it is necessary to have detailed information, both of the mechanisms responsible for the magnetic properties of the materials studied, and also of the metallurgical state of the specimens as a function of heat treatment. It is unfortunate that in the regions of interest here, completely satisfactory and tractable theories of the magnetization processes do not exist, although a number of theories have been published, e.g. the single domain theory of Stoner and Wohlfarth (1948) and the ' disperse field ' theory of Néel (1946). The detailed metallurgical aspect is also obscure. The work of Heidenreich and Nesbitt, discussed in §1, shows that we are here mainly

concerned with processes occurring in the very early stages of precipitation, about which little is at present known. However, it has been found possible to account for the broad features of the experimental results in terms of Néel's theory of magnetization processes and the work of Geisler (1949, 1953) on coherency hardening.

In the disperse field theory it has been shown that in a ferromagnetic material there may be regions of dispersion in which the divergence of the spontaneous magnetization vector, div $\mathbf{J}_s$, is non-zero. Such a region within a domain will function as a magnetic unipole but when intersected by a boundary wall a magnetic dipole will be created and there may be a diminution in the local magnetostatic energy. For low values of applied internal field, domain structures in which boundary walls intersect regions of dispersion will have minimum energy. In order to release the boundary walls it is necessary to supply sufficient magnetostatic energy to convert the dipole into a unipole ; the critical field required is interpreted as the coercive force. Regions of dispersion may be produced, for example, by the changes in magnitude of the magnetization vector caused by cavities and inclusions, or by fluctuations in the direction of the magnetization vector due to internal strains. Of particular interest here are the local internal strains of large magnitude which may be associated with coherent precipitation ; for Geisler (1953) has shown that there is an empirical relation between coercive force and the disregistry of the precipitate and matrix for a variety of ferromagnetic precipitation alloys.

Before the coercive force point, domain walls will be prevented from moving by regions of dispersion, but even when the applied field is constant, thermal agitation may provide sufficient energy to release the wall which will then move to a different position of equilibrium giving rise to magnetic viscosity. The volume of material which is affected in this way is the effective volume over which div $\mathbf{J}_s \neq 0$, and as shown in IV this volume is related to the parameter q. $\bar{\imath}$, the average increase in intensity of magnetization caused by a successful activation is a function of the volume through which the wall moves after being released and of the angle between the magnetization vectors of the domains separated by the wall.

These ideas may now be applied to the present experimental results. For all the materials studied, it was found that rapid quenching from 1250°C, which inhibits precipitation, produces low values of H_c. In this state, large localized internal strains due to precipitation do not exist and it is therefore likely that the coercive force is determined primarily by the relatively small internal strains, developed by the rapid quenching, which are not highly localized. Thermal activation in relatively large volumes must occur if magnetic viscosity is to proceed and this necessarily implies that q for these materials in this condition will be relatively large, as was in fact observed (see fig. 1(*b*)). In this state although it might be expected that $\bar{\imath}$ would be large, the distribution function, p, of the

domain activation energies, will be small. This is reflected in the experimental fact that $S_0 \propto \bar{\imath}p$ is small (fig. 1(*a*)). Subsidiary experiments showed that these materials did in fact exhibit the Barkhausen effect under these conditions, i.e. domain processes involving volumes of at least 10^{-10} cm^3 must occur during magnetization. Barkhausen discontinuities, however, could not be detected in materials developed to have high coercive force. Further examination of rapidly quenched specimens by Bitter figure techniques proved that the process of magnetization was one of 180° boundary wall movement.

Growth of the precipitate phase, either by slower cooling from 1250°C or by annealing, will take place at a large number of nuclei. As a result, localized coherent strains will appear in the lattice structure, and become of increasing and eventually predominating importance compared with the non-localized strains and the effects of the precipitate considered as inclusions. Thus the coercivity will increase, accompanied by a decrease in the volume of material in which activation occurs. As H_c increases from the initial rapidly quenched state, the q value therefore decreases and this is shown by the results plotted in fig. 1(*b*). Since the number of nuclei impeding boundary wall movement increases with increasing precipitation, it seems likely that $\bar{\imath}$ will decrease. The observed increase in S_0 with H_c under these conditions (fig. 1(*a*)) indicates that the number of domain processes available for activation, which in turn is a measure of p, increases more rapidly than $\bar{\imath}$ decreases. In order to determine quantitatively the variation of S_0 with H_c, detailed information of the development, growth and distribution of nuclei is required. Since this is not available, it is only possible to infer from the experimental results that at the maximum S_0 in the (S_0, H_c) curves, p must be increasing at the same rate as $\bar{\imath}$ decreases and beyond this point either p ceases to increase, or the decrease in $\bar{\imath}$ predominates. The S_0 value then steadily decreases in magnitude.

With increasing development of the precipitate, H_c increases towards its maximum value while q passes through a broad minimum. The increase in H_c is accounted for by the progressive increase in the effect of the coherency strains due to growth of precipitate nuclei. This will continue until a maximum in H_c is reached, presumably corresponding to the state just before the precipitate begins to break away from the matrix, becoming incoherent and resulting in the relief of the large coherency strains. If the saturation intensity of magnetization of the precipitate and matrix are largely different, then it is conceivable that the incoherent precipitate nuclei will function as inclusions as visualized in Néel's theory. In any case, however, the effect of these inclusions in impeding boundary wall movements in the matrix will disappear when the nuclei exceed a critical size. Thus in over-aged material the magnetization processes will be governed by non-localized regions of dispersion similar to those effective in the rapidly quenched condition. This would account for the observed increase in q on over-ageing.

The above explanation covers the general variation of the magnetic viscosity parameters investigated. Differences in those parameters for the various materials and heat treatments employed must be due to their composition and the metallurgical processes involved. Details of the latter are not available, but using the above considerations it is possible to explain qualitatively the observed results. In fig. 1(*b*) the minimum q values are related as described above, to the volumes of the precipitate nuclei in the coherent state, and as expected, FeNiAl has the smallest value consistent with the smallest fraction of precipitate in this alloy. The precipitate particles produced by the quenching treatments of § 4.1 will vary in composition, depending on their temperature of formation, and this will lead to a distribution in coherency strains due not only to size and number but also to composition of the particles. This may account for the subsequent difference between the quenching and annealing curves.

The results of § 4.2 reveal the effects of differences in disregistry produced by the various compositions of the two phases which are stable at the different annealing temperatures. As expected from fig. 4, the rate of cooling from the higher annealing temperatures markedly affects the results obtained ; additional development occurs during the cooling to room temperature after each period of anneal. It is of interest to note that for the annealing treatments followed by water quenching, which will give the most accurate indication of the changes due solely to annealing, the maximum value of H_c is least for the highest annealing temperature. This correlates with the fact that the disregistry will be smallest for the two phases produced at this temperature. The larger values of $S_{0\,\max}$ and $H_{c\,\max}$ obtainable with the annealing as compared with the quenching treatments for FeNiAl are probably due to the relatively ' long distance ' diffusion necessary in this alloy for the small fraction of precipitate to grow. This requires a longer period of time than that available in the quenching treatments.

In § 4.3, the annealing treatment results from different initial states are as might be expected. Whatever the distribution of size, number and composition of precipitate particles produced in the initial quenching, annealing develops the precipitate of composition corresponding to the equilibrium phases at the particular annealing temperature, so that eventually all specimens reach a similar state as shown in fig. 8. This may involve re-solution of the particles of compositions corresponding to temperatures lower than that of the annealing temperature and this is suggested particularly by the behaviour of curves A and B in fig. 8 (*a*).

Confirmation and further elaboration of these qualitative ideas must await more detailed knowledge of the magnetization and metallurgical processes involved. In view of the difficulties associated with the theoretical interpretation, it was hoped that further elucidation of the problem would be afforded by an extension of the measurements, reported in IV, on the variation of S and S_0 with absolute temperature. At higher

temperatures, the spontaneous magnetization should vary significantly in accordance, at least approximately, with the Law of Corresponding States. There is an upper limit to the temperature of measurement set by the necessity of avoiding further metallurgical changes taking place during the course of the measurements. These changes were minimized as far as possible by subjecting the specimens used to comparatively long periods of annealing before commencing measurements. The heat treatments were chosen to give suitable values of H_c and S_0.

Measurements were made on specimens of alnico and Fe_2NiAl, using a non-inductively wound, d.c. electrically heated furnace inside the solenoid. The results are shown in fig. 9, on which are plotted values of S

Fig. 9

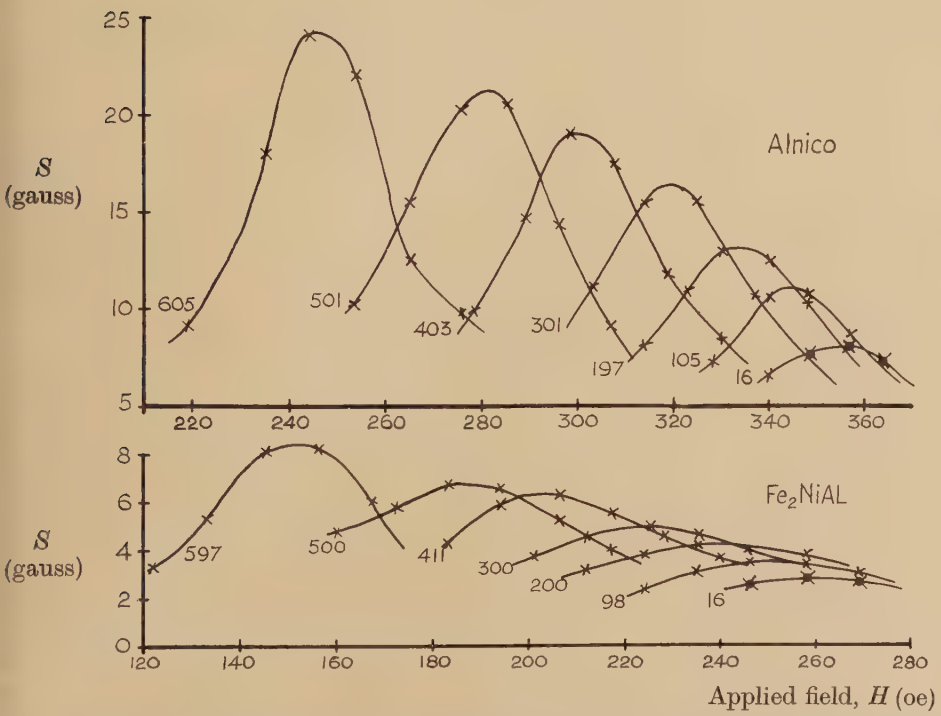

Values of S plotted as functions of the applied field, H, at different temperatures. The temperature of measurement in °C is shown on each curve. The points, shown ●, were values obtained on recooling to room temperature.

as functions of the applied field, H, at different temperatures. Also shown are values of S and H on recooling to room temperature. The differences from the initial values are very small, and thus it was shown that no significant metallurgical changes had occurred during the measurements. The highest temperatures recorded on fig. 9 represent the upper limit for measurement, since during measurements at higher temperatures metallurgical changes did take place. This was revealed by the large

differences in S and H_c on measuring again at room temperature. Within the accuracy of the measurements, the value of q for alnico was a constant, equal to $3{\cdot}74\times10^{-14}$ ergs oe^{-1},* and independent of temperature. However, in the case of Fe_2NiAl, it was found difficult, particularly at the higher temperatures, to obtain reproducible values of q and hence the values of S_0 calculated from eqn. (3) were not sufficiently precise.

Fig. 10

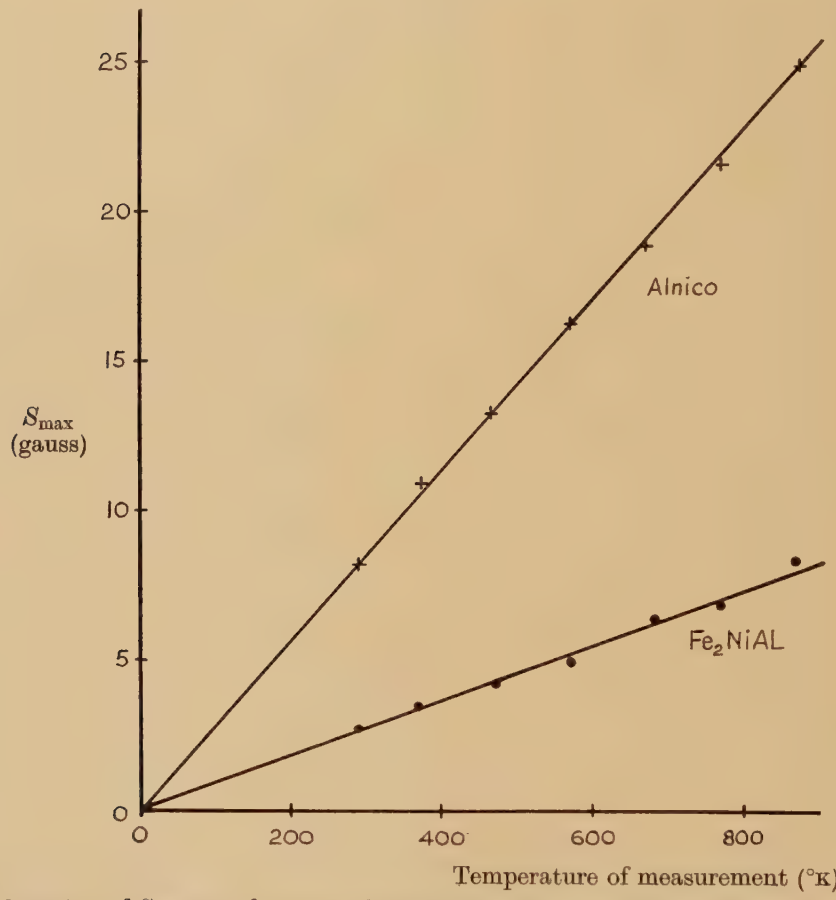

Variation of S_{max} as a function of absolute temperature for specimens of alnico and Fe_2NiAl.

Because of this, the maximum values of S, obtained from fig. 9, have been plotted against absolute temperature, T, in fig. 10. It can be seen that S_{max} is a linear function of T up to about 900°K for both materials. If S_{max} is a linear function of T, it is to be noted that $S_{0\,max}$ is also a linear

* As shown in IV, assuming magnetization to proceed by 180° boundary movements, the volume of material which undergoes thermal activation is $q/2J_s$. Therefore in this case this volume is approximately 2×10^{-17} cm^3.

function if q is constant and the term $D\chi_{rev}$ in the numerator of eqn. (3) is constant or small compared with unity. For both specimens $D\chi_{rev} < 0{\cdot}02$ and thus it is reasonable to infer from the linearity of the (S_{max}, T) graph for Fe_2NiAl that q remains constant for this material also. Combination with the results given in IV indicates that S_0 is a linear function of T over the range 90°K to 900°K and that over this range q is approximately constant.

In view of the fact that the Curie Temperature of Fe_2NiAl is about 1000°K (Sucksmith 1939) and that the spontaneous magnetization for this material decreases by about a factor 0·7 on heating from 90°K to 900°K, it is at first sight surprising that S_0 $(=\bar{\imath}pkT)$ is linearly dependent on T. A possible explanation of this is to be found in the Néel theory outlined above. The unipolar volume density in a region of dispersion, not intersected by a boundary wall, is given by div $\mathbf{J}_s$. To a first approximation, which neglects the detailed nature of the cause of the dispersion, the

Fig. 11

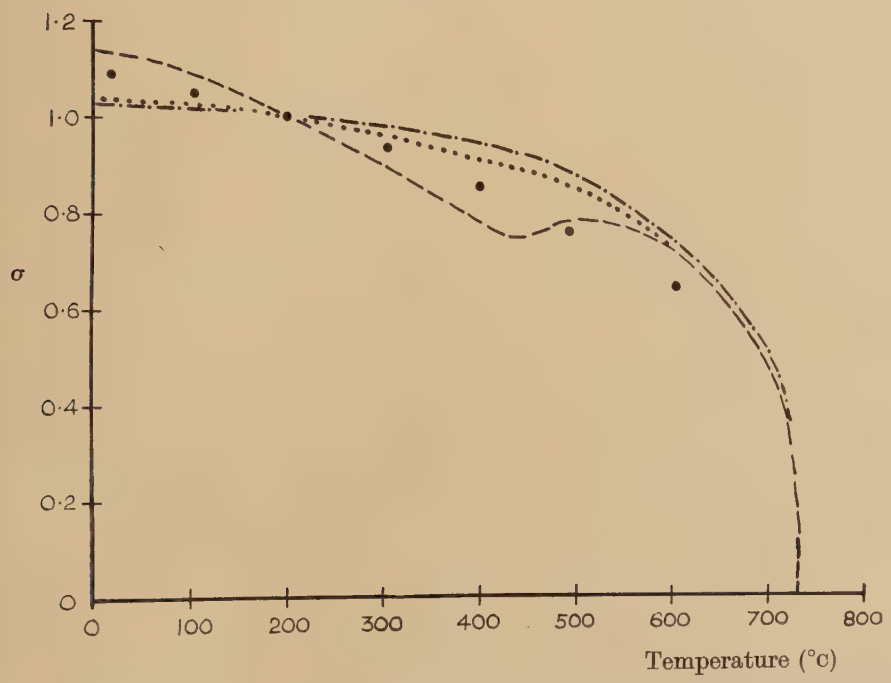

Temperature variation of the spontaneous magnetization of Fe_2NiAl subjected to different heat treatments (Sucksmith, 1939).

— — — — Quenched from 800°C.
. . . . . ,, ,, 500°C.
— · — · — Annealed (by slow cooling).

● H_c values of Fe_2NiAl specimen normalized to unity at 200°C.

energy required to release a boundary wall from a region of dispersion is equal to the magnetostatic energy of such an isolated unipole in the applied field. This energy is therefore proportional to J_s. If now J_s decreases due to an increase in temperature, and no metallurgical changes take place, the number of metastable magnetization processes, within a given energy range, will increase by a factor $1/J_s$. Hence to this order of approximation p varies as $1/J_s$ and since $\bar{\imath}$ is proportional to J_s, the product $\bar{\imath}p$ is independent of temperature in agreement with the experimental results. If the mechanism responsible for the deviation in $\mathbf{J}_s$ is itself temperature dependent, which would for example be the case if the expansion coefficients of the precipitate and matrix were appreciably different, then the above explanation would no longer be valid.

The impedance to boundary wall movement presented by regions of dispersion is proportional to the unipolar density given by div $\mathbf{J}_s$. Thus to a first approximation, subject to the conditions specified at the end of the preceding paragraph the coercive force of a specimen should vary with temperature in the same way as the spontaneous magnetization. In the case of the specimen of Fe_2NiAl it was possible to test this prediction directly. Sucksmith (1939) has determined the temperature variation of spontaneous magnetization of specimens of Fe_2NiAl subjected to different heat treatments. These results are plotted in fig. 11, where for convenience the values of spontaneous magnetization are expessed as ratios of the common value at 200°C. On this figure are plotted the measured values of the coercive force of the Fe_2NiAl specimen used in the present experiments. These values have also been normalized to unity at 200°C. Considering the nature of the approximations made the observed agreement between the temperature variation of the spontaneous magnetization and the coercive force is satisfactory. The Sucksmith curves effectively represent the extremes of heat treatment, rapidly quenched and well annealed, whilst the H_c values correspond to a specimen in an intermediate state of heat treatment.

It appears of interest to test these theories by investigating the phenomena of magnetic viscosity in precipitation alloys other than the rather complex alnico type, e.g. Co–Pt and Ni–Au. It is hoped to report these investigations at a later date.

Acknowledgments

The authors wish to thank Professor L. F. Bates for his interest and continued support of this work. Their thanks are also due to Imperial Chemical Industries Ltd. for the loan of electronic equipment, Dr. Alun Edwards and the Permanent Magnet Association for the provision of specimens and Mr. D. H. Martin for the Bitter figure investigation. One of us (R. S.) thanks the Royal Society for a grant for the purchase of the recording potentiometer.

References

Bozorth, R. M., 1951, *Colloque de Ferromagnétisme et Antiferromagnétisme* (Grenoble: C.N.R.S.), p. 160.
Bush, H. D., and Tebble, R. S., 1948, *Proc. Phys. Soc.*, **60,** 370.
Fisher, J. C., Hollomon, J. H., and Turnbull, D., 1948, *J. Appl. Phys.*, **19,** 775.
Geisler, A. H., 1949, *Trans. Amer. Inst. Min. and Met. Engrs.*, **180,** 230 ; 1953, *Rev. Mod. Phys.*, **25,** 316.
Heidenreich, R. D., and Nesbitt, E. A., 1952, *J. Appl. Phys.*, **23,** 352.
Hollomon, J. H., and Turnbull, D., 1953, *Progress in Metal Physics*, Vol. 4 (London : Pergamon Press), p. 333.
Hoselitz, K., 1952, *Ferromagnetic Properties of Metals and Alloys* (Oxford : Clarendon Press), p. 266.
Néel, L., 1946, *Ann. Univ. Grenoble*, **22,** 299.
Stoner, E. C., and Wohlfarth, E. P., 1948, *Phil. Trans. Roy. Soc.*, **240,** 599.
Street, R., and Woolley, J. C., 1949, *Proc. Phys. Soc.* A, **62,** 562 ; 1950, *Ibid.* B, **63,** 509.
Street, R., Woolley, J. C., and Smith, P. B., 1952 a, *Proc. Phys. Soc.* B, **65,** 461 ; 1952 b, *Ibid.* B, **65,** 679.
Sucksmith, W., 1939, *Proc. Roy. Soc.* A, **171,** 525.

LX. *Elastic Scattering of* 125 MeV *Electrons by Mercury*

By Sheila Brenner and G. E. Brown
Department of Mathematical Physics, University of Birmingham
and
L. R. B. Elton
Wheatstone Department of Physics, King's College, London*

[Received February 27, 1954]

Abstract

We have calculated the elastic scattering of 125 MeV electrons by the nucleus of mercury, assuming various spherically symmetric models for the charge distribution. We find that a square distribution (i.e. $\rho=\rho_0$, $r<R$; $\rho=0$, $r>R$) gives rise to a rather large oscillatory differential cross section at wide angles, whereas the cross section from a distribution of radius $R=1{\cdot}2\times10^{-13}A^{1/3}$ cm in which the sharp edge of the square distribution is smoothed reproduces the smooth, monotonically decreasing differential cross section required by the experimental data.

§ 1. Introduction

In this note we report phase-shift calculations of the scattering of 125 MeV electrons by mercury ($Z=80$). We consider only elastic Coulomb scattering, which is coherent, from a static nuclear charge distribution. The experiments (Hofstadter, Fechter and McIntyre 1953) have been designed so as to detect only scattered electrons which have lost energy of the order of 1 MeV or less, and consequently exclude most of the incoherent scattering. We neglect radiative corrections since we believe them to be small, of order α ($=1/$" 137 ") of the main effect. Work is proceeding in Birmingham to estimate these corrections. Any deviation from spherical symmetry in the shape of the nucleus is small and therefore probably alters the result very little. Scattering by the atomic electrons only affects the result for angles much smaller than those considered here.

The electron scattering experiments by Hofstadter, Fechter and McIntyre (1953) have been analysed by these authors with the use of Born approximation. This analysis has given the impression that the charge distribution has a rather large central concentration, tapering off slowly, as, for example, an exponentially decreasing charge distribution $\rho=\rho_0\exp(-r/a)$. However, Born approximation is not reliable in this problem and we shall show that this impression of a large central charge is misleading and that, in fact, the general features of the experimental scattering can be obtained from charge distributions which do not have a large central charge and which appear more reasonable to us.

* Communicated by Professor R. E. Peierls, F.R.S.

The experimental data show a differential cross section which decreases smoothly with angle from 35° to 120°. This is in disagreement with results obtained using Born approximation for a square nuclear charge distribution (i.e. $\rho=\rho_0$, $r<R$; $\rho=0$, $r>R$), the cross section for which oscillates in a pronounced manner. It has been shown by Yennie, Wilson and Ravenhall (1953) that these oscillations are less pronounced in the phase-shift calculation. The oscillations are, however, still present in the theoretical differential cross section to a greater degree than they appear to be in the experimental data. These authors carried out their calculations for electrons of energy $E=150$ MEV scattered by Au with an assumed nuclear radius R such that $ER/\hbar c=5{\cdot}4$. Using the fact that, except for a scale factor, the differential cross section depends only on the product ER (Feshbach 1952), we see that we can apply the calculations of these authors to obtain the scattering of 125 MEV electrons by Hg with nuclear radius given by $R=5{\cdot}4\hbar c/125$ MEV, if we neglect the difference between the Z values of Au and Hg (79 and 80). This gives a nuclear radius $R=1{\cdot}45\times10^{-13}\,A^{1/3}$ cm*. We have obtained a rather similar curve for $R=1{\cdot}40\times10^{-13}\,A^{1/3}$ cm. (See fig 1.)

The square distribution is not, however, a realistic one. The charge in the nucleus does not drop sharply from its maximum value to zero, but decreases smoothly over a certain transition region. It is very probable that this model will give rise to a more smoothly varying differential cross section than the square distribution.

We have considered two extreme cases, between which we would expect the reasonable case to lie, of a nuclear model with a transition range :

(i) A square distribution with charge density ρ_0 and radius R ; i.e. a model with zero transition range.

(ii) A distribution with a rather long transition range, such that the charge density is approximately homogeneous from $r=0$ to $r\sim0{\cdot}74R$, and then decreases smoothly to zero between $r\sim0{\cdot}74R$ and $r\sim1{\cdot}3R$. Explicitly

$$\rho=1{\cdot}89\rho_0/[1+\exp\{2(r^2/0{\cdot}54R^2-1)\}]$$

where we have chosen $R=1{\cdot}2\times10^{-13}\,A^{1/3}$ cm for both models, and the choice of parameters is such that (i) and (ii) reproduce the same low-energy scattering effects, as will be explained in § 3. The effects of these two models are shown in fig. 1.

We expect the actual model of the nucleus to lie somewhere between models (i) and (ii). The experiments at this stage are only accurate enough to determine rather general features of the nucleus, and since the models (i) and (ii) both satisfy the general experimental requirements, we see that not much can be said of the precise nuclear shape. It is clear, of course, that the differential cross section is rather sensitive to the choice of the nuclear radius, and the square distribution with

* It should be pointed out that Yennie *et al.* (1953) did not carry out their calculations to fit the experimental data mentioned here, but rather to test the validity of Born approximation, which they found to be very bad in this case.

$R=1{\cdot}4\times10^{-13}A^{1/3}$ cm does not fit the experimental data well, but with respect to the more specific features by which two models with the same approximately correct radius differ, not much can be said until more accurate large angle measurements have been made. Of course scattering at higher energies will also be more sensitive to these specific features. This will then allow a test of the two separate questions: (*a*) How large is the central charge density? (*b*) How sharp is the edge of the nucleus? For example, if the differential cross section at an energy in the region 150–200 Mev remains more or less smooth, we can conclude that the edge of the nucleus is not very sharp, because a sharp edge would give rise to an oscillatory differential cross section in this region.

Fig. 1

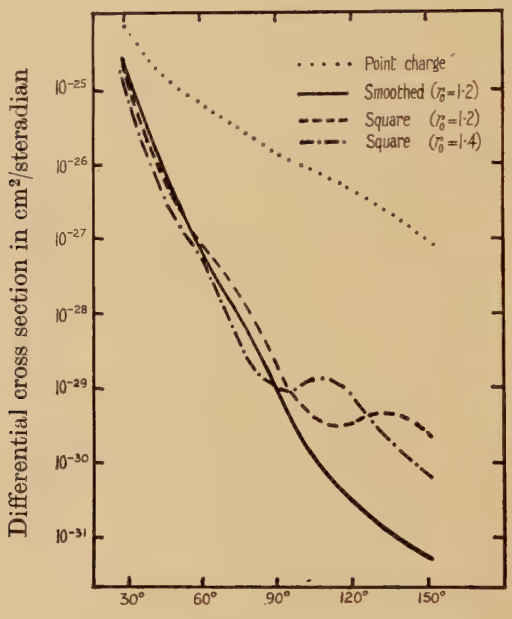

Exact (phase shift) differential cross sections in cm²/steradian *vs.* angle for the scattering of 125 Mev electrons by mercury assuming a finite nucleus of radius $R=r_0\times10^{-13}A^{1/3}$ cm and the following charge distributions:

(i) A smoothed distribution

$$\rho=1{\cdot}89\rho_0/[1+\exp\{2(r^2/0{\cdot}54R^2-1)\}]$$

with $r_0=1{\cdot}2$.

(ii) Two square distributions

$$\rho=\rho_0,\quad r<R\,;\qquad \rho=0,\quad r>R$$

with $r_0=1{\cdot}2$ and $1{\cdot}4$.

§ 2. Procedure

To find the differential scattering cross section we must solve the Dirac equation for an electron in the potential arising from the particular charge distribution considered. This solution may be broken up into a sum of partial waves, each representing a given total angular momentum

of the electron. In fact, in the relativistic theory, to each total angular momentum correspond two partial waves, which can be specified as eigenstates of Dirac's operator k having eigenvalues $k=\pm(j+\frac{1}{2})$, where j is the total angular momentum. It is known (Feshbach 1951) that if one can neglect the rest mass term in Dirac's equation, as is the case for high energies, the two solutions corresponding to the same j have the same phase shift. We shall therefore work with only one of the partial waves corresponding to a given j, namely that for which $k=j+\frac{1}{2}$. In fact, as we shall demonstrate in the appendix, the mass term enters the solution of Dirac's equation first in order $(m/E)^2$ if its effects are considered as perturbations, and we are certainly justified in neglecting it in this problem.

Fig. 2

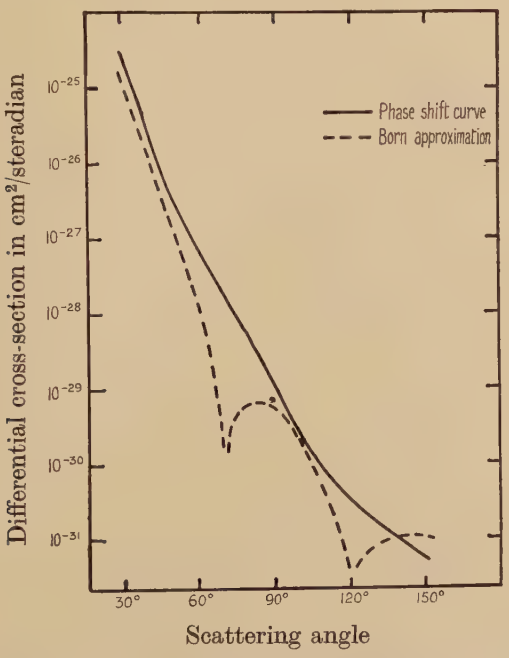

Differential cross section in cm²/steradian *vs.* angle for a smoothed distribution

$$\rho=1{\cdot}89\rho_0/[1+\exp\{2(r^2/0{\cdot}54R^2-1)\}],$$

with $r_0=1{\cdot}2$. Comparison between exact (phase shift) calculation (full curve) and Born approximation (dashed curve).

Dirac's equations for the radial functions f and g of the kth partial wave are*

$$\left.\begin{aligned}\frac{dg}{dr}+\frac{k+1}{r}g+(E-V)f=0\\ \frac{df}{dr}-\frac{k-1}{r}f-(E-V)g=0\end{aligned}\right\} \quad \ldots\ldots \quad (1)$$

where we have already neglected the mass term. Here E is the energy

* We employ relativistic units $\hbar=c=1$.

and V the potential. Introducing new functions R and S equal to $-rf$ and rg, respectively, and choosing units such that $E=1$, we find that

$$\left.\begin{aligned}\frac{dS}{dr}+\frac{k}{r}S-(1-V)R=0\\ \frac{dR}{dr}-\frac{k}{r}R+(1-V)S=0\end{aligned}\right\} \quad . \quad . \quad . \quad . \quad . \quad . \quad . \quad (2)$$

The solutions of these equations have the asymptotic forms

$$\left.\begin{aligned}R\sim&\cos\,(r+Z\alpha\,\log\,2r-\tfrac{1}{2}k\pi+\chi_k)\\ S\sim&\sin\,(r+Z\alpha\,\log\,2r-\tfrac{1}{2}k\pi+\chi_k)\end{aligned}\right\} \quad . \quad . \quad . \quad . \quad . \quad (3)$$

where χ_k is the phase shift and α is the fine structure constant. The differential cross section can be expressed simply in terms of χ_k (Mott and Massey 1949, p. 76). This cross section is equal to $|f(\theta)|^2+|g(\theta)|^2$ with the amplitudes f and g given by

$$\left.\begin{aligned}f(\theta)=&\frac{1}{2i}\sum_{k=1}^{\infty}k\exp\,(2i\chi_k)[P_k\,(\cos\,\theta)+P_{k-1})\cos\,\theta)]\\ g(\theta)=&\frac{1}{2i}\sum_{k=1}^{\infty}\exp\,(2i\chi_k)[P_k^{\,1}\,(\cos\,\theta)-P_{k-1}^{1}\,(\cos\,\theta)]\end{aligned}\right\} \quad . \quad . \quad (4)$$

where we have reduced the general expression of Mott and Massey to the expression for high energies, i.e. we have set the two phase shifts corresponding to the same j equal. It is convenient to split the phase shifts χ_k into $\eta_k+\delta_k$ where η_k is the Coulomb phase shift for a point charge and δ_k is the 'anomalous' phase shift produced by the deviation of the charge distribution from a point charge. This separation is advantageous because η_k is known analytically and δ_k is different from zero for only the first few partial waves. The η_k, however, do not go to zero with increasing k; therefore it is convenient to express the scattering amplitude $f(\theta)$ as $f_P(\theta)+[f(\theta)-f_P(\theta)]$, where $f_P(\theta)$ is the amplitude which would result from a point charge. The quantity $f_P(\theta)$ has been calculated by Feshbach (1952). The quantity $f(\theta)-f_P(\theta)$ involves only a few terms in a summation in k.

If we integrate eqns. (2) to a point outside the nucleus, we can determine δ_k, providing we know the regular Coulomb functions R_R and S_R and the irregular Coulomb functions R_I and S_I at this point. The regular functions have the asymptotic behaviour

$$\left.\begin{aligned}R_R\sim&\cos\,(r+Z\alpha\,\log\,2r-\tfrac{1}{2}k\pi+\eta_k)\\ S_R\sim&\sin\,(r+Z\alpha\,\log\,2r-\tfrac{1}{2}k\pi+\eta_k)\end{aligned}\right\} \quad . \quad . \quad . \quad . \quad . \quad (5)$$

and we choose irregular functions such that

$$\left.\begin{aligned}R_I\sim&-\sin\,(r+Z\alpha\,\log\,2r-\tfrac{1}{2}k\pi+\eta_k)\\ S_I\sim&\cos\,(r+Z\alpha\,\log\,2r-\tfrac{1}{2}k\pi+\eta_k)\end{aligned}\right\} \quad . \quad . \quad . \quad . \quad . \quad (6)$$

In this case, if r_0 is a point such that the potential is Coulombian, i.e. $\rho(r)=0$, $r>r_0$, then

$$\tan\delta_k=\frac{R_R(r_0)-u(r_0)S_R(r_0)}{R_I(r_0)-u(r_0)S_I(r_0)}, \quad \ldots\ldots \quad (7)$$

where $u(r_0)=R(r_0)/S(r_0)$.

We have found it convenient to compute the Coulomb functions directly from the asymptotic series (see, for example, Mott and Massey 1949, p. 51). The expansion in inverse powers of r is straightforward and we give only the results:

$$\begin{aligned}
S_R=&\sin(r+Z\alpha\log 2r-\tfrac{1}{2}k\pi+\eta_k)+\frac{k(k+1)}{2r}\sin(r+Z\alpha\log 2r-\tfrac{1}{2}k\pi+\eta_k+\tfrac{1}{2}\pi)\\
&+\frac{k(k+2)}{2!\,(2r)^2}[(k^2-1^2)^2+(2.1Z\alpha)^2]^{1/2}\sin(r+Z\alpha\log 2r-\tfrac{1}{2}k\pi+\eta_k+\sigma_2)\\
&+\frac{k(k+3)}{3!\,(2r)^3}[(k^2-1^2)^2+(2.1Z\alpha)^2]^{1/2}[(k^2-2^2)^2+(2.2Z\alpha)^2]^{1/2}\\
&\times\sin(r+Z\alpha\log 2r-\tfrac{1}{2}k\pi+\eta_k+\sigma_3)+\ldots.\\
R_R=&\cos(r+Z\alpha\log 2r-\tfrac{1}{2}k\pi+\eta_k)+\frac{k(k-1)}{2r}\cos\left(r+Z\alpha\log 2r-\tfrac{1}{2}k\pi+\eta_k+\frac{\pi}{2}\right)\\
&+\frac{k(k-2)}{2!\,(2r)^2}[(k^2-1^2)^2+(2.1Z\alpha)^2]^{1/2}\cos(r+Z\alpha\log 2r-\tfrac{1}{2}k\pi+\eta_k+\sigma_2)\\
&+\ldots.
\end{aligned}$$

with

$$\left.\begin{aligned}
\sigma_2&=\frac{2\pi}{2}+\tan^{-1}\frac{2.1Z\alpha}{k^2-1^2}\\
\sigma_3&=\frac{3\pi}{2}+\tan^{-1}\frac{2.1Z\alpha}{k^2-1^2}+\tan^{-1}\frac{2.2Z\alpha}{k^2-2^2}
\end{aligned}\right\}. \quad \ldots \quad (8)$$

The expansion of S_I is obtained from that for S_R by changing all sines to cosines of the same argument, and that for R_I is obtained from that for R_R by changing all cosines to negative sines.

§ 3. Definition of Nuclear Radius and Calculation of Starting Values

We shall define the nuclear radius of any charge distribution as the radius of the homogeneous distribution which would give rise to the same low-energy scattering as the particular model considered. It is well known (Feshbach 1951) that low-energy scattering is model-independent; i.e. any reasonable model will give the same scattering as a homogeneous distribution, provided the parameters occurring in it are chosen appropriately.

It follows from Feshbach's results that any charge distribution that satisfies the conditions

$$\left.\begin{aligned} 4\pi\int_0^\infty \rho(x)x^2\,dx &= Ze, \\ 4\pi\int_0^\infty \rho(x)x^4\,dx &= \tfrac{3}{5}ZeR^2 \end{aligned}\right\} \quad \ldots\ldots \quad (9)$$

will give the same low-energy scattering.

If we put

$$\rho(x)=A/[1+\exp\{2(x^2/B^2)-1\}] \quad \ldots\ldots \quad (10)$$

we find that

$$A=1{\cdot}89\rho_0, \qquad B^2=0{\cdot}54R^2 \quad \ldots\ldots \quad (11)$$

where ρ_0 and R are the charge density and radius of the corresponding square distribution. (This is the result quoted in § 1.) We may call R the (effective) nuclear radius of the distribution. The nuclear parameter r_0 is defined by $R=r_0\times 10^{-13}A^{1/3}$ cm.

Lastly, we show how to calculate starting values for our functions R and S. We see from eqn. (7) that only the ratio from R to S enters into our calculation of phase shifts, and, consequently, that the amplitude of the functions is immaterial as long as we employ the correct ratio. If we denote $S/R=1/u=w(r)$, then from eqns. (2) we find

$$\frac{dw}{dr}+\frac{2k}{r}w=(1-V)w^2+(1-V). \quad \ldots\ldots \quad (12)$$

If we expand

$$\left.\begin{aligned} w &= w_0+w_1r+w_2r^2+\ldots \\ V &= V_0+V_1r+V_2r^2+\ldots \end{aligned}\right\} \quad \ldots\ldots \quad (13)$$

we find easily from (8) that

$$\left.\begin{aligned} w_0 &= 0 \\ w_1 &= +\frac{1-V_0}{1+2k} \\ w_2 &= -\frac{V_1}{2+2k} \quad \text{etc.} \end{aligned}\right\} \quad \ldots\ldots \quad (14)$$

and we can calculate w conveniently from this series at a distance $r\ll k$ from the origin and so arrive at starting values.

§ 4. Calculation and Results

We have integrated the eqns. (2) numerically by the Runge–Kutta method on the Cambridge electronic computor EDSAC, and so obtained $u(15)$ of (7). To obtain the Coulomb functions we have employed eqns. (8). In this expansion, $k+2$ or $k+3$ terms were necessary to obtain the functions to five decimal places. Our checks show the machine calculations for $k=1$, 2 to be accurate to 5 or 6 units in the fifth decimal place and for $k\geqslant 3$ to be accurate to within 2 to 5 units in the fifth decimal place. We show the phase shifts for the various models in the table We estimate that these have an error only in the fifth decimal place.

We have employed the point charge amplitudes of Feshbach (1952) in the manner discussed in § 2. Feshbach gives amplitudes for $Z=80$ in his Table I, to three significant figures for that part of the Coulomb amplitude which must be summed numerically. We can thus easily obtain figures at large angles to three significant figures. This is sufficient to define our curves reasonably, although at 150° the anomalous amplitudes almost cancels the Coulomb amplitude. We have the Coulomb

Summary of Phase Shifts

k	Square distr. $r_0=1{\cdot}4$	Square distr. $r_0=1{\cdot}2$	Smoothed distr. $r_0=1{\cdot}2$
1	−1·01562	−0·92996	−0·90839
2	−0·39683	−0·32241	−0·31196
3	−0·15998	−0·10615	−0·10994
4	−0·05178	−0·02568	−0·03348
5	−0·01229	−0·00433	−0·00874
6	−0·00218	−0·00052	−0·00197
7	−0·00032	−0·00005	−0·00039
8	−0·00004	—	−0·00007

The square and smoothed distributions are defined below fig. 1.

amplitude to this accuracy only at 90°, 120° and 150°, with a less accurate value at 100° from his Table II, so that our curve for wide angles is not well defined. We are at present extending both the accuracy of the point charge calculations and the number of angles at which they are made. We believe, however, that the present accuracy is sufficient to define the general features of these curves even at large angles.

We see from fig. 1 that the oscillatory nature of the differential cross section for a square charge distribution can be eliminated completely by smoothing the sharp edge of the charge cut-off. The smoothed distribution reproduces the general shape of the experimental results (Hofstadter *et al.* 1953). We have made no attempt to fit these results in detail, but we are extending our present calculations and hope, at a later date, to analyse the experimental results in detail when the accuracy of these is improved.

We wish to thank Professor Peierls and Professor Hartree for many useful discussions. We are particularly indebted to the Mathematical Laboratory at Cambridge for much assistance, and for the use of EDSAC. We wish also to express our gratitude to Dr. Yennie and Dr. Ravenhall, who communicated many interesting results of theirs before publication. One of us (S. B.) is receiving a grant from the Department of Scientific and Industrial Research. We are grateful to the Research Committee of the University of Birmingham for a grant which assisted our work.

APPENDIX

We shall show that if we consider the effects of the rest mass as a perturbation for high electron energies, these effects enter first in order $(m/E)^2$; i.e. in order m^2 in the units employed in this note, which are such that energies are measured in units of E (and $\hbar=c=1$). The complete Dirac equation in these units is

$$(1-V+\boldsymbol{\alpha}\cdot\mathbf{p}+\beta m)\psi=0 \quad . \quad . \quad . \quad . \quad . \quad . \quad . \quad \text{(A1)}$$

where $\boldsymbol{\alpha}$ and β are the Dirac matrices corresponding to the classical quantities v/c and $(1-v^2/c^2)^{1/2}$. We shall find it convenient to choose a representation of $\boldsymbol{\alpha}$ and β which is different from the usual one. In fact, we use $\boldsymbol{\alpha}=\rho_3\boldsymbol{\sigma}$; $\beta=\rho_1$, where ρ_3 and ρ_1 are the matrices introduced by Dirac, p. 256 (1947), and $\boldsymbol{\sigma}$ is the Pauli spin operator. We express the wave function ψ in terms of two two-component functions, namely,

$$\psi=\begin{pmatrix}u_1\\u_2\end{pmatrix}; \quad . \quad . \quad . \quad . \quad . \quad . \quad . \quad . \quad . \quad \text{(A2)}$$

the eqn. (A1) is equivalent to the two equations

$$\left.\begin{aligned}(1-V+\boldsymbol{\sigma}\cdot\mathbf{p})\,u_1&=-mu_2\\(1-V-\boldsymbol{\sigma}\cdot\mathbf{p})\,u_2&=-mu_1\end{aligned}\right\} \quad . \quad . \quad . \quad . \quad . \quad . \quad . \quad \text{(A3)}$$

In the zero-order approximation, neglecting m, the phases of u_1 and u_2 are completely arbitrary. In (A3) we can employ, on the right side, m times the zero-order approximations of u_2 and u_1 to obtain the first-order corrections to u_2 and u_1, which will appear on the left in the usual way. Since the phases of u_1 and u_2 are arbitrary, the substitution of u_2 by $-u_2$ cannot change any observable results. But this change has the same effect as changing m to $-m$. Consequently all observables such as the scattering cross section can depend only on even powers of m ; otherwise they would change with the change of sign of m. Hence no term linear in m can occur.

References

Dirac, P. A. M., 1947, *The Principles of Quantum Mechanics*, 3rd ed. (Oxford : University Press).

Feshbach, H., 1951, *Phys. Rev.*, **84,** 1206 ; 1952, *Ibid.*, **88,** 295.

Hofstadter, R., Fechter, H. R., and McIntyre, J. A., 1953, *Phys. Rev.*, **92,** 978.

Mott, N. F., and Massey, H. S. W., 1949, *The Theory of Atomic Collisions*, 2nd ed. (Oxford : University Press).

Yennie, D. R., Wilson, R. N., and Ravenhall, D. G., 1953, *Phys. Rev.*, **92,** 1325.

LXI. *On the Mass of the Λ^0-Particle*

By M. W. Friedlander, D. Keefe,* M. G. K. Menon,† and M. Merlin‡
H. H. Wills Physical Laboratory, University of Bristol §

[Received April 5, 1954]

Summary

In a stack of stripped photographic emulsions, twenty events of type $2+0_n$ have been observed, in each of which the outgoing particles are a proton and a negative π-meson respectively; the latter particle was identified by the characteristic star it produced when brought to rest in the emulsion. Assuming that each of these events represents the decay in flight of a neutral hyperon according to the scheme $\Lambda^0 \rightarrow \pi^- + \mathrm{p} + Q$, values of the energy release Q have been calculated. In eleven of the events the proton could be traced to the end of its range; the energies of both particles could then be deduced using appropriate range–energy relations. In the remaining nine examples, the energy of the proton was deduced from grain density considerations and was accordingly less well determined.

Ten cases yield Q-values in the interval 35·5–38·5 Mev. These have been interpreted as examples of the decay of a Λ^0-particle with a unique Q of $\sim$37 Mev. The weighted mean Q-value obtained for the ten examples is then $36{\cdot}92 \pm 0{\cdot}22$ Mev.

It is not yet possible to decide whether there are neutral hyperons with a similar decay scheme but with a different release of energy.

It is clear from these and other measurements, that results of high precision can be obtained with the use of stripped emulsions. At the present stage in their use, however, there is one possibly serious source of error, namely uncertainties in the stopping power of the emulsions. This and other errors are discussed in detail and their effects evaluated in obtaining the final results.

The mass of the Λ^0-particle as deduced from these experiments is $2181 \pm 1\, m_e$.

§1. Introduction

Since the original observations of Rochester and Butler (1947), a large number of papers has appeared, describing further measurements on V-events in Wilson chambers. It was soon established that those

* On leave of absence from University College, Dublin.
† Senior Scholar of the Royal Commission for the Exhibition of 1851.
‡ On leave of absence from the University of Padua.
§ Communicated by Professor C. F. Powell, F.R.S.

V-events representing the decay in flight of neutral particles, could be divided broadly into two classes, according as the primary particle had a mass greater or less than that of the proton. The present paper is concerned only with those of mass greater than the proton. These were originally called ' V_1^0-particles ', but, following the nomenclature proposed at the Bagnères Conference (Amaldi *et al.* 1954) the name ' hyperon ' and the symbol ' Λ^0 ' will be used in this paper.

From work with expansion chambers, there is very strong evidence for the existence of a Λ^0-particle, which decays according to the scheme

$$\Lambda^0 \rightarrow p + \pi^- + Q ,$$

where the energy release, Q, is about 37 Mev ; for example, the Manchester group obtain $Q = 42^{+3}_{-2}$ Mev (Armenteros, *Bagnères Report* 1953, p. 18), the M.I.T. group 37 (± 2) Mev (Bridge *et al.* 1953) and the Pasadena group 35 ± 3 Mev (Leighton *et al.* 1953). Besides this value of Q, there is also some evidence for at least one other Q-value at ~ 75 Mev (Leighton *et al.* 1953). The position at the end of 1952 is well summarized in the review article by Rochester and Butler (1953) and the results obtained since are discussed in the Bagnères (1953) and Rochester (1954) Conference Reports.

A V-event observed in an expansion chamber can in very nearly all cases be attributed to the decay of a neutral particle, the probability of a nuclear disintegration in the gas of the chamber being extremely low. In addition, the V-event is often associated with a visible disintegration in a lead plate or the walls of the chamber, and the association can be confirmed by testing the coplanarity of the V-event and the disintegration centre. This also serves to show that the decay is a two-body process, and that it does not involve any neutral secondaries. In a photographic emulsion the greater stopping power of the solid medium is of no advantage in dealing with uncharged particles, and the V-event will very rarely be in the same emulsion as the parent disintegration. Thus, in an investigation on Λ^0-particles using photographic emulsions, a first approach could be to select those two prong stars in which the outgoing particles are a proton and a negative π-meson respectively, and then to calculate the Q-values for these cases assuming each of them to represent the decay of a Λ^0-particle. The presence of genuine Λ^0 decays amongst the group of two prong stars examined would then be indicated by a concentration of Q-values about a particular energy. Some observations have already been reported using photographic emulsions (see *Bagnères Report* 1953, pp. 166–178). Amongst these however, only in one case were both the decay products brought to rest, and in most cases it has not been possible to show that the L-meson was in fact a π^-- and not a π^+-particle. Even with these limitations, the power of the photographic technique is well illustrated by these results.

Some Λ^0-decays have been observed in emulsions in which both the proton and π^--meson are brought to rest (Bonetti *et al.* 1953 and private

communications from Kaplon, Yagoda and the Padova group). It is not possible to compare these observations with those of the present work because of the possibility of systematic differences in techniques.

In the present experiment, we have used a stack of 40 Ilford G5, 600 μ, emulsion strips, flown for 7 hours above 85 000 ft. in the 1953 International Sardinian Expedition (Flight S.35) and a stack of 46, Ilford G5, 600 μ, emulsion strips flown for 3 hours above 83 000 ft. in England (Flight H.A. 54).

Two lines of approach have been adopted. In the first, π-mesons arrested in the emulsion have been traced back to their origins inside the stack, or until the point at which they entered the stack from outside. In the other method, $2+0_n$ events recorded by scanners have been investigated and those involving a proton and a negative π-meson have been selected. In all, 20 events of the (p, π^-) type have been found. In the following sections are described the measurements and analysis. Full details of the number of positive and negative π-mesons followed, the classification of the origins, and an analysis of the relative frequencies of π-mesons, τ-mesons, and Λ^0-particles will be discussed in a later paper. Our present observations show that there is a high frequency of Λ^0-decays in our emulsions and it has therefore been possible to carry out such a statistical analysis.

§ 2. Experimental Results

Full details of the 20 (p, π^-) events found are presented in the table. The Q-values given in column 9 have been evaluated on the assumption that each represents the two-body decay of a Λ^0-particle with an energy release given by the formula

$$Q=(M_1+M_2)\left\{\left(1+\frac{2Q_1}{M_1+M_2}\right)^{1/2}-1\right\}$$

where

$$Q_1=\frac{E_1E_2-M_1M_2-P_1P_2\cos\theta}{M_1+M_2}.$$

M_1, M_2, and E_1, E_2, and P_1, P_2 are the masses, (MeV) total energies (MeV), the momenta (MeV/c) of the proton and π-meson respectively. The energies have been deduced from the ranges of the particles in the manner discussed in § 3 (*c*). θ is the angle between the two tracks. The value of M_1 and M_2 used for the calculations are $M_1=1836{\cdot}13\ m_e=938{\cdot}23$ MeV (Du Mond and Cohen 1953) and $M_2=272{\cdot}5\ m_e=139{\cdot}24$ MeV (Smith, Birnbaum and Barkas 1953).

The Q-values listed in the table are presented in graphical form in fig. 1. It is clear from this histogram that there is a pronounced peak between 34 MeV and 40 MeV centred at about 37 MeV which it is reasonable to attribute to the decay of a Λ^0-particle. It may be noted that most of the events of high quality, in which both particles are observed to come to rest, are in fact contained in this group. This is

somewhat fortuitous but may be interpreted in terms of a high relative frequency of Λ^0-particles compared to 2 prong (p, π^-) stars ; the latter would be expected to display a broad background spread. At this stage,

Event No.	Proton			π^--meson			Angle (deg.)	Q (MeV)	Whether Proton ends in stack	Weighting factor
	Range (mm)	Energy (MeV)	Momentum (MeV/c)	Range (mm)	Energy (MeV)	Momentum (MeV/c)				
14	4·4±0·5	32·4	249	0·25	2·76	27·82	20·7	0·5	Out	—
1	114±10	216	668	23·70	39·40	111·91	28·6	8·3	Out	—
19	3·99	30·7	242	10·91	24·60	86·40	64·0	18·3	Ends	—
12	—	310*	824	4·83	15·21	66·71	50·0	26·2	Out	—
17	9·20	49·5	308·8	6·29	17·79	72·61	130·2	35·6	Ends	1·0
2	7·74	44·8	293·5	6·11	17·58	72·15	140·7	36·6	Ends	1·0
15	14·49	64·4	353·6	7·19	19·22	75·65	116·4	36·6	Ends	1·0
5	10·05	52·1	317·1	4·90	15·40	67·28	146·8	36·8	Ends	1·5
9	13·94	63·0	349·5	3·07	11·74	58·38	167·1	36·9	Ends	1·5
11	23·42	85·0	408·4	2·34	10·04	53·82	148·1	37·2	Ends	1·5
16	0·147	4·52	92·2	18·05	33·43	102·11	159·0	37·4	Ends	0·5
10	48±2	129·5	512	8·82	21·70	80·41	85·4	37·4	Out	0·5
7	0·313	7·15	116·1	19·87	35·43	105·46	126·4	38·1	Ends	0·5
6	0·294	6·89	113·9	42·06	55·70	136·43	42·2	38·4	Ends	0·5
8	22·21	82·5	401·9	25·60	41·28	114·89	79·8	41·4	Ends	—
18	112±10	215	666	5·53	16·21	69·01	87·4	42·6	Out	—
4	60±10	147	551	65·8	73·01	160·20	65·5	54·1	Out	—
13	24±5	84·2	412	36·5	51·10	129·61	97·0	63·3	Out	—
20	47±8	127	504	9·50	22·70	82·70	143·5	67·7	Out	—
3	102±15	203	649	14·0	28·61	91·52	128·4	85·0	Out	—

* Event 12 : Proton energy determined by measurements of scattering along the track.

Fig. 1

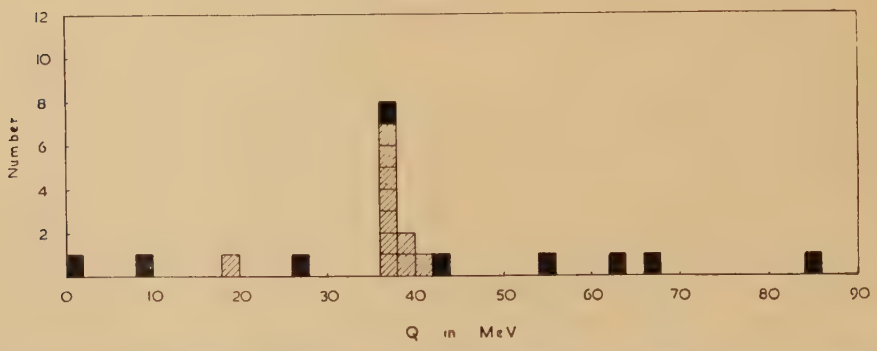

Histogram showing the distribution of Q-values for the twenty (p, π^-) events. Details of the events are given in the table. The Q-values have been calculated under the assumption that each event represents the two body decay of a neutral hyperon according to the scheme $\Lambda^0 \rightarrow p + \pi^- + Q$.

▨ Events in which both the proton and the π^--meson came to the end of their range within the stack.

■ Events in which only the π^--meson was arrested within the stack; the energy of the proton was then determined from grain density and scattering considerations.

it is appropriate to point out that nineteen out of the twenty events were found by tracing back σ-mesons to their origins and the remaining one by direct observation of the V-event. The histogram of fig. 2 shows in greater detail that part of the Q-value distribution lying between 34 MeV and 40 MeV. The geometry of the events is such that each cannot be given the same weight in assessing a mean Q and accordingly, approximate errors were assigned to the measured quantities and the error in Q derived therefrom. On the basis of this, weighting factors were obtained for each event and these are indicated in column 11 of the table. The weighted mean Q-value found for the nine events shown in fig. 2 is

$$Q = 36{\cdot}92 \pm 0{\cdot}22 \text{ MeV}.$$

The error quoted is the standard deviation of the mean and does not include any due to effects of a systematic nature, which are discussed in § 3. The mass of the Λ^0-particle is therefore $2181 \pm 1\ m_e$.

Fig. 2

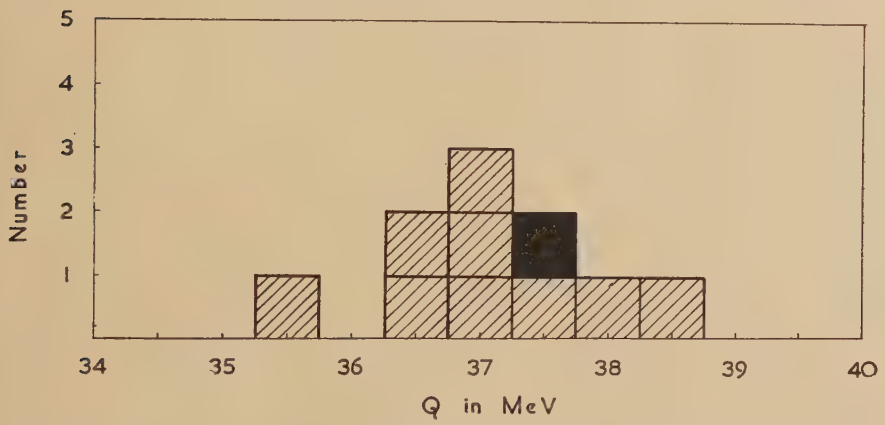

Histogram showing in greater detail the Q-value distribution for the interval 34 MeV $< Q <$ 40 MeV.

§ 3. Experimental Procedure

The calculation of Q-values requires an accurate knowledge of the energies of the two particles and of the angle between them. These quantities in turn depend on

(*a*) the ranges of the particles,

(*b*) the projection of the included angle upon, and the inclinations of the two tracks to the plane of the emulsion,

(*c*) the deduction of energies from these ranges using a range-energy relation appropriate to the experimental conditions,

(*d*) energy determinations on the protons which do not come to the end of their range in the emulsion.

(*a*) *Range Measurements*

(i) *Projected Lengths*

The projected lengths of the tracks in the emulsions they traversed, were determined by means of the stage micrometer and an eyepiece graticule, both of which were calibrated against Leitz 'etalons'. Measurements on these events were made on Cooke M4000-type microscopes. Care was taken to ensure that the calibration of the eyepiece graticule and subsequent measurements using it, were all made at the same interocular distance, and at or very close to a chosen position of the fine focus control. These precautions are essential since the magnification can change by several per cent between the extremes of adjustment, and can lead to corresponding systematic errors in the length measurements. In the plates employed, the conditions of processing were such that it was possible to define accurately the points of entrance and exit of each particle. The true ranges in unprocessed emulsion were then calculated from a knowledge of the individual emulsion thicknesses.

(ii) *Emulsion Thickness*

The entire stack used in this work was kept for several days in an enclosure of uniform humidity to ensure that the contours of the unprocessed emulsion were faithfully reproduced in the processed conditions. Projected range and dip measurements were carried out on the tracks of 207 μ-mesons arising from the decay at rest of π-particles observed in several plates, and adopting a modification of a procedure discussed by Fry and White (1953) the shrinkage factor appropriate to the conditions of measurement was obtained. At the same time, the thickness at several points in every emulsion was also measured. Apart from inequalities in the average thicknesses of the various emulsion strips, it was found that there existed departures from uniformity in thickness within single plates. The average unprocessed thickness for all plates of the stack was 610 μ and varied from 574 μ to 643 μ while differences within single plates sometimes amounted to as much as 12%. These conclusions were independently supported by measurements on the relative projected lengths of heavy primary particles traversing the stack. In view of these considerations it was necessary to determine the actual thickness at those points where the V-events occurred, and also to take account of these effects in evaluating the particle ranges. It was considered inadvisable to use a single value for the mean emulsion thickness over the entire stack as this would lead to errors both of a statistical and systematic nature.

(*b*) *Angles*

Dip measurements on the tracks and their errors were determined from the repeated measurements of several observers using different microscopes, and the corresponding angles of dip deduced from the original

and the processed thicknesses. Using then the projected angle as measured with a conventional eyepiece protractor, the space angle was calculated analytically.

(c) *Range–Energy Relation*

The relation between range and energy has been fairly well established experimentally for protons with energies below about 40 Mev (i.e. for ranges smaller than about 6 mm). Fay, Gottstein and Hain (1954) have shown that the experimental values of Bradner, Smith, Barkas and Bishop (1950), Rotblat (1951), and Catala and Gibson (1951) for proton ranges in emulsions in the region of 0·7 mm–6 mm may be represented by the relation

$$E=kR^{0\cdot568}$$

(E in Mev, R in microns, $k=0\cdot281$ for 'dry' G5 emulsion) with an accuracy of 0·7%. In considering the differences between C2 and G5 emulsions and to allow for variation in moisture content it would seem sufficient to modify the constant 'k' and retain unaltered the exponent. For the work described in this paper, in this region of energy, we have used the above relation and adopted a value of k appropriate to our emulsions. The measured mean range of μ-mesons (corrected for finite emulsion thickness) was $601\cdot6\pm3\,\mu$. Using the known mass $m_\mu=207\cdot0\,m_e$ of the μ-meson and its kinetic energy $E_\mu=4\cdot12$ Mev in the π–μ-decay process (Smith *et al.* 1953) we find $k=0\cdot276$. We thus obtain for 0·7 mm$<R<$6 mm,

$$E=0\cdot276\,R^{0\cdot568}. \quad \ldots\ldots\ldots \quad \text{(A)}$$

For proton ranges <1 mm, a curve was fitted to the experimental points of Rotblat (1951) and Catala and Gibson (1951) obtained for 'dry' C2 emulsions, and a new curve derived for our emulsions using the μ-meson data in conjunction with the stopping power figures given by Wilkins (1951).

For ranges >6 mm only one experimental point exists, that of Heinz (1954), who reports that protons of energy 342·5 Mev have an average range of $92\cdot68\pm0\cdot25$ g/cm^2 in Ilford C2 emulsions of average density 3·815 g/cm^3. The density of our emulsions at exposure was known to be very close to this value and accordingly we have used a range of 24·29 cm for 342·5 Mev protons.

A direct extension up to 342·5 Mev of the power law (A) yields a value of range considerably smaller than that obtained by Heinz. Since the energies of most of the particles considered in this investigation correspond to proton energies >40 Mev, it became necessary to adopt some suitable interpolation procedure.

The energy corresponding to a range of 6 mm was deduced from the power law (A), and, on a log–log plot, a straight line was then drawn between this point and the 24·29 cm point of Heinz. The equation of this is

$$E=0\cdot230\,R^{0\cdot589}. \quad \ldots\ldots\ldots \quad \text{(B)}$$

Energies of the particles have been deduced using this formula but these

are probably overestimates of the true value. On the other hand we have employed the extensive calculations on the range–energy relation in C2 emulsions which have been presented by Vigneron (1953) and which appear to be in satisfactory agreement with the experimental data in the lower energy region ($R<6$ mm). We find that Vigneron's results may be well fitted by the same power law (A) up to proton ranges of $\sim$5 cm. Accordingly we have also adopted a double chord fit of the following type.

(i) For 1 mm$<R<$5 cm : Power law (A).

(ii) For $R>5$ cm : Power Law

$$E=0{\cdot}1605\,R^{0{\cdot}618} \qquad \ldots\ldots\ldots \quad \text{(C)}$$

which is the equation on a log–log plot, of the straight line joining the 5-cm point determined according to (i), and the 24·29 cm point of Heinz. The true energies are probably slightly higher than given by this procedure.

At present there is no evidence, as to the true shape of the range–energy curve in the region above 6 mm. It appears reasonable to consider, however, that the two types of interpolation described above yield estimates not very different from the true values and that they represent reasonable upper and lower bounds. The maximum difference between the estimates derived by the two procedures is $\sim$5% (for a proton range of $\sim$5 cm). Hence we have deduced energies by both methods and taken a mean value as the best estimate. This may require revision when the range–energy relation becomes better established experimentally.

(*d*) *Energy Determinations on Tracks which left the Emulsion Stack*

Normalized grain density measurements were carried out at different places along the tracks of particles which did not come to the end of their range in the emulsion. Except in the case of Event No. (12) the true ranges of the particles in emulsions were then estimated using these values in conjunction with previously determined calibration grain density *vs.* range curves for protons. For Event (12), in view of the rather high energy of the proton, this procedure could not be applied. Instead, scattering measurements were carried out on the track and the energy thence determined.

§4. Discussion

(*a*) *Identities of the Secondary Particles*

As has been stated previously, the Q-values have all been calculated on the assumption that the particles involved are a proton and a negative π-meson respectively. The nature of the disintegrations produced by the mesons at the end of their range makes it virtually certain that all these were indeed π- and not μ-particles. In the favourable cases, the mass of the other secondary particle was obtained by measurements of grain density, photometric track density and multiple scattering as a function of range. All the measurements yielded masses consistent with that of the proton.

(*b*) *Errors*

The errors affecting the observations are partly of a statistical and partly of a systematic nature and may be considered in the following terms.

The determination of range is subject to errors in measurement which were reduced to negligible proportions by the procedures described in § 3. Straggling in range results in an uncertainty in energy of approximately 1% for protons and ~2·5% for π-mesons. Also, if the particle suffers an inelastic scattering the measured range will yield an underestimate of the true energy. The magnitude of this is probably small, since no such effect could be detected from the grain density and multiple scattering measurements along the tracks.

The effect of distortion and Coulomb scattering of the tracks, on the measurement of angles, has been dealt with in detail by Lal *et al.* (1953). The correction for distortion in the case of our emulsions is negligible, whilst errors due to Coulomb scattering are small and will increase only slightly the statistical spread of Q-values.

Since the precise form of the range–energy relation in the region of higher energies is not yet known, it has been necessary to use a somewhat arbitrary interpolation procedure to deduce energies. The Q-values thus obtained may therefore require adjustment when further experimental data becomes available, but it seems improbable that the mean value will change by more than 1%.

Acknowledgments

We wish to express our gratitude to Professor C. F. Powell, F.R.S., for the hospitality and facilities of his laboratory and for his constant encouragement. We are indebted to Mr. L. van Rossum who kindly carried out the photometric track density measurements for us. We are grateful to Mrs. D. M. Ford and Miss Rosemary Mitchell for assistance rendered.

Certain of us wish to thank the following bodies for financial grants: National University of Ireland for a Travelling Studentship and University College, Dublin, for additional assistance (D. K.); The Royal Commission for the Exhibition of 1851, for a Senior Studentship (M. G. K. M.); Consiglio Nazionale delle Ricerche, Roma (M. M.).

One of us (M. M.) is grateful for the Istituto di Fisica dell'Universita di Padova for leave of absence.

References

Amaldi, E., Anderson, C. D., Blackett, P. M. S., Fretter, W. B., Leprince-Ringuet, L., Peters, B., Powell, C. F., Rochester, G. D., Rossi, B., and Thompson, R. W., 1954, *Nature, Lond.*, **173**, 123.

Bonetti, A., Levi Setti, R., and Locatelli, B., 1953, *Bagnères Report*, p. 171.

Bradner, H., Smith, F. M., Barkas, W. H., and Bishop, A. S., 1950, *Phys. Rev.*, **77**, 462.

Bridge, H. S., Peyrou, C., Rossi, B., and Safford, R., 1953, *Phys. Rev.*, **91,** 362.
Catala, J., and Gibson, W. M., 1951, *Nature, Lond.*, **167,** 551.
DuMond, J. W. M., and Cohen, E. R., 1953, *Rev. Mod. Phys.*, **25,** 691.
Fay, H., Gottstein, K., and Hain, K., 1954, *Report of the* 1953 *Varenna Summer School* (in press).
Fry, W. F., and White, G. R., 1953, *Phys. Rev.*, **90,** 207.
Heinz, O., 1954, private communication.
Lal, D., Yash Pal, and Peters, B., 1953, *Proc. Ind. Acad. Sci.*, 38, V, 398.
Leighton, R. B., Wanlass, S. D., and Anderson, C. D., 1953, *Phys. Rev.*, **89,** 148.
Report of the International Conference on the Cosmic Radiation, Bagnères de Bigorre, 1953.
Report of the Rochester Conference on High Energy Physics, 1954.
Rochester, G. D., and Butler, C. C., 1947, *Nature, Lond.*, **160,** 855 ; 1953, *Rep. Prog. Phys.*, **16,** 364.
Rotblat, J., 1951, *Nature, Lond.*, **167,** 550.
Smith, F. M., Birnbaum, W., and Barkas, W. H., 1953, *Phys. Rev.*, **91,** 765.
Vigneron, L., 1953, *J. de Phys.*, **14,** 145.
Wilkins, J. J., 1951, *A.E.R.E.* (*Harwell*) *Report* G/R 664 (unpublished).

LXII. CORRESPONDENCE

The State of Ionization of Fast Nitrogen Ions Passing through Matter

By K. G. Stephens and D. Walker
Physics Department, University of Birmingham

[Received March 9, 1954]

A high-energy ion passing through matter undergoes a process of charge exchange by losing electrons in collisions with, or capturing electrons from, the stationary atoms of the matter traversed. The time average of the degree of ionization of the moving ion depends on the velocity of the ion and on its atomic number, being greater the higher the velocity and the smaller the atomic number.

In the case of fast ^{4}He ions (α-particles) this variation in the degree of ionization was early investigated by Henderson (1922, 1925). It was shown that for low-energy α-particles the mean charge carried is appreciably less than $2e$, falling continuously to zero as the velocity is reduced. Much other work has been done to investigate the charge-exchange phenomenon for hydrogen and helium ions. Dissanaike (1953) and Allison and Warshaw (1953) give adequate bibliographies.

Interest in ions heavier than ^{4}He arose in studies of the ranges of fission fragments and of recoil nuclei from nuclear reactions. Theoretical estimates of the degree of ionization of these heavier ions at various velocities have been made (Brunings *et al.* 1941, Bohr 1948) in order to calculate range-energy relations for these ions. It is a feature of these theoretical investigations that only the mean degree of ionization at a given velocity is estimated and no attempt is made to compute the relative probabilities of various states of ionization. It is assumed in the theory that, at any given ion velocity, there are only a few electron states of the ion for which the probabilities of electron-capture and of electron-loss are comparable. These electron states are such that the average orbital velocity of the electrons is of the same order of magnitude as the ion velocity. Brunings *et al.* (1941) use a factor γ, of the order of unity, to relate the characteristic electron orbital velocity V_e to the ion velocity V by the relation $V_e=\gamma V$.

Direct measurements of the relative probabilities of various states of ionization of a heavy ion at a given velocity are of interest, not only in checking the above theory, but also from the practical point of view of accelerating highly-charged heavy ions in a cyclotron (Walker and Fremlin 1953, Walker *et al.* 1954, Rossi *et al.* 1954). Some measurements have therefore been carried out with an external beam of 15 Mev $^{14}N^{2+}$ ions (velocity$=1{\cdot}43\times10^9$ cm/sec) from the Birmingham 60-inch cyclotron.

A narrow beam of 15 MeV $^{14}N^{2+}$ ions was defined by means of a slit system in the fringing magnetic field of the cyclotron. This beam impinged on an organic film 0·1 micron thick, the mean atomic number of the constituents of the film being 4. The energy loss of the ions in passing through the film was of the order of 1% only. Beyond the film the ions, now carrying various charges, were separated into groups by the action of the magnetic field and recorded in a photographic plate. The figure shows the result of scanning the plate in a direction at right

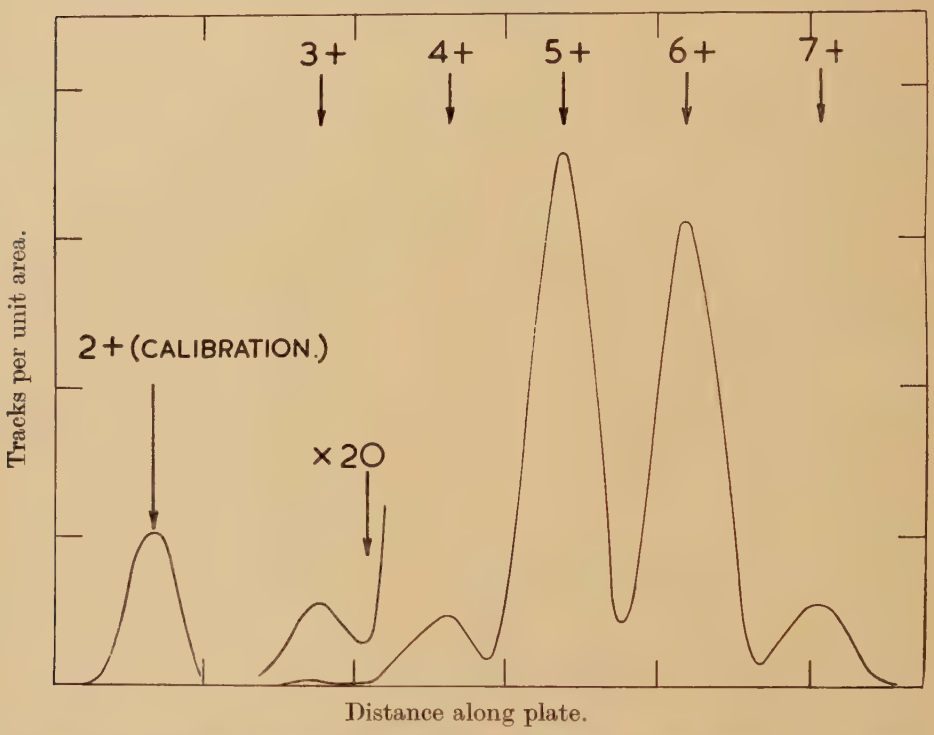

Density of nitrogen tracks observed in the photographic emulsion. The peaks due to ions with 3, 4, 5, 6 and 7 positive charges respectively are indicated. The 3+ peak obtained by scanning a strip 20 times the standard width is also shown. The relative height of the 2+ calibration peak is arbitrary.

angles to the directions of the magnetic field and of the incident ion beam. Individual points on the distribution curve are not shown since large numbers of tracks could be counted and thus high statistical accuracy achieved. The calibration peak was obtained by leaving a small hole in the organic film through which $^{14}N^{2+}$ ions passed without losing electrons.

Analysis of the distribution curve gives the probabilities of 3+, 4+, 5+, 6+, and 7+ states as 0·4%, 6·0%, 45·6%, 40·5%, and 7·5% respectively. The mean number of positive electron charges carried by the ions after passing through the film is computed from the distribution

curve to be 5·49. (Experiments with slightly thicker films yield slightly lower values of the mean charge, in accordance with the reduction in velocity of the ions in passing through the films. Thus we may infer that a film 0·1 micron thick is already sufficient for the equilibrium degree of ionization to have been reached.) The mean charge found agrees with the prediction of that form of the analysis of Brunings *et al.* (1941) which assumes that V_e is the velocity of the outermost electron on the Thomas–Fermi atomic model. For this assumption our result corresponds to $\gamma=0{\cdot}6$.

The measurements are being extended.

References

Allison, S. K., and Warshaw, S. D., 1953, *Rev. Mod. Phys.*, **25,** 779.
Bohr, N., 1948, *Kgl. Danske Videnskab. Selskab., Mat.-fys. Medd.*, **18,** No. 8.
Brunings, J. H. M., Knipp, J. K., and Teller, E., 1941, *Phys. Rev.*, **60,** 657.
Dissanaike, G. A., 1953, *Phil. Mag.*, **44,** 1051.
Henderson, G. H., 1922, *Proc. Roy. Soc.* A, **102,** 496 ; 1925, *Ibid.*, **109,** 157.
Rossi, G. B., Jones, W. B., Hollander, J. M., and Hamilton, J. G., 1954, *Phys. Rev.*, **93,** 256.
Walker, D., and Fremlin, J. H., 1953, *Nature, Lond.*, **171,** 189.
Walker, D., Fremlin, J. H., Link, W. T., and Stephens, K. G., 1954, *Brit. J. Appl. Phys.* (in press).

Paramagnetic Resonance in Activated Carbon

By D. J. E. Ingram and J. E. Bennett
University of Southampton

[Received March 15, 1954]

We have found that narrow paramagnetic resonance absorption lines can be obtained from samples of activated carbon. The samples can be divided into two classes (i) those which give a single strong line corresponding to a free electron spin, (ii) those which give a weaker, but well resolved, hyperfine structure, which is probably due to paramagnetic impurities trapped in the carbon.

Samples of powdered activated carbon (normally termed ' decolourizing charcoal ') freshly supplied by Hopkins and Williams, or B.D.H., show the single narrow line. This has a 'g' value of $2{\cdot}004\pm0{\cdot}002$, and a width of 10 ± 3 gauss, no change in either being detectable between 270°K and 90°K. The carbon may be heated to over 900°K with no resultant change in the absorption line, and may also be boiled in concentrated nitric, hydrochloric or sulphuric acids with no effect. Carbon giving an identical absorption can also be made in the laboratory by heating the organic salt of a diamagnetic metal. Thus zinc or

magnesium acetate can be heated, either in an atmosphere of carbon dioxide, or in air if the decomposition products are not allowed to burn, and a small amount of the salt will then char to produce black specks of carbon. These may be separated from the rest of the residue by boiling with hydrochloric acid, when the carbon remains as a fine black precipitate after filtration. The narrow line obtained from these specimens has the same 'g' value, and width, as those obtained from the commercial samples of activated carbon. We assume that the presence of the diamagnetic atoms has produced defects in the carbon structure, and that electrons have become trapped in these to give the narrow absorption lines.

The second type of spectrum was obtained from granulated activated carbon, and consisted of six hyperfine structure lines, equally spaced with a separation of 90 gauss between each line, the centre of the pattern corresponding to a 'g' value of $2{\cdot}01 \pm 0{\cdot}01$. The most likely explanation of this would be some small quantity of paramagnetic impurity, such as manganese, which has become distributed throughout the carbon structure. This seems to be confirmed by the fact that the intensity of these lines varies from sample to sample.

Recent work by Griffiths, Owen and Ward (1954) has shown that narrow paramagnetic absorption lines can be obtained from irradiated diamonds; our results seem to show that defects can also be produced in the carbon structure by other means, and that even powdered carbon has sufficiently large lattice units for them to be seen.

Absorption lines, which are very similar to the single one observed in powdered carbon, were first noticed in a residue obtained from the preparation of metallic phthalocyanine derivatives (Ingram and Bennett 1954). All the diamagnetic derivatives so far investigated (zinc, magnesium, aluminium and lead) produce a residue which gives a strong narrow line, with a 'g' value of $2{\cdot}004 \pm 0{\cdot}002$ and a width of 12 ± 5 gauss. The exact nature of this residue has not yet been determined, but it may be isolated by boiling in concentrated nitric acid, when small black particles are left undissolved, these being responsible for the absorption line. This would suggest that it might be a form of active carbon produced by charing, but it also appears to be slightly soluble in concentrated sulphuric acid and α-chloro-naphthalene, so it may be some form of polymerized carbon chain.

It is of interest that none of the paramagnetic metallic derivatives so far produced (copper, cobalt, iron, manganese, vanadium and platinum) give a residue that has this absorption line, although the actual metallic phthalocyanines all show a resonance corresponding to the particular metal. The one exception to this is nickel, the residue from this does give a line with a 'g' value of $2{\cdot}004 \pm 0{\cdot}002$, but its width is considerably greater than the others, being 30 ± 5 gauss. It would seem that the presence of the paramagnetic atom in this case causes a broadening of the free electron resonance.

Work on these compounds is continuing and we would like to thank the Royal Society for a grant towards the cost of the apparatus.

Note added in proof.—An exactly similar single narrow absorption line of 8 gauss width can be obtained by simply charring any natural carbohydrate; this may be the same as reported by Castle (1953) although its width does not appear to be dependent on the size or direction of the charred particles.

Castle, J. E., 1953, *Phys. Rev.*, **92**, 1063.

References

Griffiths, J. H. E., Owen, J., and Ward, I. M., 1954, *Nature, Lond.*, **173**, 439.
Ingram, D. J. E., and Bennett, J. E., 1954, *J. Chem. Phys.* (in the press).

Collisional Effects and the Conduction Current in an Ionized Gas

By A. A. Ware
Research Laboratory, Associated Electrical Industries Ltd., Aldermaston, Berks.

[Received March 17, 1954]

In a recent paper in this journal (Westfold 1953) an approximate expression is derived for the collision term in the current transport equation for a binary ionized gas in a large magnetic field ($\omega/\nu \gg 1$). This is obtained from the second approximations for the velocity distribution functions of the ions which are of the form

$$f_1^{(0)}(1+\Phi_1^{(1)}), \qquad f_2^{(0)}(1+\Phi_2^{(1)}),$$

where, using Westfold's notation,

$$\Phi_1^{(1)} = -\boldsymbol{A}_1 \cdot \frac{\partial T}{\partial \boldsymbol{r}} - \mathbf{B}_1 : \frac{\partial}{\partial \boldsymbol{r}} \boldsymbol{c}_0 - n\boldsymbol{D}_1 \cdot \boldsymbol{d}_{12}, \quad . \quad . \quad . \quad (1)$$

$$\Phi_2^{(1)} = -\boldsymbol{A}_2 \cdot \frac{\partial T}{\partial \boldsymbol{r}} - \mathbf{B}_2 : \frac{\partial}{\partial \boldsymbol{r}} \boldsymbol{c}_0 - n\boldsymbol{D}_2 \cdot \boldsymbol{d}_{12}. \quad . \quad . \quad . \quad (2)$$

To obtain approximations for the current density $\boldsymbol{j}$ and the collision term $\Delta\boldsymbol{j}$ the vector functions $\boldsymbol{A}$ and $\boldsymbol{D}$ are replaced by $\mathbf{a} \cdot \boldsymbol{C}$ and $\mathbf{d} \cdot \boldsymbol{C}$ and only the first terms in the expansions of the components of $\mathbf{a}$ and $\mathbf{d}$ in Sonine polynomials are taken. The coefficients of $\partial T/\partial \boldsymbol{r}$ and $\boldsymbol{d}_{12}$ are then linear in C, and to this approximation the current transport equation is

$$\frac{\partial \boldsymbol{j}}{\partial t} - \frac{\rho_1\rho_2}{\rho}\left(\frac{e_1}{m_1\rho_1} + \frac{e_2}{m_2\rho_2}\right)\boldsymbol{j} \wedge \boldsymbol{H} - \Delta\boldsymbol{j} = p\left(\frac{e_1}{m_1} - \frac{e_2}{m_2}\right)\boldsymbol{d}_{12}, \quad . \quad (3)$$

where

$$\Delta\boldsymbol{j} = -\nu\boldsymbol{j}, \quad . \quad . \quad . \quad . \quad . \quad . \quad . \quad . \quad (4)$$

and ν is the mean collision frequency. This expression for $\Delta\boldsymbol{j}$ is analogous with the results obtained by ' free path ' treatments.

The essential basis for this result is the rejection of all terms beyond the first in the expansions for $\boldsymbol{A}$ and $\boldsymbol{D}$. In the case of $\boldsymbol{D}$ the work of Cowling (1945) has shown that the higher order terms do not contribute substantially to $\boldsymbol{j}$, so that the approximation is valid in this case. It is the purpose of this note to consider the importance of the higher terms in $\boldsymbol{A}$.

From the nature of the Maxwellian distribution a temperature gradient will cause molecules with velocity magnitude in the range dC to have a mean drift parallel to the gradient for small values of C and in the opposite direction for large C. (The transition will occur somewhere near the velocity magnitude $\{3kT/m\}^{1/2}$.) Thermal diffusion is the resultant of these two particle currents, and the question as to which predominates depends on the variation of mean free path with velocity.

These simple considerations show that the contribution to $\Phi^{(1)}$ due to a temperature gradient must be of opposite sign for large and small values of C. But since the first term in $\boldsymbol{A}$ is proportional to C this condition is not satisfied by the above approximation. It follows that the sum of higher terms in $\boldsymbol{A}$ must be comparable to the first so as to make $\boldsymbol{A}$ change signs for different magnitudes of C.

Solutions have been obtained for the higher terms in $\boldsymbol{A}$ only in two particular but important cases where the negative ions are electrons and where the approximation $m_2 \ll m_1$ can be made. These are (i) the case of a slightly ionized gas where momentum transfer to only the neutral atoms is considered (Davydov 1937) and (ii) the case of a completely ionized gas (Landshoff 1949). In (i) the coefficients in the first order terms are zero and only the second order terms have non-zero coefficients; in (ii) for large ω/ν the coefficients in the second order terms are about half those in the first order terms for a singly ionized gas.

A direct check of the validity of the approximation is obtained by comparing the current transport equations for the steady state case $\partial \boldsymbol{j}/\partial t = 0$. From (3) and (4) with $m_2 \ll m_1$ the components of current produced by a temperature gradient normal to a magnetic field are given by

$$\boldsymbol{j} = -\frac{n_2 e_2 k}{\nu m_2}\left\{\alpha \frac{\partial T}{\partial \boldsymbol{r}} - H^{-1}\beta \boldsymbol{H} \wedge \frac{\partial T}{\partial \boldsymbol{r}}\right\},$$

where for $\omega/\nu \gg 1$ the coefficients α and β are

$$\alpha = (\nu/\omega)^2, \qquad \beta = (\nu/\omega).$$

The corresponding values for these coefficients in cases (i) and (ii) are

$$(\alpha)_1 = \frac{3\pi}{4}(\nu/\omega)^2, \qquad (\beta)_1 = \frac{3\pi}{8}(\nu/\omega),$$

$$(\alpha)_2 = -\tfrac{1}{2}(\nu/\omega)^2, \qquad (\beta)_2 = (\nu/\omega).$$

It is seen that β is a good approximation for both cases, whereas α is a good approximation in neither case. In fact it has the wrong sign for

a completely ionized gas. In general it must be concluded that eqn. (4) is a good approximation only for an isothermal plasma.

The author would like to acknowledge the benefit of a discussion with Professor T. G. Cowling, F.R.S., and to thank Dr. T. E. Allibone, F.R.S., for permission to publish this letter.

References

Cowling, T. G., 1945, *Proc. Roy. Soc.* A, **183,** 453.
Davydov, B., 1937, *Phys. Z. Sowjet.*, **12,** 269.
Landshoff, R., 1949, *Phys. Rev.*, **76,** 904.
Westfold, K. C., 1953, *Phil. Mag.*, **44,** 711.

ERRATA

On the Nature of the Discrete Radio Sources, by R. Q. Twiss, 1954, *Phil. Mag.*, **45,** 249.

(1) The exponent of ν_c in the denominator of eqn. (14) should be 0·4 *not* 0·9.

(2) The first term under the integral sign in the equation determining $\alpha(\nu)$ in page 254 should be

$$\frac{dE}{E_0} \text{ not } \frac{\theta E}{E_0}.$$

LXIII. *Notices of New Books and Periodicals received*

Modern Developments in Fluid Dynamics—High Speed Flow. Edited by L. Howarth. [2 vols., pp. 875.] (Oxford : University Press.) Price 84*s*.

The last war lead to a great advance in our understanding of the problems of compressible flow, and by 1946 there was a clear need for a systematic account of the more important results in one convenient work.

The book under review was composed under the aegis of the Fluid Motion Sub-Committee of the Aeronautical Research Council, who recognized the need for it and took the necessary steps to secure its production. It follows the example of its predecessor (*Modern Developments in Fluid Mechanics* (1938) edited by S. Goldstein) in recognizing the mutual dependence of theory and experiment, a fact so clearly exemplified by the subject of compressible flow. The first volume is entirely devoted to the theoretical aspects of the subject. Volume II deals with the experimental techniques and numerical results and also contains a chapter on heat transfer. The latter is a combination and revision of two chapters of the earlier work mentioned above, the present book being considered a more appropriate place for them.

The scope of the book is wide, and the reader will find an account of all the more important aspects of compressible flow. With such an ambitious programme it is inevitable that the authors could not include too much detail and the general aim is to explain the underlying theory and experiment and refer the reader to original sources for further information.

The book is the collective effort of 16 authors, each of them an expert in his own particular field. It is an authoritative work and is sure to be welcomed by everyone interested in the subject. W. C.

Signal, Noise and Resolution in Nuclear Counter Amplifiers. By A. B. Gillespie. (Pergamon Press Ltd.) [Pp. 155.] Price 21*s*.

This book is an excellent and clear summary of the problems involved in determining the best choice of parameters in circuits used for nuclear counting. The emphasis is on the fundamental problems of input stage design and optimum frequency response, the questions of choice and design of the most suitable counter for a particular application is considered only insofar as it is necessary to explain the amplifier working. Although no complete amplifier circuits are given, the approach is thoroughly practical and many of the results presented in immediately applicable graphical form.

Most of the book is concerned with an analysis of the performance of an ionization chamber and amplifier, and later it is shown how the results must be modified to apply to proportional and scintillation counters. An analysis of the advantages to be obtained by coincidence counting might perhaps have made the book more useful to the experimenter, though admittedly this is hardly to be expected from the title.

Although there is probably insufficient explanation for a newcomer to signal to noise problems, the mathematics is for the most part easily followed and even comparatively straightforward integrations and other calculations are carefully worked through in a series of appendices. The least satisfactory part in the reviewer's opinion is the treatment of the counting of noise crests.

D. F. G.

[The Editors do not hold themselves responsible for the views expressed by their correspondents.]